

AD

AD 675445

USAAVLABS TECHNICAL REPORT 68-23

**RESEARCH IN MANEUVERABILITY
OF THE
XH-51A COMPOUND HELICOPTER**

By

F. P. Lottine
W. P. Groth
T. H. Oglesby

June 1968

ADDC
RECEIVED
OCT 1 1968
RILEY

**U. S. ARMY AVIATION MATERIEL LABORATORIES
FORT EUSTIS, VIRGINIA**

**CONTRACT DA 44-177-AMC-365(T)
LOCKHEED-CALIFORNIA COMPANY
BURBANK, CALIFORNIA**

*This document has been approved
for public release and sale; its
distribution is unlimited.*



Reproduced by the
CLEARINGHOUSE
for Federal Scientific & Technical
Information Springfield Va. 22151

**Best
Available
Copy**



DEPARTMENT OF THE ARMY
U S ARMY AVIATION MATERIEL LABORATORIES
FORT EUSTIS, VIRGINIA 23604

This report was prepared by the Lockheed-California Company under the terms of Contract DA 44-177-AMC-365(T).

The program, which consisted primarily of a flight investigation of the maneuvering capability of the XH-51A compound helicopter, is part of a progressive series of flight research programs being pursued by this Command to provide increased performance of rotary-wing type aircraft. Included in the program was an investigation of flight in turbulence and nap-of-the-earth operation. The XH-51A was also flown by NASA and U. S. Army personnel to evaluate performance, handling qualities, and general flight characteristics.

In general, the objectives of the flight program were met. Data were obtained on dynamic stresses, vibration, stability and control, and performance to a maximum flight speed of 263 knots (302 miles per hour) true airspeed.

The conclusions and recommendations contained herein are concurred in by this Command.

DISCLAIMERS

The findings in this report are not to be construed as an official Department of the Army position unless so designated by other authorized documents.

When Government drawings, specifications, or other data are used for any purpose other than in connection with a definitely related Government procurement operation, the United States Government thereby incurs no responsibility nor any obligation whatsoever; and the fact that the Government may have formulated, furnished, or in any way supplied the said drawings, specifications, or other data is not to be regarded by implication or otherwise as in any manner licensing the holder or any person or corporation, or conveying any rights or permission, to manufacture, use, or sell any patented invention that may in any way be related thereto.

DISPOSITION INSTRUCTIONS

Destroy this report when no longer needed. Do not return it to originator.

ACCESSION BY	
ADVIS	ADVIS SECTION <input checked="" type="checkbox"/>
REC	REC SECTION <input type="checkbox"/>
CHALLENGED	<input type="checkbox"/>
JUSTIFICATION	
BY _____	
EXTENSION/AVAILABILITY _____	
DEL.	MAIL DEL/SPCL
<input checked="" type="checkbox"/>	

Task LF121401A4301
Contract DA 44-177-AMC-365(T)
USAAVLABS Technical Report 68-23
June 1966

RESEARCH IN MANEUVERABILITY
OF THE
XH-51A COMPOUND HELICOPTER

Final Report

Lockheed Report 20894

By

F. P. Lentine
W. P. Groth
T. H. Oglesby

Prepared by

Lockheed-California Company
Burbank, California

for

U. S. ARMY AVIATION MATERIEL LABORATORIES
FORT EUSTIS, VIRGINIA

This document has been approved
for public release and sale; its
distribution is unlimited.

SUMMARY

This report discusses the results of a research program conducted by the Lockheed-California Company to evaluate the maneuvering capability and critical rotor stresses of the rigid-rotor XH-51A compound helicopter (Figure 1) under Contract DA 44-177-AMC-365(T).

As shown in Figure 2, the maneuvering envelope was expanded beyond the specified program objectives. These data are referenced to the design gross weight of 4500 pounds.

In demonstrating this test envelope, the effects of rotor RPM, cyclic control system sensitivity, and center of gravity position were evaluated in terms of aircraft response and structural loads to determine the optimum combination of these variables. The testing conducted to investigate these effects consisted of longitudinal and lateral control response, short-period damping, autorotation characteristics, maneuvering stability, static stability, and level flight performance. Also investigated were the effects of atmospheric turbulence and nap-of-the-earth operations on aircraft response and rotor stresses.

The following significant results were obtained:

- A maximum flight speed of 262.7 KTAS was attained in a shallow descent of 800 to 1000 fpm with a rotor RPM of 95.5 percent.
- Autorotation entries at speeds in excess of 230 KTAS were simulated using high-speed entry techniques.
- Forward centers of gravity had a favorable effect on high-speed handling qualities.
- Desensitizing the longitudinal cyclic control system helps to reduce the excessive response characteristics of the aircraft at high forward speeds. Aircraft response at low speeds, however, is reduced to the extent that it appears doubtful that a single control system sensitivity will suffice for all speeds and conditions.
- Main rotor loads obtained in rough air were more severe than those obtained in level flight at comparable airspeeds. However, the effect of the load increase on fatigue life does not appear to be severe.
- Reduced rotor RPM at high speed had an adverse effect on rotor plane oscillations.

Two factors prevented the RPM-airspeed envelope shown in Figure 3 from being expanded further. The first of these is a strong vibration above 220 KTAS at high rotor RPM settings which is associated with the advancing blade Mach number. The second factor is a mild rotor plane oscillation at high airspeeds which becomes more pronounced as rotor RPM is reduced below intermediate values.



Figure 1. XH-51A Compound Helicopter in Flight.

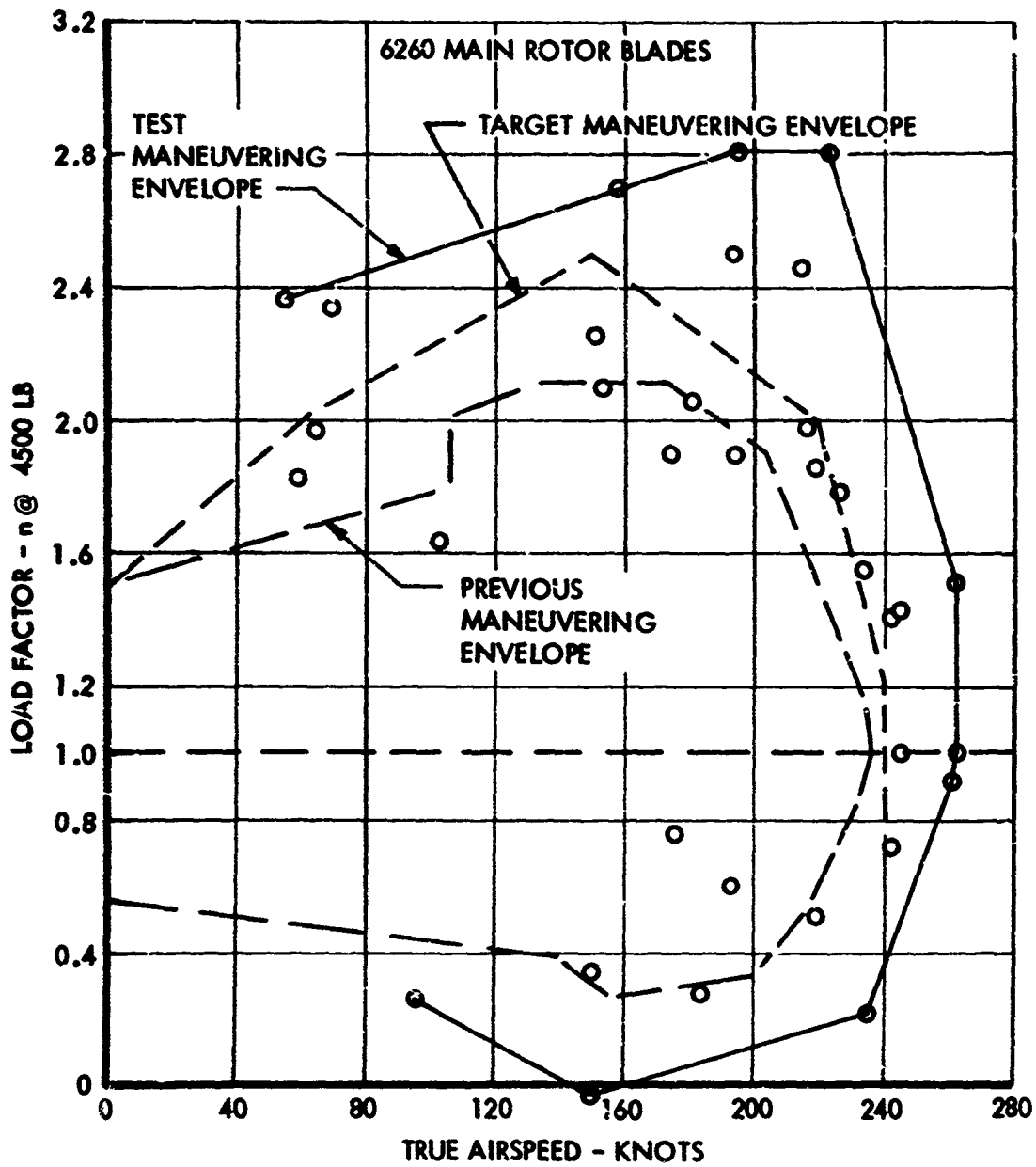


Figure 2. Maneuvering Envelope - Referenced to Design Gross Weight of 4500 Pounds.

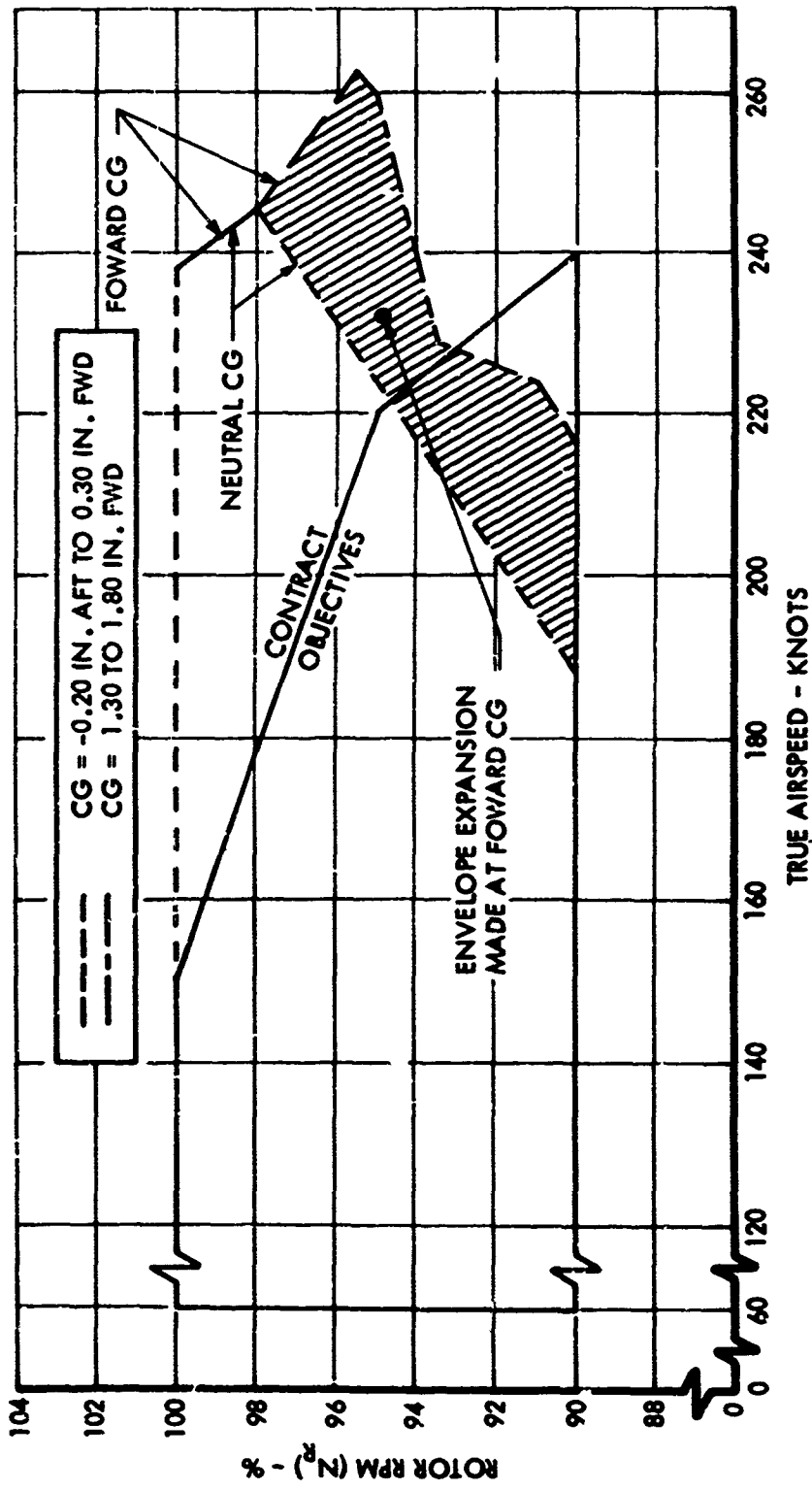


Figure 3. Power-On Rotor RPM Envelope as a Function of True Airspeed.

FOREWORD

This report describes the results of the research in the maneuverability program conducted with the Lockheed Rigid-Rotor XH-51A compound helicopter. This program was conducted by the Lockheed-California Company under Contract DA 44-177-AMC-365(T) with the U.S. Army Aviation Materiel Laboratories (USAAVLABS), Fort Eustis, Virginia.

Flying began on 4 August 1966 and continued through 11 July 1967. It was conducted by members of the helicopter staff under the direction of Mr. A. W. Turner, Flight Test Division Engineer. The Lockheed test pilots were Messrs. R. Goudey and D. Segner.

The NASA evaluation during the program was performed by Messrs. L. Jenkins, Engineer, and P. Deal, Test Pilot.

Technical monitoring of the program for USAAVLABS, as well as a separate flight evaluation, was performed by Messrs. R. Dumond, Engineer and D. Simon, Test Pilot.

TABLE OF CONTENTS

	<u>Page</u>
SUMMARY	iii
FOREWORD	vii
LIST OF ILLUSTRATIONS	xii
LIST OF TABLES	xviii
LIST OF SYMBOLS	xix
INTRODUCTION	1
DESCRIPTION OF TEST ARTICLE	2
AGILITY AND MANEUVERABILITY	9
Envelope Expansion	9
Power-On Rotor RPM/Airspeed Envelope	9
Maximum Airspeeds	11
Maneuvering Envelope	13
Control Response and Short-Period Damping	17
Longitudinal Control Response	17
Longitudinal Short-Period Damping	21
Lateral Control Response	25
Lateral Short-Period Damping	28
Maneuvering Stability	32
Turning Flight	32
Symmetrical Pull-Ups	38
Rotor RPM Characteristics	43
Cyclic Control Trim Requirements	45
Nap-of-the-Earth Flying	52

	<u>Page</u>
Structural Loads	54
General	54
Main Rotor Blade Loads	55
6261-1100-01 Model 286 Prototype Blades with XH-51A Cuff Fittings	56
6260-1100-01 Standard XH-51A Main Rotor Blades	59
6260-1100-01 Main Rotor Blades with 20 Pound Anti-Nodal Weights	59
6260-1100-01 Standard XH-51A Main Rotor Blades	60
Level Flight Conditions	60
Maneuvering Conditions	63
Gyro Arm Bending	67
Vibration	73
Rotor Plane Oscillations	73
Horizontal Stabilizer Loads	75
Pitch Link Loads	76
Miscellaneous Loads	76
Tail Rotor Loads	76
Map-of-the Earth Testing	78
Side Hill Landing	78
ROUGH AIR OPERATION	81
General	81
Vertical Acceleration Due to Gusts	81
Derived Gust Velocities	86
Main Rotor Load Measurements	89
HOVERING AND HOVER MANEUVERS	95
General	95
Hovering Over a Spot	95
Sideward Flight	95
Rearward and Low Speed Forward Flight	97
Turn On a Spot	97
Crosswind Hover	99

	<u>Page</u>
AUTOROTATION	100
Rotor RPM Decay Characteristics	100
Autorotation Entries	102
Simulated Failure of PT6B-9 Main Rotor Engine	102
Simulated Failure of J-60-P-2 Auxiliary Thrust Engine	104
Simulated Simultaneous Failure of Both Engines	104
Structural Loads	106
LEVEL FLIGHT PERFORMANCE CHARACTERISTICS	107
Airspeed Calibration	107
Power and Thrust Sharing Characteristics	116
Rotor/Wing Lift Sharing Characteristics	116
Rotor/Wing Lift Sharing Characteristics in Turning Flight	121
Theoretical Comparison	125
NASA PARTICIPATION	132
U.S. ARMY PARTICIPATION	133
CONCLUSIONS	134
RECOMMENDATIONS	136
LITERATURE CITED	137
DISTRIBUTION	138

LIST OF ILLUSTRATIONS

<u>Figure</u>		<u>Page</u>
1	XH-51A Compound Helicopter in Flight	iv
2	Maneuvering Envelope - Referenced to Design Gross Weight of 4500 Pounds	v
3	Power-On Rotor RPM Envelope as a Function of True Airspeed	vi
4	XH-51A Compound Helicopter in Hover	3
5	Power-On Rotor RPM Envelope as a Function of True Airspeed	10
6	Approximate Collective Blade Angle Test Envelope as a Function of True Airspeed	12
7	Maneuvering Envelope - Referenced to Design Gross Weight of 4500 Pounds	14
8	Longitudinal Control Response as a Function of True Airspeed - Effect of Rotor RPM - Neutral CG	18
9	Longitudinal Control Response as a Function of True Airspeed - Effect of Collective Blade Angle - Neutral CG	19
10	Longitudinal Control Response as a Function of True Airspeed - Effect of Longitudinal System Sensitivity - Neutral CG	20
11	Longitudinal Control Response as a Function of True Airspeed - Effect of CG Location	22
12	Time History of Longitudinal Short-Period Damping - 83% Longitudinal System Sensitivity - Neutral CG	23
13	Time History of Longitudinal Short-Period Damping - 66% Longitudinal System Sensitivity - Neutral CG	24

<u>Figure</u>		<u>Page</u>
14	Time History of Longitudinal Short-Period Damping - $N_R = 100\%$ - Neutral CG	26
15	Time History of Longitudinal Short-Period Damping - $N_R = 91.5\%$ - Neutral CG	27
16	Lateral Control Response as a Function of True Airspeed - Effect of Lateral System Sensitivity - Neutral CG	29
17	Time History of Lateral Short-Period Damping - 154% Lateral System Sensitivity - Neutral CG	30
18	Time History of Lateral Short-Period Damping - 200% Lateral System Sensitivity - Neutral CG	31
19	Time History of Lateral Short-Period Damping - $N_R = 100\%$ - Neutral CG	33
20	Time History of Lateral Short-Period Damping - $N_R = 90.5\%$ - Neutral CG	34
21	Maneuvering Stability During Steady Turns as a Function of True Airspeed for Various Collective Blade Angles and Rotor RPM Settings - Neutral CG	36
22	Variation of Maneuvering Stability With True Airspeed During Steady Turns - Effect of Longitudinal System Sensitivity - Neutral CG	37
23	Maneuvering Stability During Symmetrical Pull-Ups as a Function of True Airspeed for Various Collective Blade Angles and Rotor RPM Settings - Neutral CG	39
24	Maneuvering Stability During Symmetrical Pull-Ups as a Function of True Airspeed for Various Collective Blade Angles and Rotor RPM Settings - Forward CG	40
25	Variation of Maneuvering Stability With True Airspeed During Symmetrical Pull-Ups - Effect of Longitudinal System Sensitivity - Neutral and Forward CG	41
26	Variation of Rotor RPM with Load Factor in Steady Turns - Neutral CG	44
27	Variation of Cyclic Control Positions With True Airspeed - Effect of Control Gyro Tab Installation - Neutral CG	47

<u>Figure</u>		<u>Page</u>
28	Variation of Cyclic Control Positions with True Airspeed - Effect of System Sensitivity - Neutral CG	48
29	Variation of Cyclic Control Positions With True Airspeed - Effect of Collective Blade Angle and Rotor RPM Setting - Neutral CG	50
30	Variation of Cyclic Control Positions With True Airspeed - Effect of Longitudinal System Sensitivity - Forward CG	51
31	Main Rotor Hub Loads as a Function of Equivalent Airspeed	57
32	Harmonic Components of Cyclic Flapwise Bending Moment at Sta. 6 as a Function of Equivalent Airspeed	58
33	Main Rotor Hub Loads as a Function of Equivalent Airspeed	61
34	Harmonic Components of Cyclic Flapwise Bending Moment at Sta. 6 as a Function of Equivalent Airspeed	62
35	Harmonic Components of Cyclic Flapwise Bending Moment at Sta. 6 as a Function of Main Rotor Advancing Tip Mach Number	64
36	Roll and Pitch Components of Cyclic Flapwise Bending Moment at Sta. 6 as a Function of Equivalent Airspeed	65
37	Maximum Main Rotor Blade Loads as a Function of Load Factor	66
38	Flapwise Bending Moment at Sta. 6 as a Function of Pitch Angular Acceleration	68
39	Main Rotor Blade Loads as a Function of Maximum Load Factor	69
40	Right Wing Bending Moment and Rotor Lift as a Function of Maximum Load Factor	70
41	No. 1 Gyro Arm Chord Cyclic Bending Moment as a Function of Main Rotor RPM	71

<u>Figure</u>		<u>Page</u>
42	Horizontal Stabilizer, Gyro Arm, and Pitch Link Loads as a Function of Equivalent Airspeed	72
43	Cabin Vibration as a Function of Equivalent Airspeed . .	74
44	Collective Blade Angle, Rotor Lift, and Right Wing Bending Moment as a Function of Equivalent Airspeed . .	77
45	Tail Rotor Loads, Control Positions, and Horsepower as a Function of Equivalent Airspeed	79
46	Comparison of CG Vertical Acceleration in Gusts	82
47	Exceedance of CG Acceleration Increments in Rough Air for a Test Time of 4.9 Minutes	84
48	Exceedance of CG Acceleration Increments in Rough Air for a Test Time of 11.9 Minutes	85
49	Exceedance of CG Acceleration Increments in Rough Air for a Test Time of 13.5 Minutes	87
50	Distance to Reach or Exceed a Given Gust Velocity . . .	88
51	Time History of Blade Loads and CG Vertical Acceleration in Turbulence at 130 KEAS	90
52	Time History of Blade Loads and CG Vertical Acceleration in Turbulence at 200 KEAS	91
53	Gust Loading Spectrum - Chordwise Bending Moment at Sta. 6	92
54	Gust Loading Spectrum - Flapwise Bending Moment at Sta. 6	93
55	Control Position Variation During Sideward Flight . . .	96
56	Control Position Variation During Hover, Rearward, and Low-Speed Forward Flight	98
57	Power-Off Rotor RPM Decay Rate as a Function of True Airspeed - Normal Acceleration = 1.0g	101
58	Time History of Autorotation Entry at 228.5 KTAS - Forward CG	103
59	Time History of Autorotation Entry at 232.0 KTAS - Forward CG	105

<u>Figure</u>		<u>Page</u>
60	Airspeed Calibration - Boom System	109
61	Engine Shaft Horsepower Required for Level Flight - Effect of Collective Blade Angle - Neutral CG	110
62	Tail Rotor Horsepower Required for Level Flight - Effect of Collective Blade Angle and Rotor RPM - Neutral CG	111
63	Engine Shaft Horsepower Required for Level Flight - Effect of Rotor RPM - Neutral CG	112
64	Auxiliary Thrust Required for Level Flight - Effect of Collective Blade Angle and Rotor RPM - Neutral CG	114
65	Equivalent Shaft Horsepower Required for Level Flight - Effect of Collective Blade Angle - Neutral CG	115
66	Equivalent Shaft Horsepower Required for Level Flight - Effect of Rotor RPM - Neutral CG	117
67	Power Sharing Characteristics in Level Flight - Effect of Collective Blade Angle - Neutral CG	118
68	Rotor Lift Sharing Characteristics in Level Flight - Effect of Collective Blade Angle - Neutral CG	119
69	Angle of Attack Variation With True Airspeed - Effect of Collective Blade Angle and Rotor RPM - Neutral CG	120
70	Rotor Lift Sharing Characteristics in Level Flight - Effect of Rotor RPM - Neutral CG	122
71	Rotor Lift Sharing Characteristics in Turning Flight - Effect of Airspeed - Neutral CG	123
72	Rotor Lift Sharing Characteristics in Turning Flight - Effect of Collective Blade Angle - Neutral CG	124
73	Forces Acting on the Aircraft	126
74	Helicopter Lift and Drag Characteristics	128
75	Correlation of Flight Test Data and Calculations at 100% Rotor RPM	129

<u>Figure</u>		<u>Page</u>
76	Correlation of Flight Test Data and Calculations at 95% Rotor RPM	130
77	Correlation of Flight Test Data and Calculations at 91% Rotor RPM	131

LIST OF TABLES

<u>Table</u>		<u>Page</u>
I	Compound Helicopter Description	5
II	Summary of Maximum Airspeed Conditions	13
III	Summary of Test Conditions - Neutral CG	15
IV	Summary of Test Conditions - Forward CG	16
V	Summary of Longitudinal Control Response and Short-Period Damping Test Results	25
VI	Summary of Lateral Control Response and Short-Period Damping Test Results	32
VII	Summary of Maneuvering Stability Test Results	42

LIST OF SYMBOLS

GENERAL

°C	temperature, degrees centigrade
$C_{L_{max}}$	maximum attainable lift coefficient
CG	Center of gravity referenced to rotor-mast centerline
cps	cycles per second
deg ()°	angular degrees
CAS	calibrated airspeed
KCAS	knots calibrated airspeed
EAS	equivalent airspeed - $TAS \times \sigma^{1/2}$
KEAS	knots equivalent airspeed
ESHP	equivalent shaft horsepower
F_N	Auxiliary net thrust, lb
FRL	fuselage reference line, an arbitrary longitudinal line parallel to fore and aft centerline and waterline
g	aircraft load factor
H_D	density altitude
H_{PC}	pressure altitude corrected for static system error
HP	horsepower
in.-Hg	inches of mercury
i	incidence angle
kts	knots

lb	pounds
L_R	rotor lift
L_W	wing-body lift
M	Mach number
MAC	mean aerodynamic chord
NASA	National Aeronautics and Space Administration
ND	nose down
NU	nose up
N_R	rotor speed
n	flight load factor, multiples of g where noted, adjusted to a standard gross weight by the ratio
	$n = n(\text{test}) \frac{\text{gross weight (test)}}{\text{gross weight (standard)}}$
P	notation for per revolution when relating frequencies to rotor rotating frequency, e.g.,
	1P, one per revolution 3P, three per revolution
psi	pounds per square inch
psf	pounds per square foot
q	dynamic pressure $q = \rho(TAS)^2/2$
rpm	revolutions per minute
SHP	shaft horsepower
TAS	true airspeed
THP	thrust horsepower = $F_N(KTAS)/325$
V_e	equivalent airspeed - knots
V_{in}	indicated airspeed (corrected for instrument error) - knots

V_{\max}	maximum airspeed - knots
W	weight
W_{AVG}	average weight
α_{FRL}	angle of attack (fuselage reference line)
σ	air density ratio $\sigma = \rho/\rho_0$
ρ	test condition air density
Ω	angular velocity, rad/sec
ρ_0	sea level standard day air density
θ_0	collective blade angle at blade station zero, hub center-line, + leading edge up
$\frac{-d(\%N_R)}{dt}$	rate of decay of rotor speed with respect to time

THEORETICAL COMPARISON

C_L'/σ	rotor lift coefficient, $\frac{T_R}{\rho \omega R^2 (\Omega R)^2}$
C_D'/σ	rotor drag coefficient, $\frac{D_R}{\rho \omega R^2 (\Omega R)^2}$
C_Q/σ	rotor torque coefficient, $\frac{Q_R}{\rho \omega R^3 (\Omega R)^2}$
W	aircraft gross weight
L_A	lift of helicopter without rotor
T_R	thrust of rotor
F_N	jet engine thrust
α_R	angle of attack of rotor disc
α_{∞}	angle of attack of aircraft at instrumentation boom

α_L	angle of attack of aircraft at wing
ϕ_R	downwash angle at wing induced by rotor
i_R	incidence of rotor shaft
i_j	incidence of jet exhaust
D_R	rotor drag
D_A	drag of helicopter without rotor
D_{TR}	drag of tail rotor
ρ	density of atmosphere
R	radius of main rotor
V	forward velocity
μ	tip speed ratio, $\frac{V}{\Omega R}$
ΩR	tip speed
σ	rotor solidity

INTRODUCTION

Previous research efforts on various compound helicopters have been directed largely toward speed gains and transient load factors. Although these programs were successful, their scope was limited in one important area. This was the area of maneuverability and agility over the entire speed range. With rapidly approaching compound helicopter applications, additional maneuverability and agility information and accompanying quantitative data on dynamic stresses and handling characteristics are needed to assist designers of future compound helicopters.

A high-speed extension flight test program was conducted by the Lockheed-California Company on the rigid-rotor XH-51A compound helicopter during May 1965 under Contract DA 44-177-AMC-150(T). The objective of this program was to investigate the flight characteristics of the compound helicopter with special emphasis on the areas of flying qualities, performance, structural loads, vibration, and maneuverability in the speed range of 200 to 230 KTAS. As reported in Reference 1, this objective was met and a maximum level flight speed of 236 KTAS was demonstrated.

The Lockheed-California Company was then authorized to study the maneuvering capability of the rigid-rotor XH-51A compound helicopter under Contract DA 44-177-AMC-365(T), dated 20 June 1966, with the U.S. Army Aviation Materiel Laboratories, Fort Eustis, Virginia. This is a report of the results of that study.

The principal objective of this study was to explore further the maneuvering capability of the compound helicopter in terms of envelope expansion, longitudinal and lateral control response and damping, maneuvering stability, hover maneuvers, and autorotation and level flight characteristics over the following target airspeed-load factor envelope:

- 2.0g at 60 KTAS
- 2.5g at 150 KTAS
- 2.0g at 220 KTAS
- 1.0g ($\pm 0.2g$) at 240 KTAS

The first flight under this contract was accomplished on 4 August 1966, and a maximum true airspeed of 262.7 knots was demonstrated on 19 June 1967. During the program, 209 flights were conducted, for a total of 64.3 flight hours. Of these totals, NASA participation amounted to 23 flights, accumulating 9.2 flight hours, with U.S. Army participation amounting to 15 flights, for a total of 5.5 flight hours. The flight program ended on 11 July 1967.

DESCRIPTION OF TEST ARTICLE

The XH-51A compound helicopter test article (see Figure 4) is described in Table I. At the completion of the previous compound helicopter program, certain modifications to the aircraft were considered necessary. Accordingly, prior to commencing the maneuverability program, the following modifications were incorporated:

- PT6B-9 Turbine Engine

A PT6B-9 gas turbine engine compatible to the XH-51A helicopter was installed. This engine provided more available power to compensate for the vehicle's increased gross weight, and it afforded additional low-speed maneuvering capability.

- Slip Ring Assemblies

A 40-slip ring assembly compatible to the XH-51A main rotor and an 18-slip ring assembly compatible to the XH-51A tail rotor were installed to monitor main rotor and tail rotor instrumentation parameters, respectively.

- Rate Gyros

Two rate gyros sensitive to 0.02 rad/sec were installed to sense aircraft pitch and roll responses.

- Spoiler Control

The actuation of the spoiler was revised so that the direction of the controlling switch conformed to the convention for dive-brake operation.

- Increased Fuel Capacity

A 34-gallon torso fuel tank capacity with quick-disconnect provisions and a separate fuel shutoff valve was installed in the aircraft. The torso tank is the J-60-P-2 engine primary fuel source until nearly empty, at which time it reverts to the ship's main fuel supply.

- Torso Tank Fuel Gage

A cockpit gage to indicate fuel quantity in the auxiliary torso fuel tank was installed. This gage was a differential pressure gage plumbed to measure the liquid fuel head in the tank for level flight conditions.

- Auxiliary Jet Throttle Modification

The auxiliary jet engine throttle was incorporated into the collective handle twist grip, replacing the PT6B-9 gas generator control at that location.

- PT6B-9 Gas Generator Control

The gas generator condition lever (N_1) was relocated from the collective handle twist grip to the handle previously used for the jet engine control (quadrant lever). To facilitate recovery from autorotations, an emergency solenoid actuator was added to move this quadrant lever back to the power-on condition upon actuation of a switch on the pilot's collective control.

- Collective Control

An overriding detent was incorporated into the pilot collective pitch control lever at $\theta_0 = 4.00$ degrees, the optimum blade angle for high speed flight in the compound helicopter mode. This was a spring detent which could be overridden by the pilot but would return the handle to the detent position when released. It will return the handle to the detent only from positions below the detent.

- Zero-g Hydraulic Reservoir

A zero-g type hydraulic system reservoir was installed to provide hydraulic fluid pressure to the intake port of the primary system pump regardless of the flight attitude or load factor. The emergency standby system still operates from a standpipe reserve supply contained in this reservoir.

- Control Bell Cranks and Springs

Capability to vary cyclic control system sensitivities in the longitudinal and lateral axes was utilized through the variation of booster input and output bell cranks and springs. Since the control system of the XH-51A rigid rotor helicopter is basically a rate-generating system, this approach was utilized to attain the desired results.

TABLE I. COMPOUND HELICOPTER DESCRIPTION

<u>General</u>	
Design gross weight	4,500 lb
Takeoff gross weight - neutral cg	5,165 lb
Takeoff gross weight - fwd cg	5,275 lb
Fuel capacity (includes 220-lb-capacity torso tank)	700 lb
Normal crew (plus research instrumentation)	1
Overall length	42.58 ft
Maximum ground attitude (tail low)	6 deg
Roll mass moment of inertia (including rotor)	1,500 slug-ft ²
Pitch mass moment of inertia (including rotor)	3,180 slug-ft ²
Yaw mass moment of inertia (including rotor)	3,800 slug-ft ²
<u>Neutral Center of Gravity Range</u>	
Full Fuel = 700 lb	1,550 in.-lb fwd - 19,650 in.-lb lt
Main Fuel = 480 lb	1,485 in.-lb aft - 23,170 in.-lb lt
Zero Fuel	0 in.-lb -20,900 in.-lb lt
<u>Forward Center of Gravity Range</u>	
Full Fuel = 700 lb	9,500 in.-lb fwd - 19,600 in.-lb lt
Main Fuel = 480 lb	6,070 in.-lb fwd - 23,120 in.-lb lt
Zero Fuel	6,875 in.-lb fwd - 20,900 in.-lb lt
<u>Main Rotor</u>	
Type	rigid
Diameter	35 ft
Number of blades	4
Blade Chord	13.5 in.

TABLE I - (Continued)

TABLE I - (Continued)	
<u>Main Rotor - Continued</u>	
Blade Weight	36 lb/blade
Airfoil section	modified NACA 0012
Blade taper	0
Blade twist (root to tip)	-5 deg
Rotational axes tilt	6 deg forward
Hub precone	+3.2 deg
Preset blade droop @ sta 27.85	-1 deg
Disc area	962 sq ft
Solidity	.0818
Disc loading	4.68 ps ²
Polar moment of inertia	1,013 slug-ft ²
Normal operating speed (100%)	355 rpm
Blade sweep	1.4 deg forward
<u>Control Gyro</u>	
Diameter	72 in.
Number of arms	4
Polar moment of inertia	7.5 slug-ft ²
Incidence angle of arms	5.0 deg
<u>Tail Rotor</u>	
Diameter	72 in.
Number of blades	2
Blade chord	8.5 in.
Hub type	teetering
Airfoil section	NACA 0012
Blade taper	0
Blade twist (root to tip)	-4.35 deg

TABLE I - (Continued)

<u>Tail Rotor - Continued</u>	
<u>Feathering moment balance weights:</u>	
Weight	2.25 lb/blade
Arm	3.0 in.
Delta -3 hinge	15 deg
Disc area	28.27 sq ft
Solidity	.1503
Pitch change travel	27 deg to -8 deg
Normal operating speed (100%)	2,085 rpm
<u>Wing</u>	
Span (nominal)	16.83 ft
Taper ratio	0.5
Area	70 sq ft
Aspect ratio	4.05
Sweepback (.25c)	0
Chord (MAC)	57.72 in.
Airfoil	NACA 13012
Incidence (fixed)	- 9 deg
<u>Horizontal Stabilizer</u>	
Span	108 in.
Chord (constant)	26.4 in.
Area	19.8 sq ft
Aspect ratio	4.1
Incidence	-0.25 deg
Airfoil section	NACA 0015
Tip weights	8 lb/side
<u>Vertical Stabilizer</u>	
Span	41.75 in.
Chord (tip)	38.5 in.

TABLE I - (Continued)

Vertical Stabilizer - Continued

Chord (root)	51.5 in.
Area	12.58 sq ft
Taper ratio	0.70
Aspect ratio	0.95
Airfoil section	modified NACA 4424

Powerplants

Primary

Type	Turboshaft PT6B-9
Maximum power (takeoff)	550 SHP @ sea level
Military power (30-minute limit)	500 SHP @ sea level
Fuel type	JP-4
Oil type	Turbo 35

Auxiliary

Type	Turbojet J-60-P-2
Military thrust @ 250 to 270 KTAS (specification engine-military power - standard day conditions - with no losses of any type)	2,590 lb @ sea level 2,295 lb @ 5,000 ft 2,010 lb @ 10,000 ft
Fuel type	JP-4
Oil type	Turbo 35
Thrust axis inclination	+7 deg

AGILITY AND MANEUVERABILITY

ENVELOPE EXPANSION

Power-On Rotor RPM/Airspeed Envelope

The power-on rotor RPM/airspeed envelope is presented in Figure 5 and represents a summary of test conditions evaluated during the program. The inner boundary line indicates the extent of testing at neutral centers of gravity, whereas the shaded portion indicates the envelope expansion resulting from forward centers of gravity.

At neutral centers of gravity, the boundary line for the lower rpm settings is characterized by a noticeable decrease in rotor damping which results in a feeling of reduced stability to the pilot. The pilots reported that the aircraft felt as though it were undergoing random rough air inputs.

With the high rotor RPM settings at neutral centers of gravity, the boundary line is due primarily to an overall increase in vibration levels and is associated with advancing tip Mach numbers in excess of approximately 0.91.

Shifting the aircraft center of gravity forward resulted in a significant improvement in handling characteristics and eliminated random rough air motions at high speed. Longitudinal control response and aircraft sensitivity during high speed flight were reduced and resulted in improved handling characteristics, which permitted further expansion of the flight envelope as shown in Figure 5. At low to intermediate rotor RPM settings, the limits of the outer boundary line were established by rotor plane oscillations. This phenomenon is discussed more fully in the section on Rotor Plane Oscillations.

At the highest airspeed flown with forward center of gravity, the maximum available auxiliary thrust was used; in addition, it was necessary for the aircraft to descend to meet the overall power requirements. Above 238 KTAS, the rotor RPM was gradually reduced to delay the effect of advancing tip Mach number on power required, vibration, structural loads, and general handling characteristics.

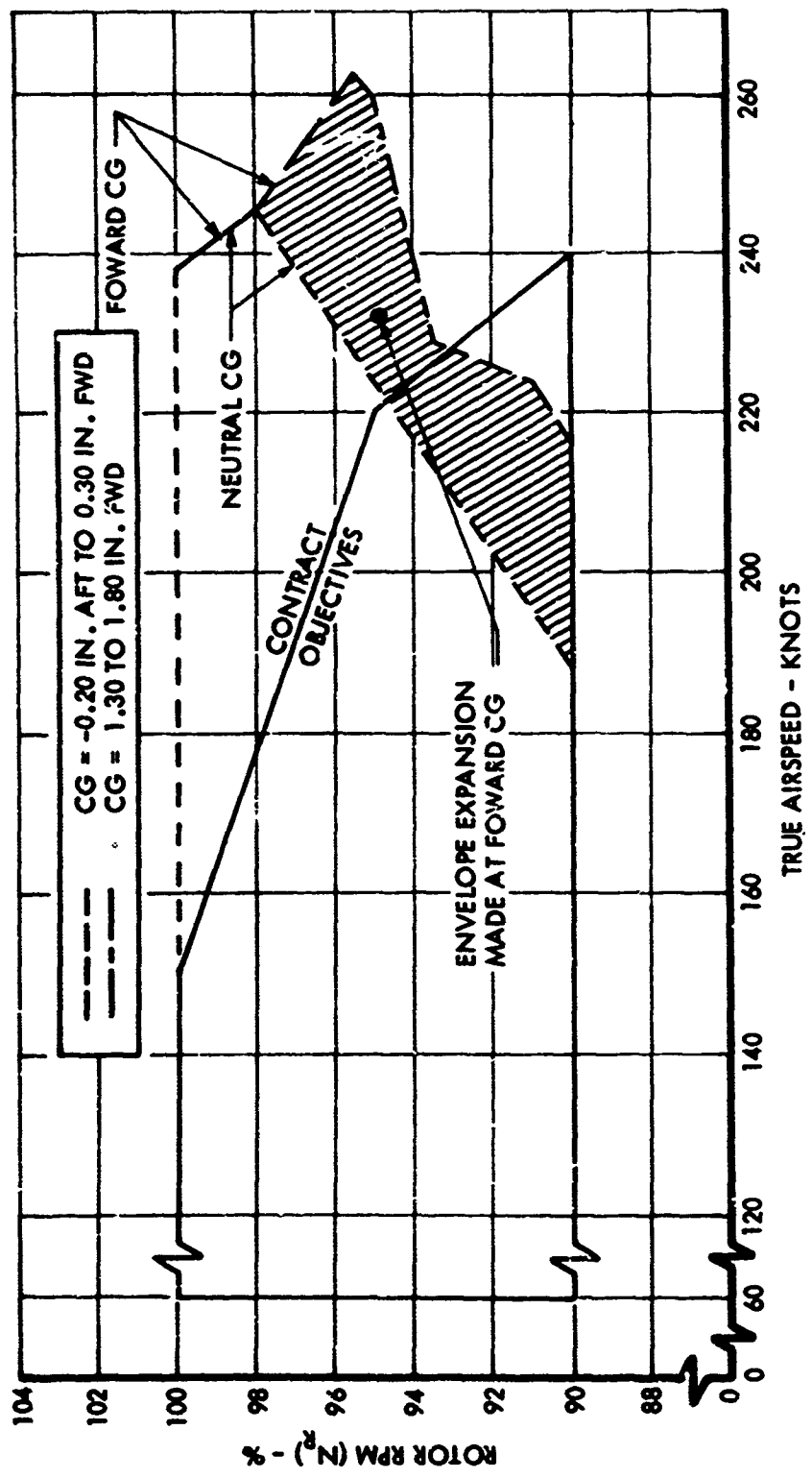


Figure 5. Power-On Rotor RPM Envelope as a Function of True Airspeed.

Ample control margins existed in those areas of the flight envelope where longitudinal system sensitivities of 100, 83 and 66 percent were found to be operationally suitable. The same is also true for lateral system sensitivities of 154 and 200 percent.

Figure 6 presents the collective blade angle/airspeed test envelope and represents an approximate summary of test conditions evaluated during the program at neutral and forward centers of gravity. This envelope covers an operational rotor speed range from 90 to 100 percent RPM.

The preceding discussion provides a general view of test conditions experienced during the program. Details of the conditions encountered during each phase of testing are described in subsequent sections of this report.

Maximum Airspeeds

The maximum true airspeed attained during this program was 262.7 knots (302.6 mph). Because of thrust limitations of the auxiliary engine, this speed was reached in a shallow descent of approximately 800 to 1000 feet per minute. With the rotor operating at 95.5 percent RPM, the advancing tip Mach number was 0.942 with a tip speed ratio of 0.716. The aircraft was flown with the center of gravity approximately 1.5 inches forward of the rotor mast with an 83 percent longitudinal system sensitivity. The forward center of gravity provided a near-constant level of stability with increasing airspeed. This effect enabled the maximum true airspeed to be extended approximately 20 knots beyond the maximum speed attained with a neutral center of gravity.

A maximum true airspeed of 223.5 knots was obtained with a forward center of gravity and 91 percent rotor speed. Under this condition, the tip speed ratio is 0.638 and the advancing tip Mach number is 0.860.

With a neutral center of gravity, a maximum true airspeed of 245 knots (282 mph) was attained. The aircraft was in a slight climb at this speed with the rotor operating at 98 percent RPM. The advancing tip Mach number was 0.937 with a tip speed ratio of 0.650. At 91 percent rotor speed the maximum true airspeed attained was 194.5 knots, resulting in a tip speed ratio of 0.556 and an advancing tip Mach number of 0.838.

The preceding information presented in this section is summarized in Table II.

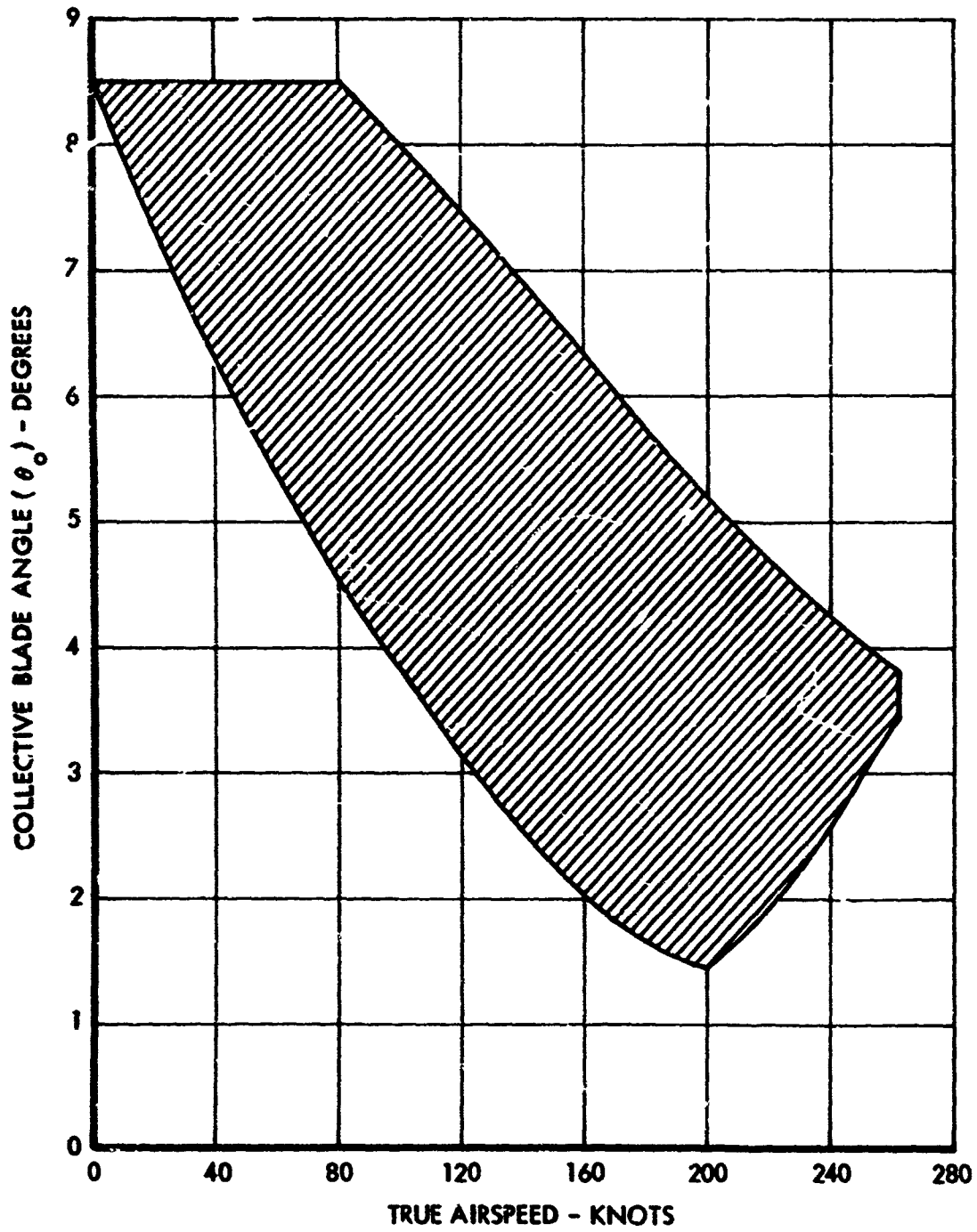


Figure 6. Approximate Collective Blade Angle Test Envelope as a Function of True Airspeed.

TABLE II. SUMMARY OF MAXIMUM AIRSPEED CONDITIONS				
KTAS	MACH NO.	μ	$N_R - \%$	CG
262.7	.942	.716	95.5	Fwd
223.5	.860	.638	91.0	Fwd
245.0	.937	.650	98.0	Neutral
194.5	.838	.556	91.0	Neutral

Data obtained at both forward and neutral centers of gravity in high-speed flight above 200 knots indicate a slight decrease in the margin of static longitudinal stability, even though the overall handling characteristics of the aircraft are significantly better at forward centers of gravity.

The pilots reported a slight decrease in static longitudinal stability and an increase in sensitivity of the longitudinal control as flight speeds exceeded approximately 200 knots. This was particularly true for the neutral center of gravity position. However, a shift of the center of gravity to the 1.5-inch forward location tended to compensate for these characteristics at the higher speeds. A rapid increase in 1P and 4P vibration was noted as the maximum airspeeds were approached. Pilot observations indicated a slightly lower level of 4P vibration with the forward center of gravity.

Maneuvering Envelope

As shown in Figure 7, the maneuvering envelope was expanded well above the proposed target maneuvering envelope. These load factors are referenced to the design gross weight of 4500 pounds. Modifications made during previous programs along with those required prior to starting this program resulted in a takeoff weight increase to 5275 pounds, 775 pounds above the design value of 4500 pounds. To be consistent with results previously reported for the 4500-pound aircraft, the load factors presented in Figure 7 for the test envelope are those attained in flight multiplied by the actual weight at the test condition/4500. The maximum load factor of 2.81g was obtained at 225 KTAS. The minimum load factor of -0.025g was obtained at 150 KTAS. The forward speed was expanded to 262.7 KTAS (234.0 KEAS). The high load factor points at speeds below 220 KTAS were obtained with a rotor RPM of 100 percent. The points at maximum speed were with a rotor RPM of 95.5 percent.

Tables III and IV summarize the boundaries of the flight envelope investigated during the program and the goals which were achieved at neutral and forward centers of gravity, respectively.

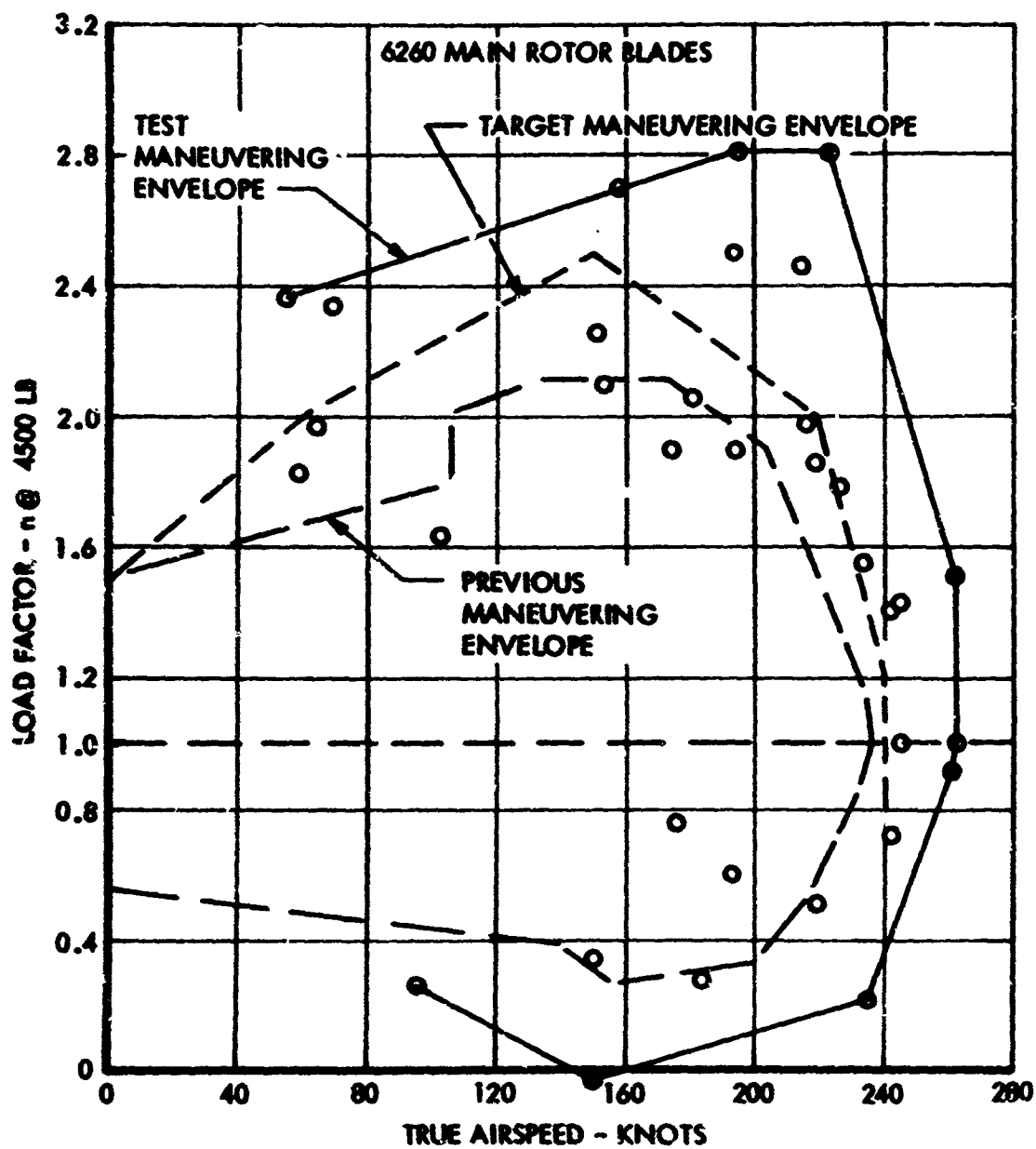


Figure 7. Maneuvering Envelope - Referenced to Design Gross Weight of 4500 Pounds.

TABLE III. SUMMARY OF TEST CONDITIONS - NEUTRAL CG

Maximum equivalent airspeed @ 98% N_R	221.5 knots
Maximum true airspeed @ 98% N_R	245 knots
Auxiliary thrust required @ max TAS	1950 lb *
Engine power required @ max TAS	245 SHP
Test pressure altitude @ max TAS	5160 ft
Test density altitude @ max TAS	6700 ft
Maximum equivalent airspeed @ 91% N_R	174 knots
Maximum true airspeed @ 91% N_R	194.5 knots
Maximum takeoff gross weight flown	5165 lb
Maximum and minimum load factors corrected to the design gross weight of 4500 lb	2.81g @ 195 KTAS 2.70g @ 158 KTAS 2.46g @ 215 KTAS 2.34g @ 70 KTAS 1.43g @ 245 KTAS 0.72g @ 242 KTAS 0.22g @ 235 KTAS
Maximum autorotation entry speed	212 KTAS
Lowest collective blade angle evaluated	1.45° θ_0
* Maximum available auxiliary thrust for the test conditions	

TABLE IV. SUMMARY OF TEST CONDITIONS - FORWARD CG

Maximum equivalent airspeed @ 95.5% N_R	234 knots
Maximum true airspeed @ 95.5% N_R	262.7 knots
Auxiliary thrust required @ max TAS	1880 lb *
Engine power required @ max TAS	250 SHP
Test pressure altitude @ max TAS	5550 ft
Test density altitude @ max TAS	7750 ft
Maximum equivalent airspeed @ 91% N_R	220.5 knots
Maximum true airspeed @ 91% N_R	223.5 knots
Maximum takeoff gross weight flown	5275 lb
Maximum and minimum load factors corrected to the design gross weight of 4500 pounds	2.81g @ 225 KTAS 2.51g @ 193 KTAS 2.37g @ 55 KTAS 2.26g @ 150 KTAS 1.51g @ 262 KTAS 0.91g @ 261 KTAS 0.59g @ 193 KTAS -0.025g @ 150 KTAS
Maximum autorotation entry speed	232 KTAS
Lowest collective blade angle evaluated	3.50° θ_0
* Maximum available auxiliary thrust for the test conditions	

CONTROL RESPONSE AND SHORT PERIOD DAMPING

Longitudinal Control Response

Longitudinal control response as defined by the steady-state angular pitch rate per inch of longitudinal cyclic control input, was evaluated over the airspeed envelope as a function of both rotor RPM and longitudinal system sensitivity.

Figures 8 and 9 indicate that longitudinal control response is relatively unaffected by changes in rotor RPM and collective blade angle. However, as summarized in Figure 10, longitudinal control response varies directly with both airspeed and system sensitivity.

As reported in Reference 1, aircraft longitudinal response becomes increasingly sensitive to pilot inputs at high forward speeds. To determine whether a simple change in the longitudinal system sensitivity* would be effective in controlling this characteristic without adversely affecting other control aspects, the control system geometry was modified so that additional system sensitivities of 83 and 66 percent of nominal could be examined. The longitudinal system sensitivity is decreased between the hydraulic booster and the rotor system and thus does not change the total available stick travel in the longitudinal axis. Therefore, larger control motions are required to produce a given pitch rate as the longitudinal system sensitivity is decreased.

Changing the system sensitivity had no significant effect on the vehicle's initial response characteristics to a step input. It takes approximately 0.25 second for the aircraft to respond to a longitudinal step input at all system sensitivities.

With a system sensitivity of 83 percent at neutral center of gravity, control response is comfortable at speeds up to about 180 KTAS. At higher speeds, however, aircraft longitudinal response is considered to be excessive when cyclic inputs are made unless special piloting precautions are observed. This is due not only to the increased control response but also to the fact that load factor varies as the product of pitch rate and airspeed and magnifies the apparent response of the helicopter.

The longitudinal system sensitivity was further reduced to 66 percent to determine how much this would improve the high-speed handling characteristics. These results are also shown in Figure 10. As expected, this resulted in a reduction in control response and increased the optimum

* Mechanical changes in the control system are referred to as system sensitivity changes throughout this report.

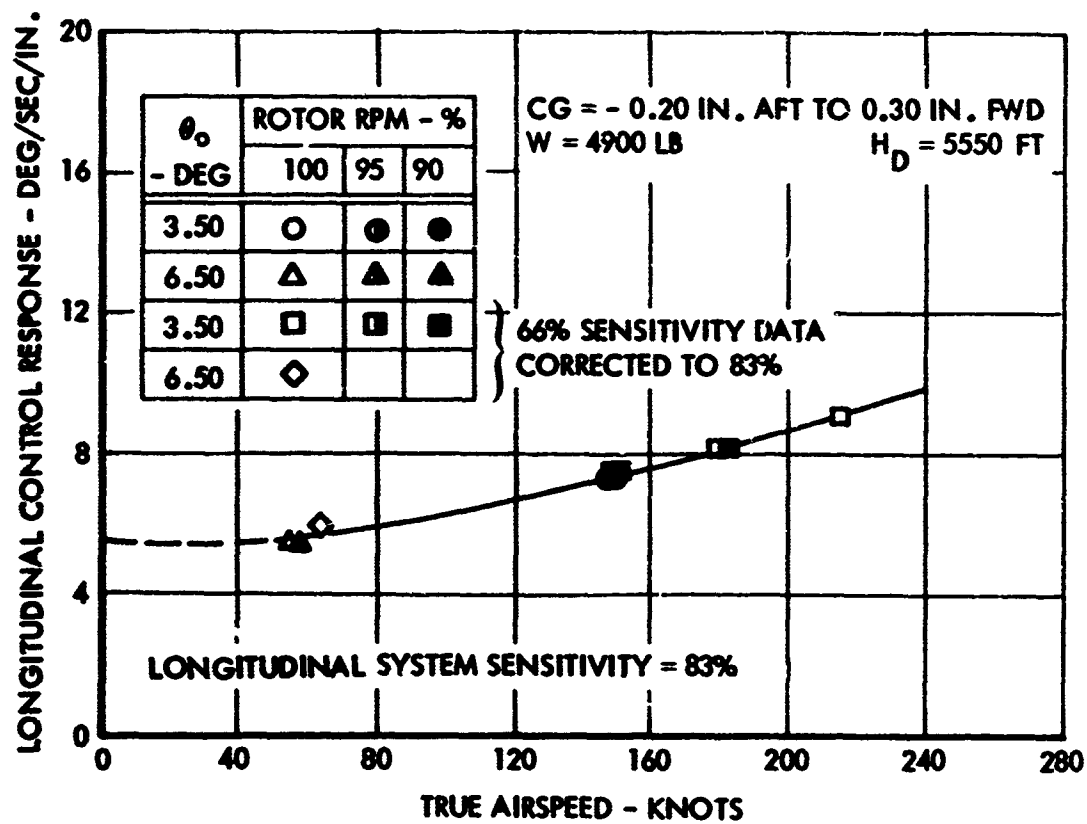


Figure 8. Longitudinal Control Response as a Function of True Airspeed - Effect of Rotor RPM - Neutral CG.

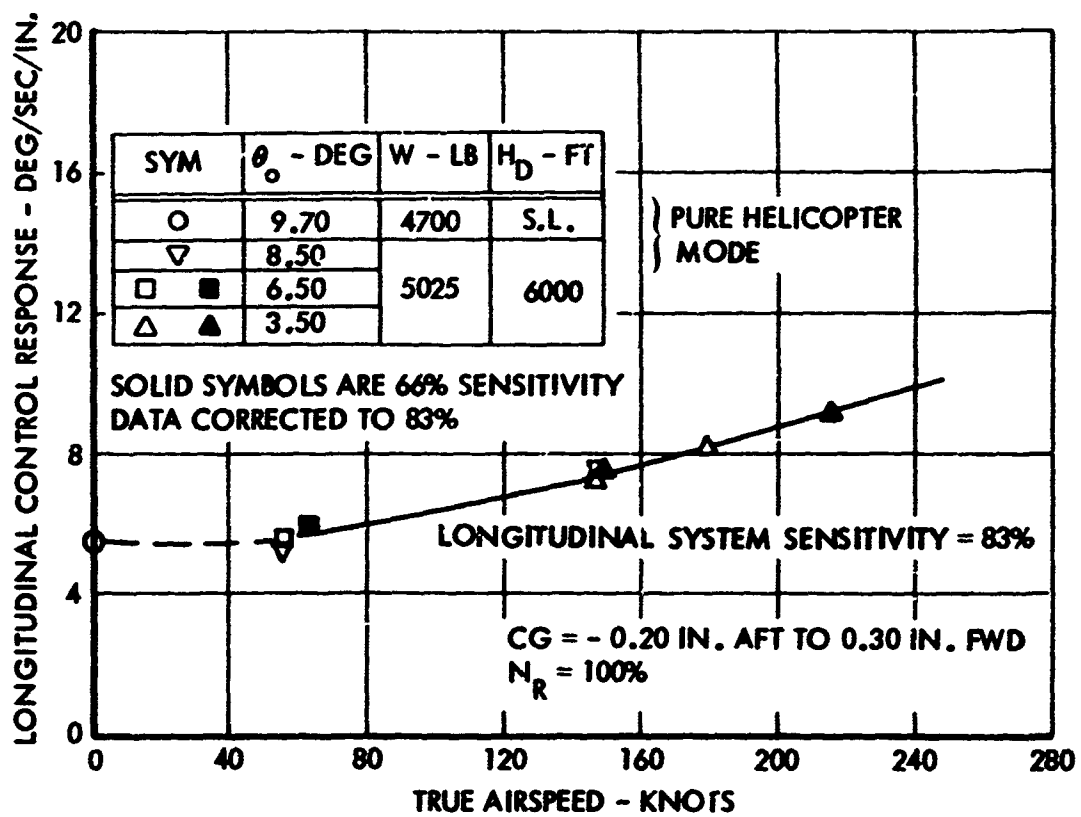


Figure 9. Longitudinal Control Response as a Function of True Airspeed - Effect of Collective Blade Angle - Neutral CG.

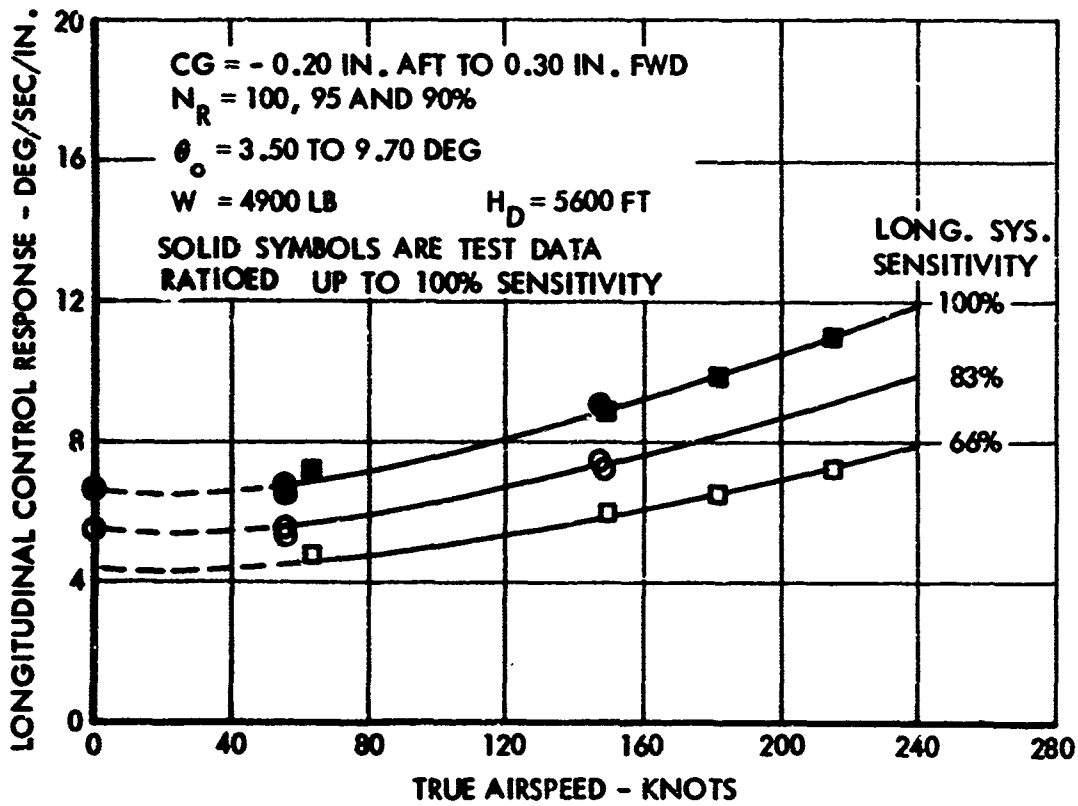


Figure 10. Longitudinal Control Response as a Function of True Airspeed - Effect of Longitudinal System Sensitivity - Neutral CG.

speed range to approximately 200 to 235 KTAS. At true airspeeds less than 200 knots, this reduction in system sensitivity requires larger control inputs to maneuver the helicopter with attendant higher-than-desired control forces. At speeds beyond 235 KTAS, longitudinal aircraft response is still above the desired level.

In view of these results, it is felt that simple changes in the control system geometry aid in handling the high-speed longitudinal response problem. It is also clear that a single longitudinal system sensitivity is probably not adequate for all speeds throughout the flight envelope.

A further attempt was made to lower the high-speed longitudinal response by evaluating the effect of shifting the aircraft center of gravity forward. This change was quite successful in that the overall longitudinal response was significantly reduced at the higher airspeeds. The aircraft was flown with a 100 percent system sensitivity, and the results are shown in Figure 11. Also included for comparison purposes in Figure 11 are the previous data obtained at a neutral center of gravity, which have been ratioed to a 100 percent system sensitivity. Examination of these two sets of data indicates that the forward center of gravity provides near-constant longitudinal control response with increasing airspeed. This is more desirable than the characteristics at neutral center of gravity, wherein the aircraft becomes more sensitive with increasing airspeed and requires additional desensitizing of the longitudinal cyclic control. Comparison of Figures 10 and 11 indicates that with a forward center of gravity at 200 KTAS, the steady-state pitch rate is almost the same with 100 percent system sensitivity as it is with 66 percent sensitivity at neutral center of gravity.

The improvement in handling characteristics was quite evident, since higher airspeeds were attained with the 100 percent system sensitivity at forward center of gravity than were possible with the 66 percent system sensitivity at neutral center of gravity. A further optimization of the high-speed handling characteristics was obtained by using the 83 percent system sensitivity, which permitted speed extension to 262.7 KTAS. It is evident that center of gravity location is an important consideration with regard to the longitudinal handling and response characteristics of high-speed helicopters.

Longitudinal Short-Period Damping

Pulse inputs were conducted to evaluate longitudinal short-period damping characteristics over the airspeed envelope at a neutral center of gravity. Figures 12 and 13 present the results obtained above 220 KTAS at 100 percent rotor speed with system sensitivities of 83 and 66 percent, respectively. Examination of these data indicates that the short period disturbance is well damped, requiring less than one-half cycle to damp. As expected, system sensitivity appears to have little or no effect on longitudinal short-period damping.

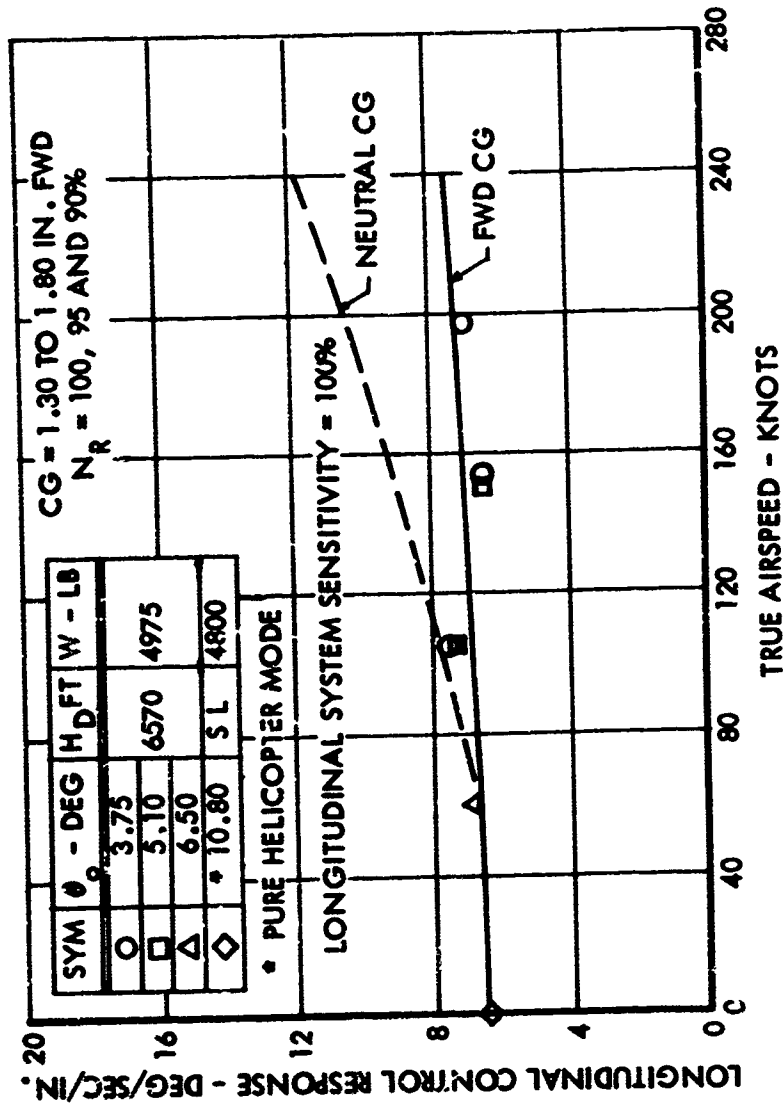


Figure 11. Longitudinal Control Response as a Function of True Airspeed - Effect of CG Location.

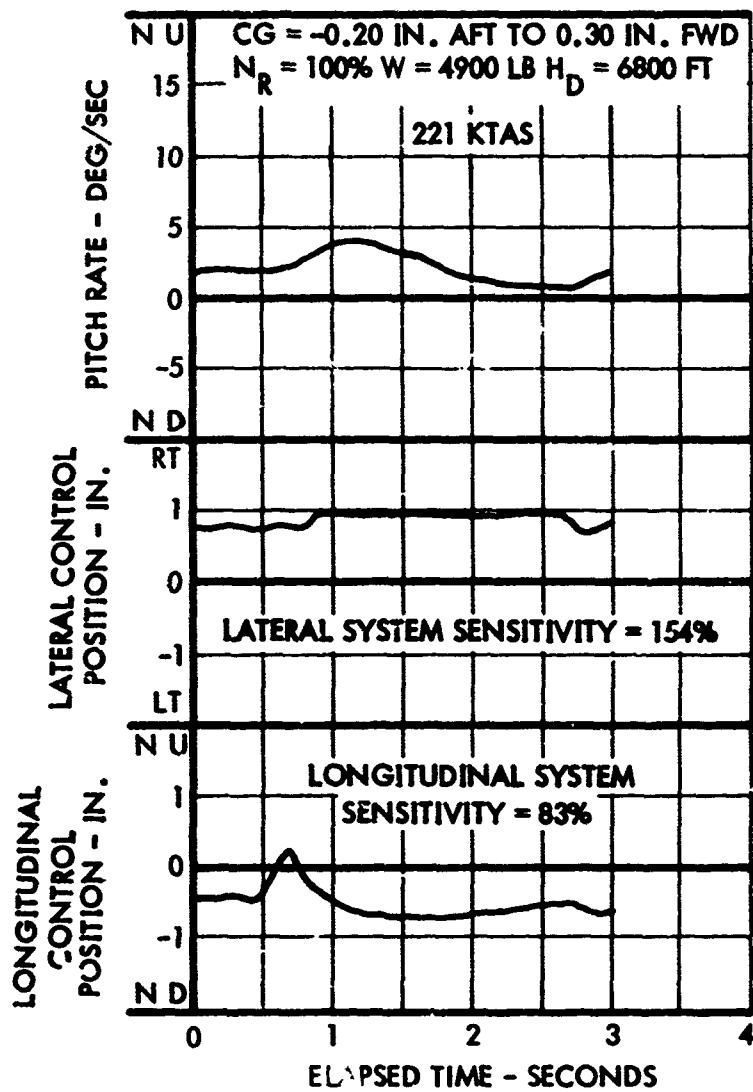


Figure 12. Time History of Longitudinal Short-Period Damping - 83% Longitudinal System Sensitivity - Neutral CG.

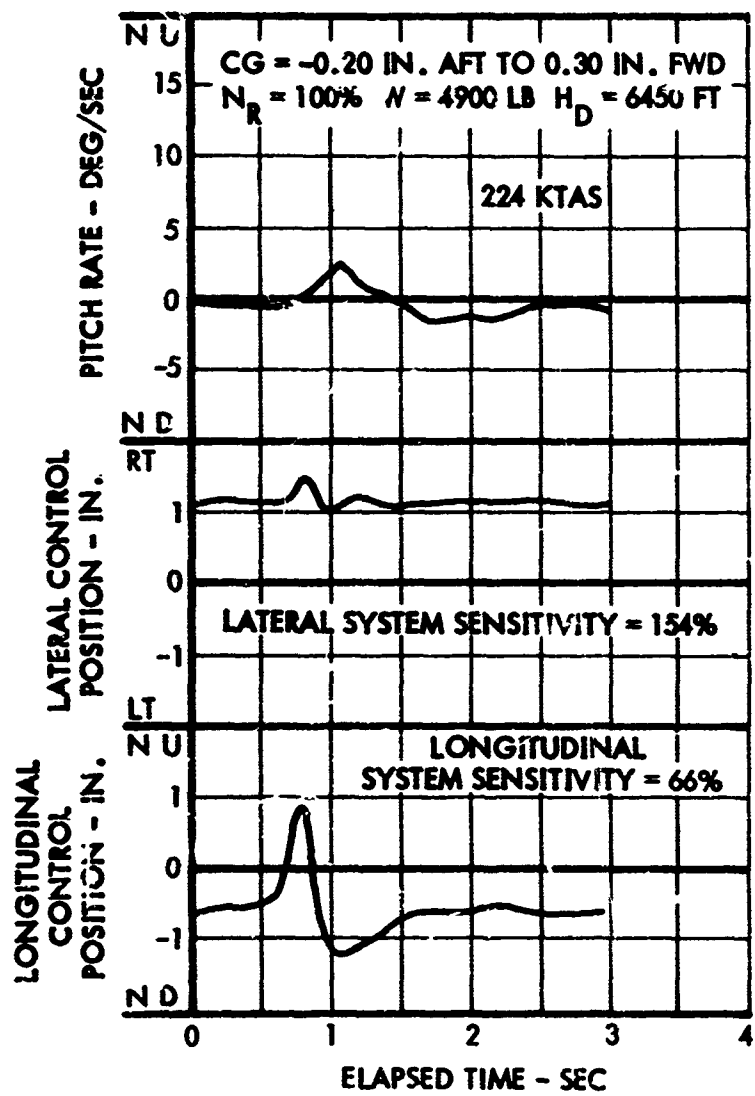


Figure 13. Time History of Longitudinal Short-Period Damping -- 66% Longitudinal System Sensitivity - Neutral CG.

Figures 14 and 15 present short-period damping at rotor speeds of 100 and 91.5 percent. These data were obtained at a true airspeed of 150 knots and indicate that rotor RPM has little or no effect on short-period damping. The same type of results was obtained at other airspeeds with variations in rotor RPM.

Pilot observations of these characteristics confirmed the strong damping in the longitudinal axis. Qualitative evaluations conducted over the airspeed envelope at forward centers of gravity indicated that the aircraft continued to be well damped in the longitudinal axis.

The results obtained from longitudinal control response and short-period damping evaluations are summarized in Table V.

TABLE V. SUMMARY OF LONGITUDINAL CONTROL RESPONSE AND SHORT-PERIOD DAMPING TEST RESULTS		
Longitudinal Control Response	Neutral CG	<ol style="list-style-type: none"> 1. Varies directly with airspeed 2. Varies directly with system sensitivity 3. Invariant with collective position 4. Invariant with rotor RPM
	Forward CG	<ol style="list-style-type: none"> 1. Nearly invariant with airspeed 2. Varies directly with system sensitivity 3. Invariant with collective position 4. Invariant with rotor RPM
Longitudinal Short-Period Damping	Neutral CG	<ol style="list-style-type: none"> 1. Varies directly with airspeed 2. Invariant with system sensitivity 3. Invariant with collective position 4. Invariant with rotor RPM
	Forward CG	<ol style="list-style-type: none"> 1. Pilot commented that aircraft continued to be well damped

Lateral Control Response

Lateral control response, as defined by the steady-state angular roll rate per inch of lateral cyclic control input, was evaluated over the airspeed envelope as a function of lateral system sensitivity and rotor RPM.

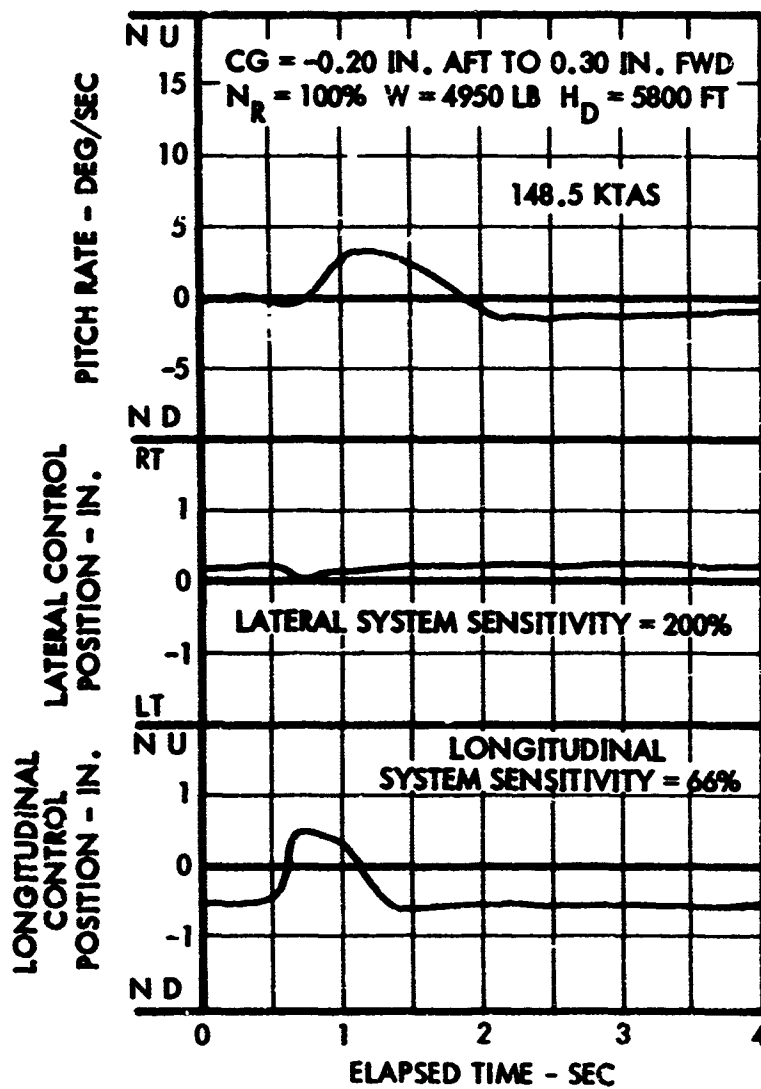


Figure 14. Time History of Longitudinal Short-Period Damping - $N_R = 100\%$ - Neutral CG.

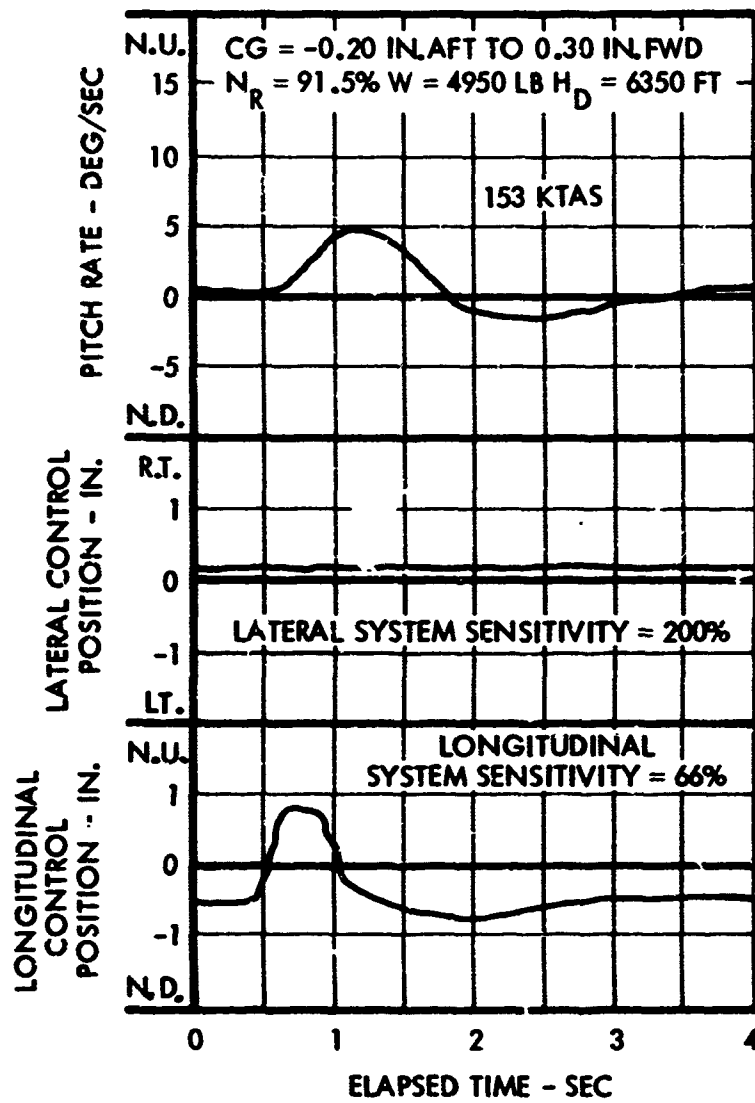


Figure 15. Time History of Longitudinal Short-Period Damping - $N_R = 91.5\%$ - Neutral CG.

As reported in Reference 1, the overall lateral control sensitivity of the aircraft was lower than desirable for maneuverability at high speeds. To determine whether an improvement in the lateral handling characteristics could be obtained without adversely affecting other control aspects, the control system geometry was modified so that system sensitivities of 154 and 200 percent of nominal could be examined. In the lateral control system, the sensitivity is increased between the cyclic control stick and hydraulic booster. This modification reduces the total stick travel in the lateral axis by an amount proportional to the increase in sensitivity. Therefore, smaller control inputs are required to produce a given roll rate as the lateral system sensitivity is increased.

System sensitivity had no significant effect on the vehicle's response characteristics to a step input. It takes approximately 0.15 second for the aircraft to respond to a lateral step input for all system sensitivities.

Figure 16 summarizes the variations of lateral control response with both system sensitivity and airspeed. An increase in system sensitivity from 154 to 200 percent results in approximately a 30 percent higher rate of roll per inch of control input. Lateral control response is relatively constant from 60 to 150 KTAS, but it decreases at an increasing rate above this speed. With a system sensitivity of 200 percent, the lateral control response is 16.5 deg/sec/in. at 150 KTAS and is reduced to 13.5 deg/sec/in. at 220 KTAS. Although the control response decreases with airspeed, an adequate level is available above 250 KTAS. These data were obtained at various collective blade angles with rotor speeds of 100, 95, and 90 percent. The results indicate that lateral control response is relatively unaffected by changes in collective blade angle and rotor RPM.

The pilots reported that lateral control response felt comfortable at the 200 percent system sensitivity. However, control system cross-coupling characteristics were somewhat magnified. With a left roll input, the aircraft pitches nose-down; during a right roll input, a nose-up tendency occurs. Pilot observations indicated that cross-coupling characteristics are more noticeable at the 66 percent longitudinal system sensitivity. While this characteristic is annoying, it is not considered to be of sufficient magnitude to cause any concern.

Lateral Short-Period Damping

Pulse inputs were conducted to evaluate lateral short-period damping characteristics over the airspeed envelope. Figures 17 and 18 present the results obtained at an airspeed of 224 KTAS at 100 percent rotor speed with system sensitivities of 154 and 200 percent, respectively. Examination of these data indicates that the short-period disturbance is well damped and does not degrade the high-speed handling characteristics of the aircraft. System sensitivity has no effect on lateral short-period damping.

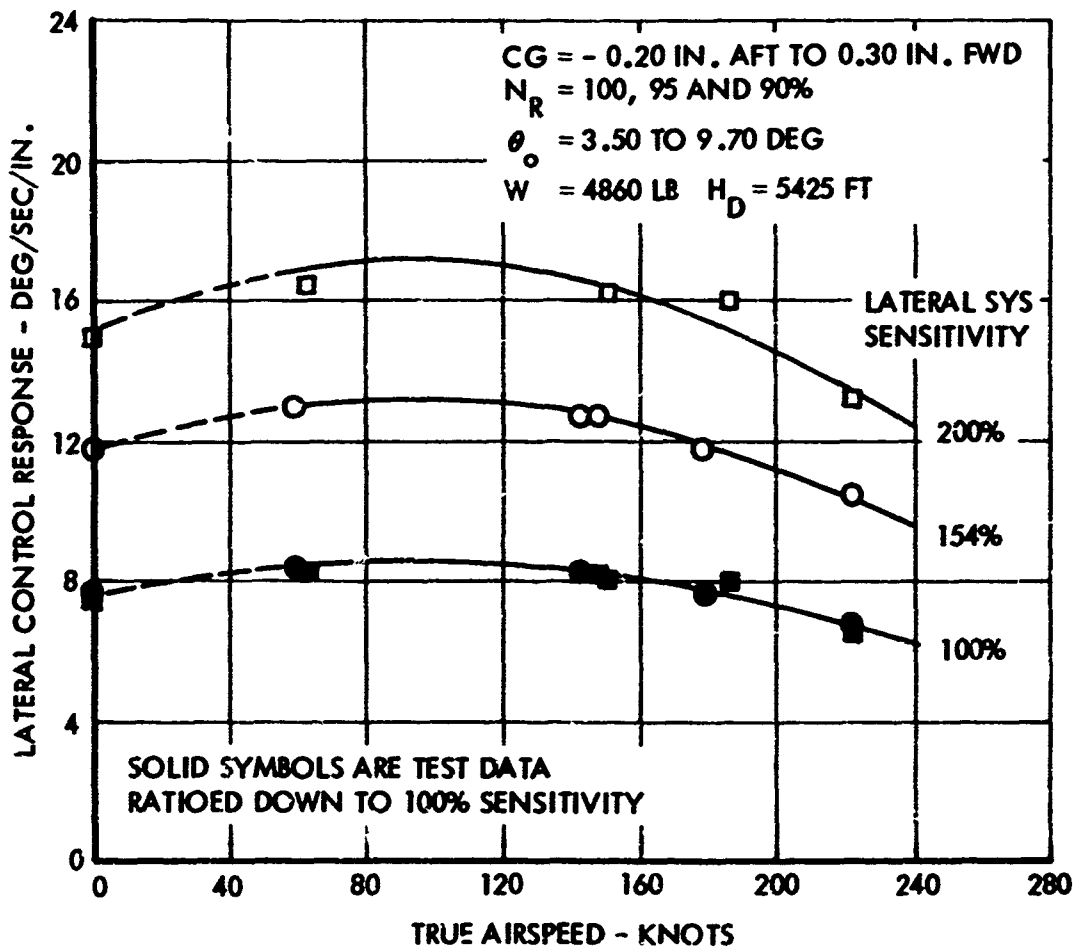


Figure 16. Lateral Control Response as a Function of True Airspeed - Effect of Lateral System Sensitivity - Neutral CG.

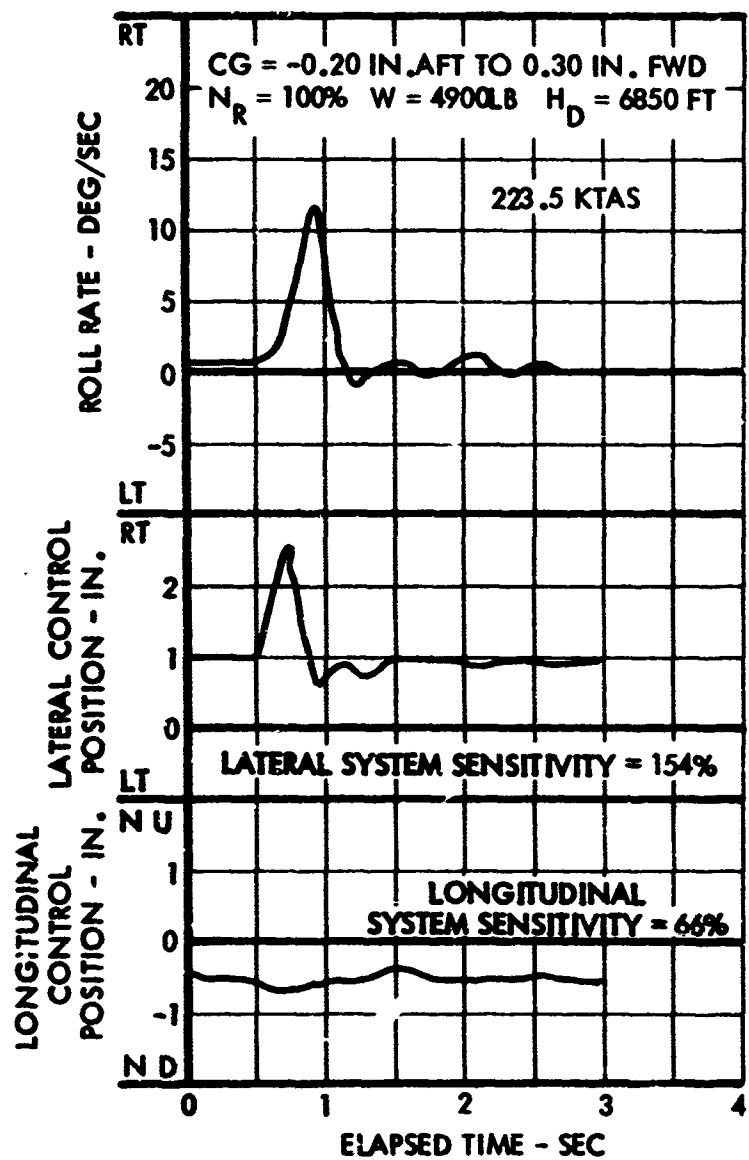


Figure 17. Time History of Lateral Short-Period Damping - 154%
Lateral System Sensitivity - Neutral CG.

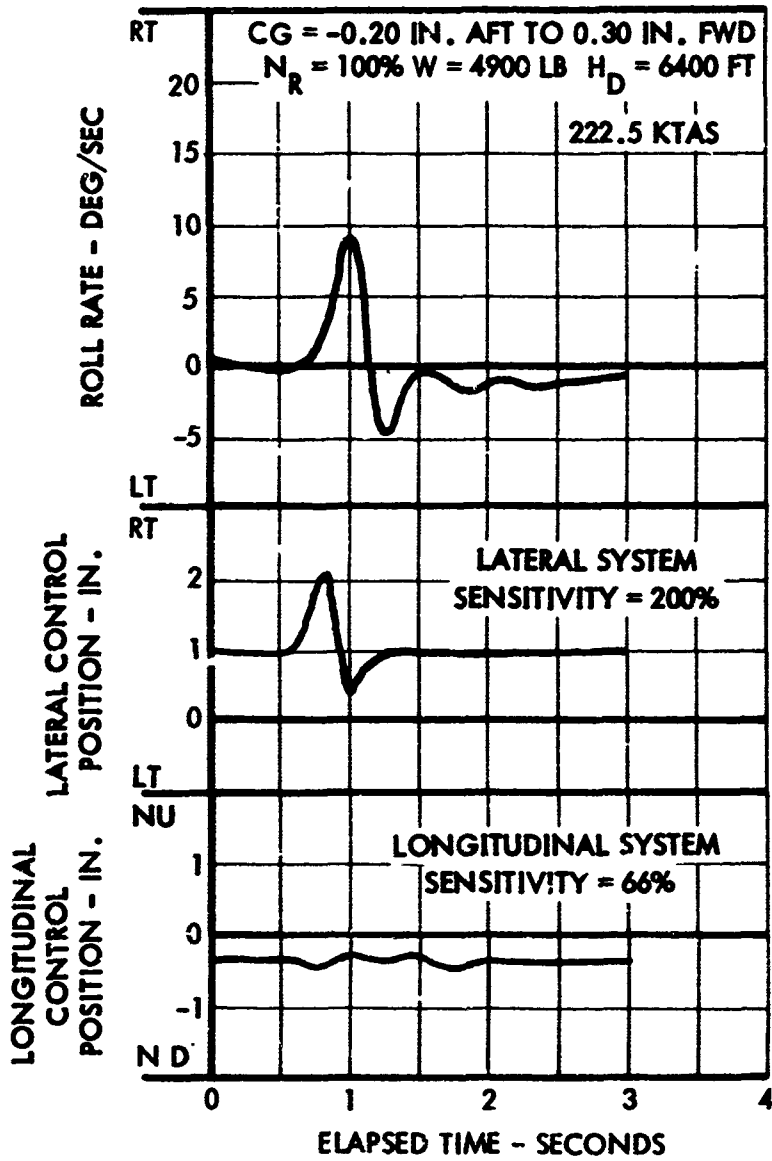


Figure 18. Time History of Lateral Short-Period Damping - 200%
Lateral System Sensitivity - Neutral CG.

Figures 19 and 20 present short-period damping at rotor speeds of 100 and 90 percent. These data were obtained at a nominal true airspeed of 150 knots, and they indicate that as rotor RPM is reduced below 100 percent, there is essentially no degradation in roll damping. The 2.5-cps roll oscillation superimposed on the roll rate trace is simply the body responding at its natural roll frequency. This frequency seems to be independent of rotor RPM.

Pilot observations of these characteristics confirmed the strong damping in roll.

The results obtained from lateral control response and short-period damping evaluations are summarized in Table VI.

TABLE VI. SUMMARY OF LATERAL CONTROL RESPONSE AND SHORT-PERIOD DAMPING TEST RESULTS AT NEUTRAL CG	
Lateral Control Response	<ol style="list-style-type: none"> 1. Invariant with airspeed from 60 to 150 KTAS 2. Decreases at an increasing rate above 150 KTAS 3. Varies directly with system sensitivity 4. Invariant with collective position 5. Invariant with rotor RPM
Lateral Short-Period Damping	<ol style="list-style-type: none"> 1. Invariant with system sensitivity 2. Invariant with airspeed 3. Invariant with rotor RPM

MANEUVERING STABILITY

Turning Flight

Maneuvering stability during steady turns, in terms of the longitudinal cyclic control force required to produce normal load factors, was measured by entering a steady descending turn from a trimmed, level-flight condition for a given collective blade angle and rotor RPM setting. J-60 engine thrust was maintained at the trim setting, and the radius of turn was decreased to produce the desired g level. This is a conventional technique which provides a method for obtaining reliable and repeatable data

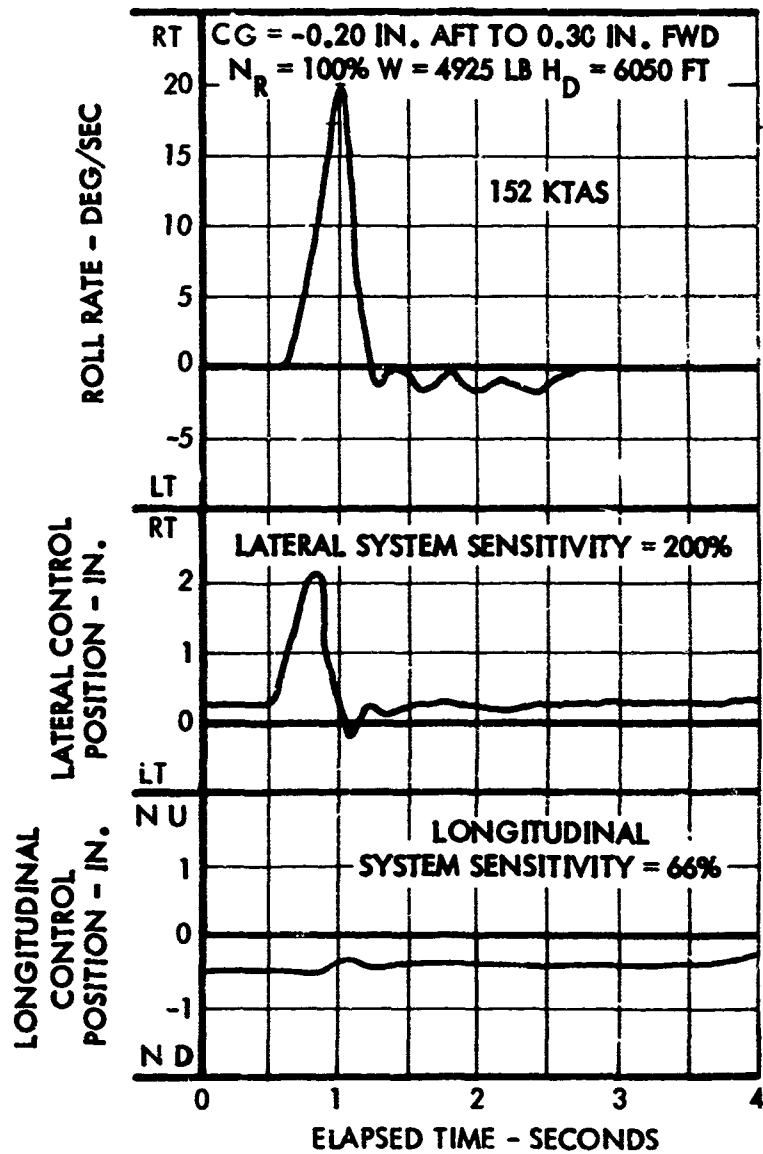


Figure 19. Time History of Lateral Short-Period Damping - $N_R = 100\%$ - Neutral CG.

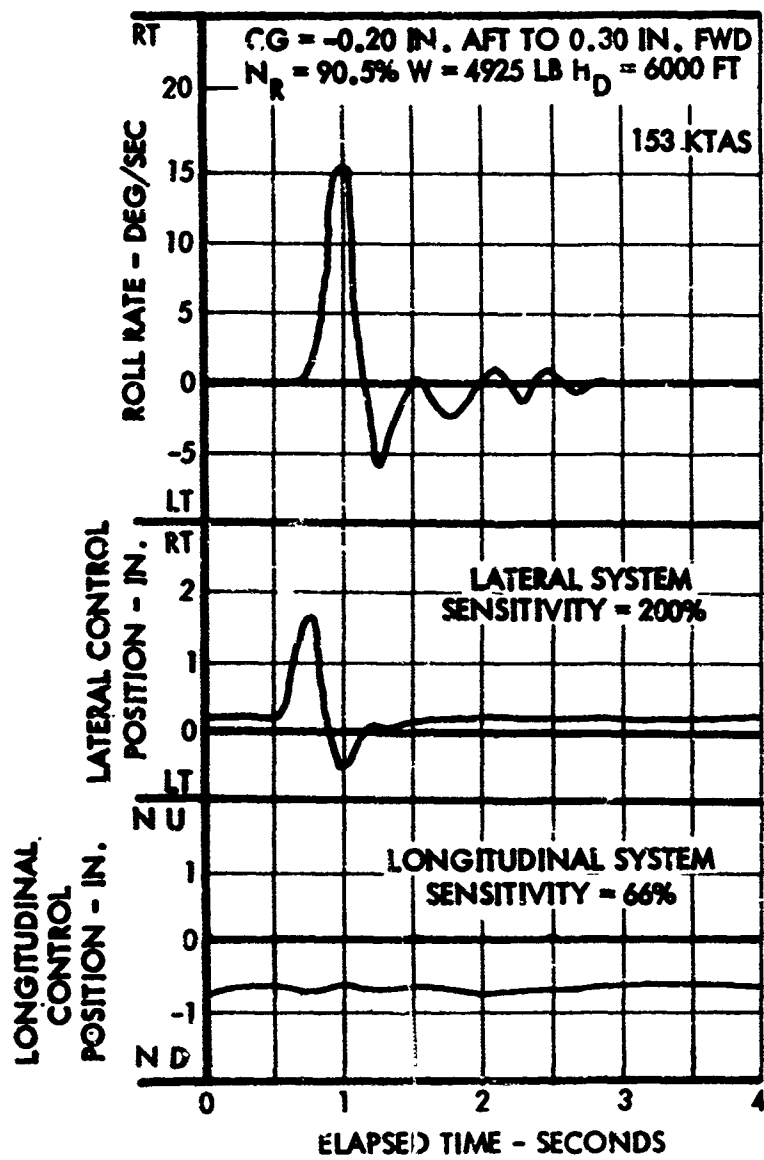


Figure 20. Time History of Lateral Short-Period Damping -
N_R = 90.5% - Neutral CG.

The results of these tests are summarized in Figures 21 and 22 as a function of airspeed for various collective blade angles and rotor speeds. The maneuvering force gradient is unaffected by the initial rotor RPM setting over the airspeed envelope. This means that the stick force required to obtain a particular load factor for a given set of test conditions does not vary due to changes in the initial rotor RPM setting.

Although rotor RPM does not affect maneuvering stability, the maximum load factor attainable in turning flight can be limited by a rotor overspeed condition. Test results indicate that the rotor can go into autorotation at various combinations of airspeed, collective blade angle, initial rotor RPM, and load factor. If an upper power-off RPM limit is observed, there is a maximum load factor for a given set of test conditions. A more complete discussion of such effects is included in a subsequent section of this report.

The pilots reported that once they became aware of this overspeed condition, it was quite easy to control rotor RPM by easing off on load factor to avoid exceeding the upper RPM limit.

Reference to Figure 21 indicates that for a given collective blade angle, the stick force per g remains positive over the airspeed envelope but decreases with both increasing airspeed and load factor. Maneuvering stability is also decreased by increasing the collective blade angle setting at a given airspeed.

Although the force gradient becomes lighter with airspeed for a given load factor and collective blade angle, the preceding data indicate that an adequate level of maneuvering stability exists within the entire operational blade angle and airspeed envelope.

The effect of varying longitudinal system sensitivity on maneuvering stability in turning flight is shown in Figure 22 over a true airspeed range of 55 to 220 knots. The maneuvering force gradient increases as the longitudinal system sensitivity is decreased. Desensitization of the longitudinal control requires larger stick deflections to produce the pitch rate required to obtain a given load factor. In turn, the increase in stick displacement provides an additional force contribution from the longitudinal feel spring and results in an overall increase in the level of maneuvering stability. At a system sensitivity of 83 percent, maneuvering stability varies from 41.5 lb/g at 55 KTAS to 16.5 lb/g at 220 KTAS for a load factor of 1.50g. A decrease in system sensitivity to 66 percent results in a maneuvering force gradient of 19.0 lb/g at a load factor of 1.50g at a speed of 220 KTAS.

The pilots reported that with a 66-percent system sensitivity, the maneuvering force gradient and response of the helicopter feel best at speeds in excess of 200 KTAS. Below this airspeed, the stick forces are considered to be excessive if held for any length of time. However, stabilizing at any test point was accomplished without difficulty.

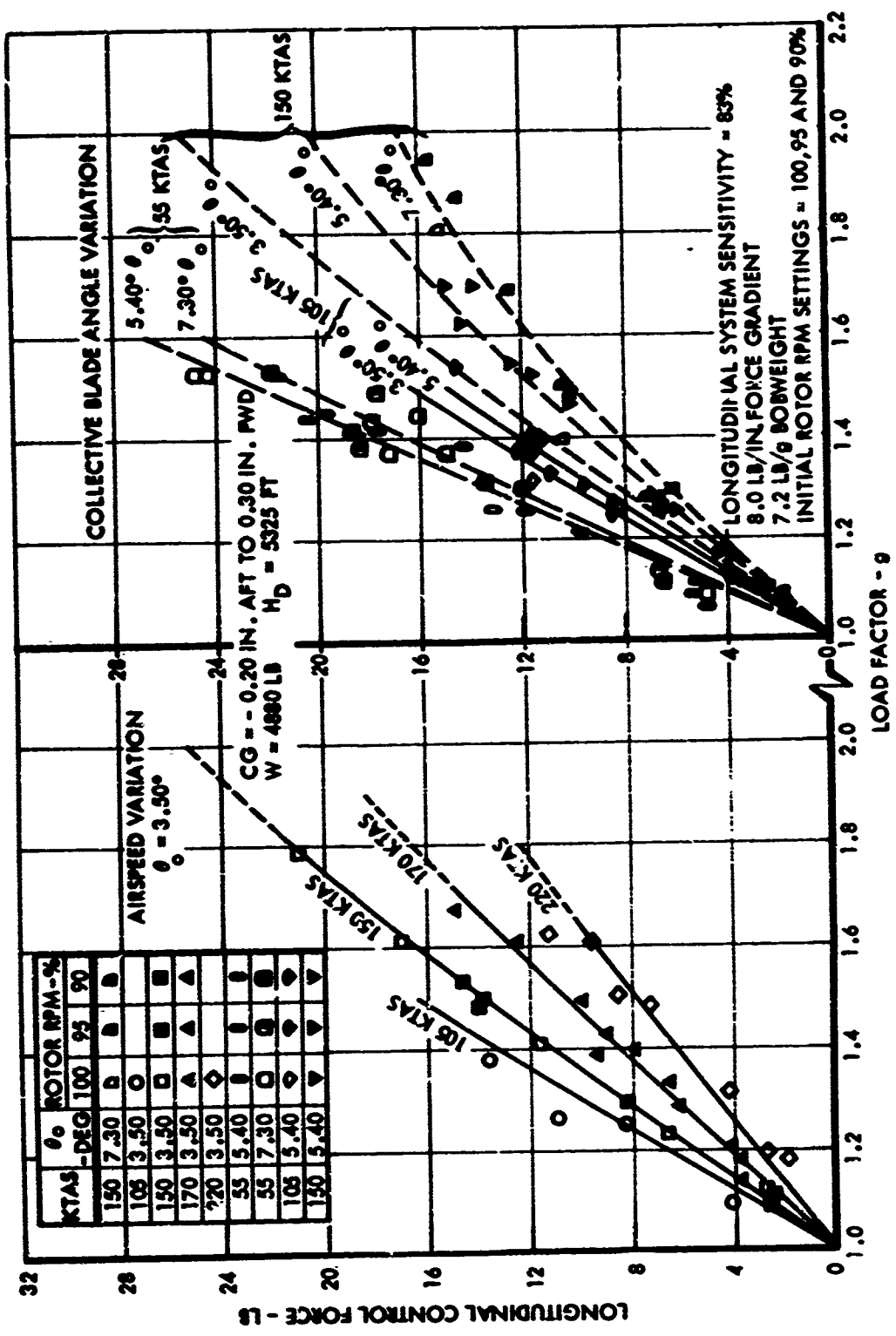


Figure 21. Maneuvering Stability During Steady Turns as a Function of True Airspeed for Various Collective Blade Angles and Rotor RPM Settings - Neutral CG.

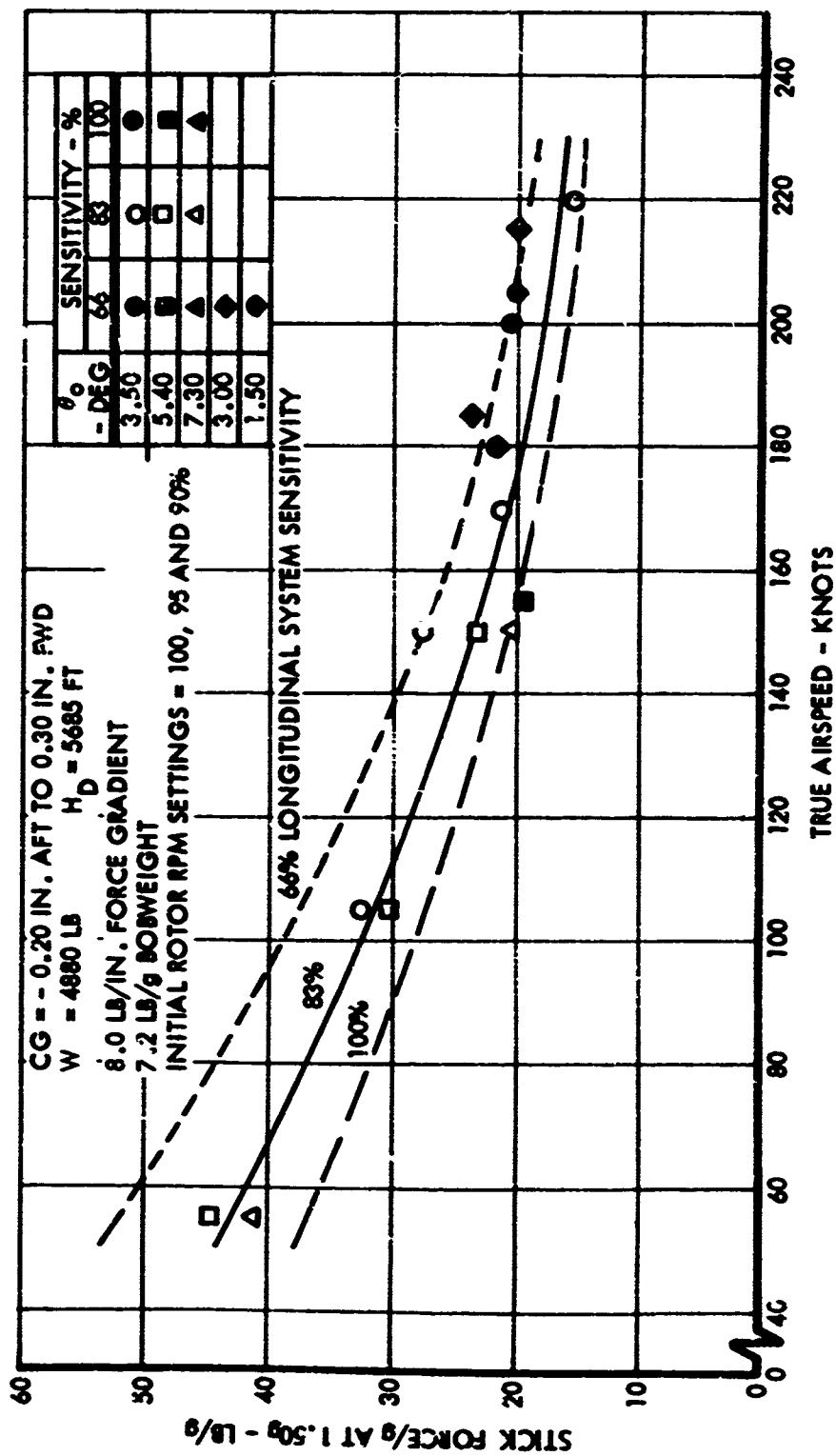


Figure 22. Variation of Maneuvering Stability with True Airspeed During Steady Turns - Effect of Longitudinal System Sensitivity - Neutral CG.

All turning flight maneuvering stability testing was conducted at neutral center of gravity.

The preceding test results indicate that speed and load factor have less effect on the maneuvering capability of the XH-51A compound helicopter operating in the compound mode than in the pure helicopter mode, or than on a conventional XH-51A helicopter (see References 1 and 2).

Symmetrical Pull-ups

Maneuvering stability during symmetrical pull-ups, in terms of the longitudinal cyclic control force required to produce normal load factors, was measured by trimming at the test altitude and airspeed for a given collective blade angle and initial rotor RPM. The aircraft was pulled up to a higher altitude, thus allowing airspeed to bleed off. This was followed by pushing over to the trim airspeed and initiating a constant load factor pull-up, trying to hit the target load factor when level at the trim altitude. This technique permits more consistent results by eliminating much of the dynamics of the maneuver and by allowing the pilot a longer time period to stabilize. Moreover, recovery from the maneuver was simplified because of the near-level attitude of the aircraft at the test altitude and target load factor.

The results of these tests are shown in Figures 23 and 24 for neutral and forward centers of gravity, respectively. As in the case for turning flight, maneuvering stability is unaffected by the initial rotor RPM setting and decreases with both increasing airspeed and collective blade angle. Also, comparison of the data in Figure 23 with the results obtained during steady turns indicates that a lower level of force gradient is achieved in a symmetrical pull-up at the same test conditions. This result was expected, since the higher pitch rate required to produce a given load factor in a turn results in a larger longitudinal cyclic control displacement from trim, thereby producing higher stick forces.

The effect of varying longitudinal system sensitivity on maneuvering stability in symmetrical pull-ups is shown in Figure 25 over a true airspeed range of 55 to 220 knots. The increase in data scatter that occurs during symmetrical pull-up testing has a tendency to mask the effect of changing system sensitivity. However, the majority of testing was performed at neutral center of gravity with a system sensitivity of 83 percent, and this data was used to establish the baseline fairing for calculating the maneuvering stability at system sensitivities of 66 and 100 percent. As the system sensitivity is reduced, larger control motions are required to produce the pitch rate needed to obtain a given load factor. This results in a larger force contribution from the longitudinal feel spring and therefore raises the overall level of maneuvering stability. At a system sensitivity of 83 percent, maneuvering stability varies from 28.0 lb/g at 60 KTAS to 14.5 lb/g at 220 KTAS for neutral center of gravity at a load factor of 1.50g.

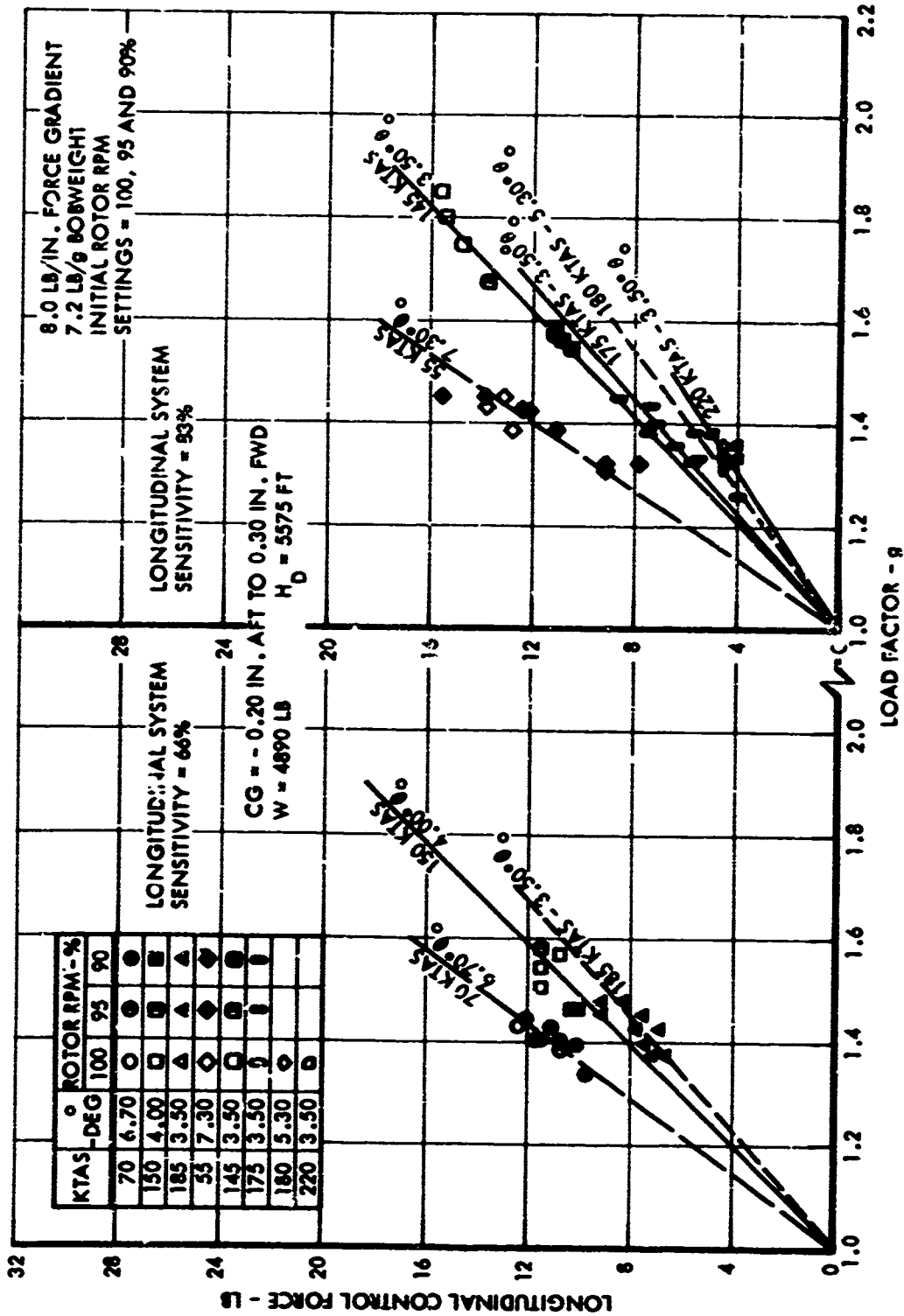


Figure 23. Maneuvering Stability During Symmetrical Pull-Ups as a Function of True Airspeed for Various Collective Blade Angles and Rotor RPM Settings - Neutral CG.

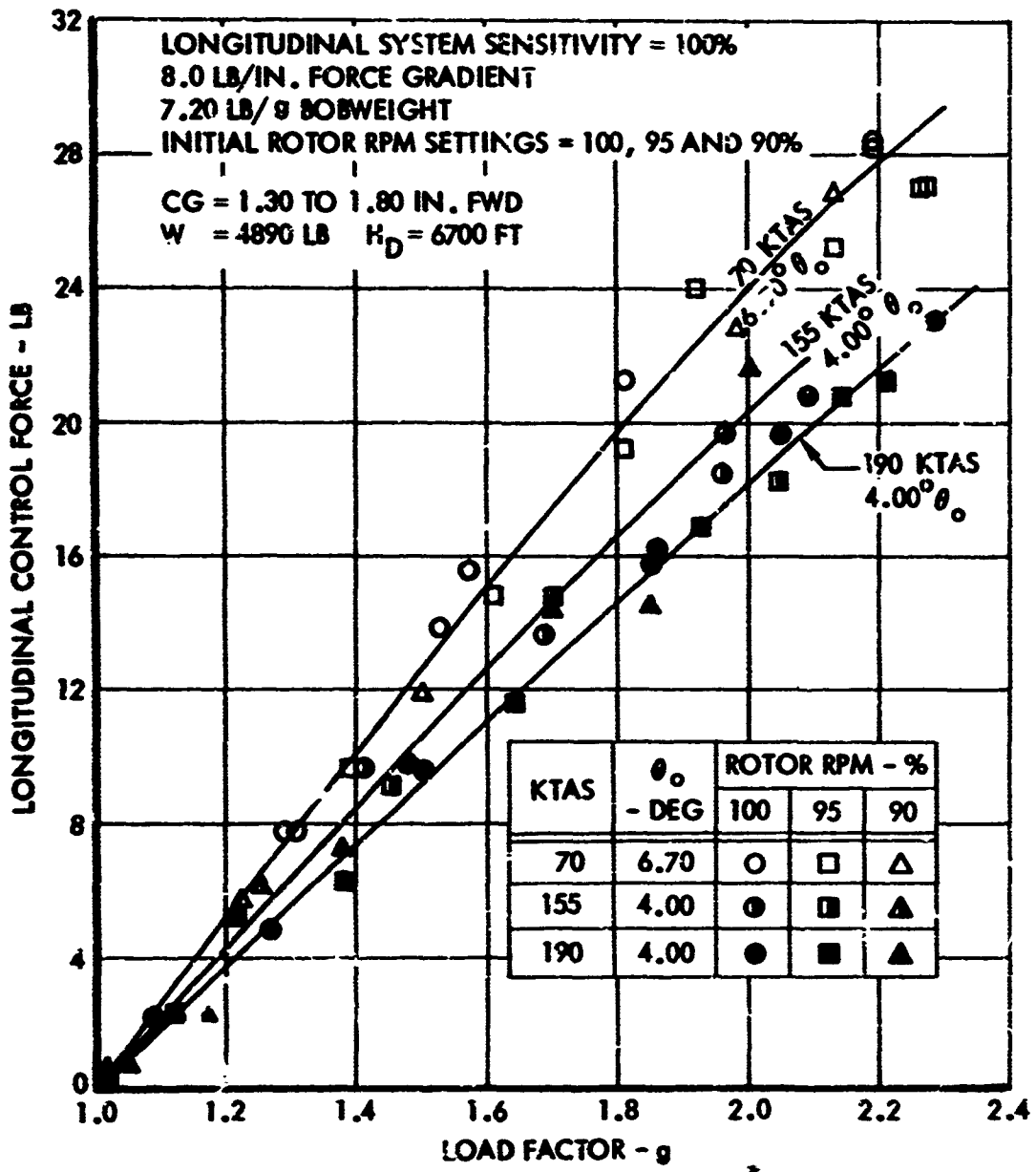


Figure 24. Manuevering Stability During Symmetrical Pull-Ups as a Function of True Airspeed For Various Collective Blade Angles and Rotor RPM Settings - Forward CG.

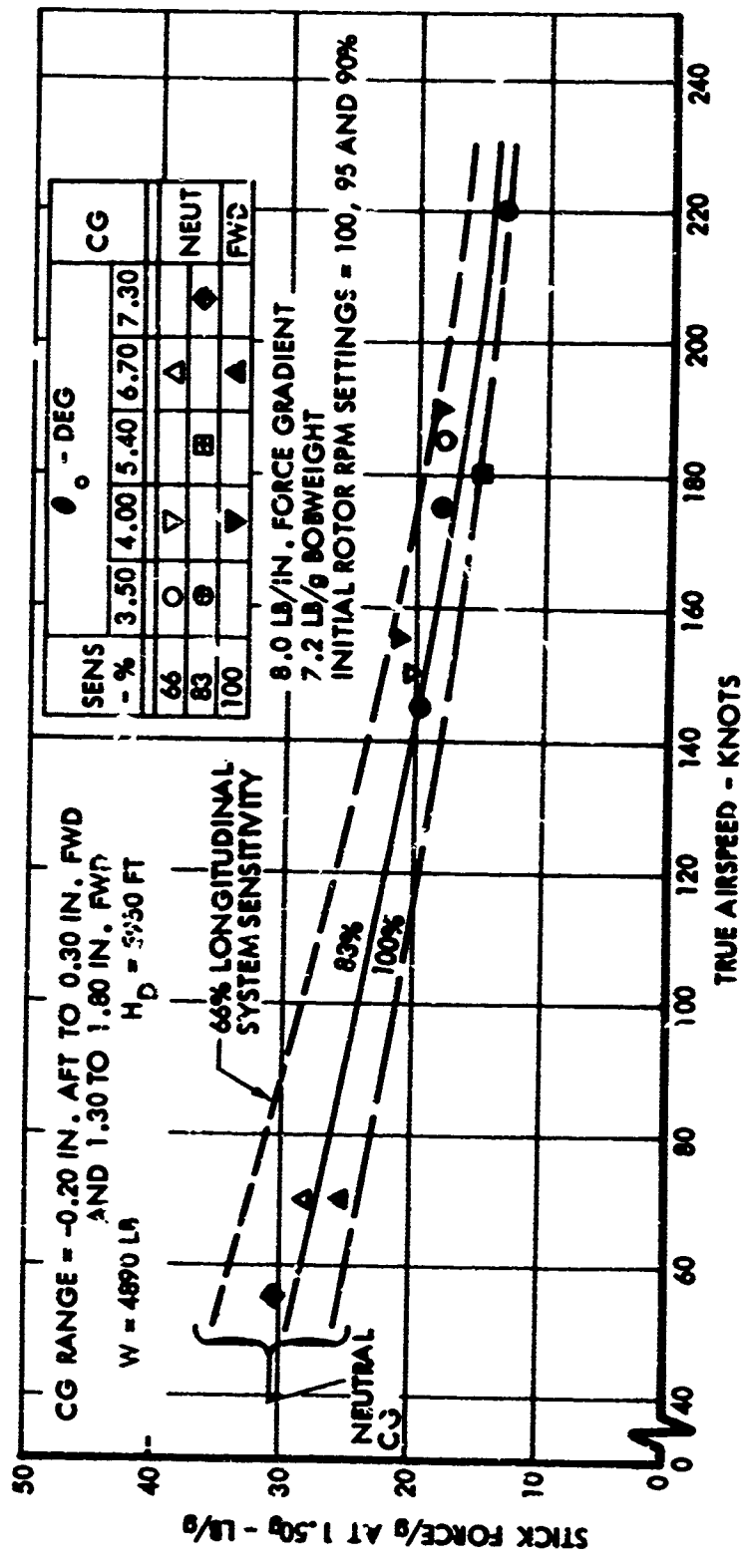


Figure 25. Variation of Maneuvering Stability with True Airspeed During Symmetrical Pull-Ups - Effect of Longitudinal System Sensitivity - Neutral and Forward CG.

Comparison of Figures 22 and 25 again illustrates that the level of maneuvering stability is lower during a symmetrical pull-up than it is in a turn at the same test conditions. This result, as stated previously, is attributable to the fact that a higher pitch rate, hence a larger control deflection, is required to obtain a given load factor in a turn. It follows that the larger control displacement from trim results in higher control forces.

Examination of Figure 25 also indicates that maneuvering stability is higher when the center of gravity is shifted forward. At forward centers of gravity with a system sensitivity of 100 percent the level of maneuvering stability is almost the same as a system sensitivity of 66 percent at a neutral center of gravity. This result is reasonable since the control response at forward centers of gravity is less than that obtained at a neutral center of gravity. Larger control motions are required to generate the pitch rate needed to obtain a given load factor with attendant higher control forces due to the longitudinal feel spring.

Table VII summarizes the results obtained from maneuvering stability testing.

TABLE VII. SUMMARY OF MANEUVERING STABILITY TEST RESULTS
1. Maneuvering stability varies inversely with airspeed
2. Maneuvering stability varies inversely with load factor
3. Maneuvering stability varies inversely with collective position
4. Maneuvering stability varies inversely with longitudinal system sensitivity
5. Maneuvering stability is invariant with the initial rotor RPM setting
6. Maneuvering stability increases as the center of gravity is moved forward

Pilot observations indicate that longitudinal system sensitivity has a noticeable effect on maneuvering stability in that a higher level of maneuvering stability exists with a decreased system sensitivity. The pilots also reported that, except for the 83 percent system sensitivity data points at neutral center of gravity, load factor values were easily anticipated and controlled during symmetrical pull-up maneuvers. At 83 percent system sensitivity and neutral center of gravity, there was a tendency to overshoot high load factor points - because of the higher aircraft response to a given control input - resulting in rotor overspeed.

This would cause the pilot to ease off on the longitudinal control and would give him the feeling of lower maneuvering capability. At forward center of gravity, the aircraft's longitudinal response to a given control input was lower; and this feeling was not encountered with a 100-percent longitudinal system sensitivity.

Rotor RPM Characteristics

During the maneuvering stability testing, it was found that at higher load factors it is possible for the rotor to overspeed as a result of autorotation. The amount of overspeed depends on airspeed, collective blade angle, initial RPM setting, and the type and severity of the maneuver. This condition is accentuated somewhat, because of the low rotor lift associated with compound vehicles, and also because of their greater high-speed maneuvering capability as compared with that of conventional helicopters.

An example of this is shown in Figure 26 for steady-state conditions. These data are for a constant 150 KTAS and show the variation of RPM with load factor for various collective blade angles and initial RPM settings. The gentle slope seen in the data as the load factor first exceeds 1g reflects the engine governor response to the reduction in power required. Under these conditions the governor is able to maintain the initially selected RPM setting reasonably well until the shaft horsepower drops to zero. This control is the reason for the separate fairings for each of the initial RPM settings.

At the break in the curves, the power requirements of the rotor are zero and the engine no longer controls rotor RPM. At load factors beyond this point, therefore, the rotor is in autorotation and the steeper slope is the variation of RPM with load factor for this condition. Naturally, there is only a single fairing which depends on the collective blade angle and airspeed, and it is independent of the initial RPM setting. There is another factor, however, which seems to affect the RPM/g characteristics in autorotation. This is the type of maneuver performed to develop a given load factor. As shown in Figure 24, symmetrical pull-ups were found to have a lesser effect on rotor overspeed than were steady turns at the same load factor. In spite of this, pilots reported several instances of transient overspeed during pull-ups in nap-of-the-earth flying. While this is believed to be due to the severity of the maneuver, data in this area are limited. Additional investigations are therefore required before any definite conclusions can be drawn.

However, based on the experience gained during this program, some general observations can be made. First, overspeeds are most likely to occur in the region of 140 to 200 knots. At speeds below 140 knots, collective blade angles are generally higher, and thus the power requirements of the rotor are high. This provides more margin from autorotation during

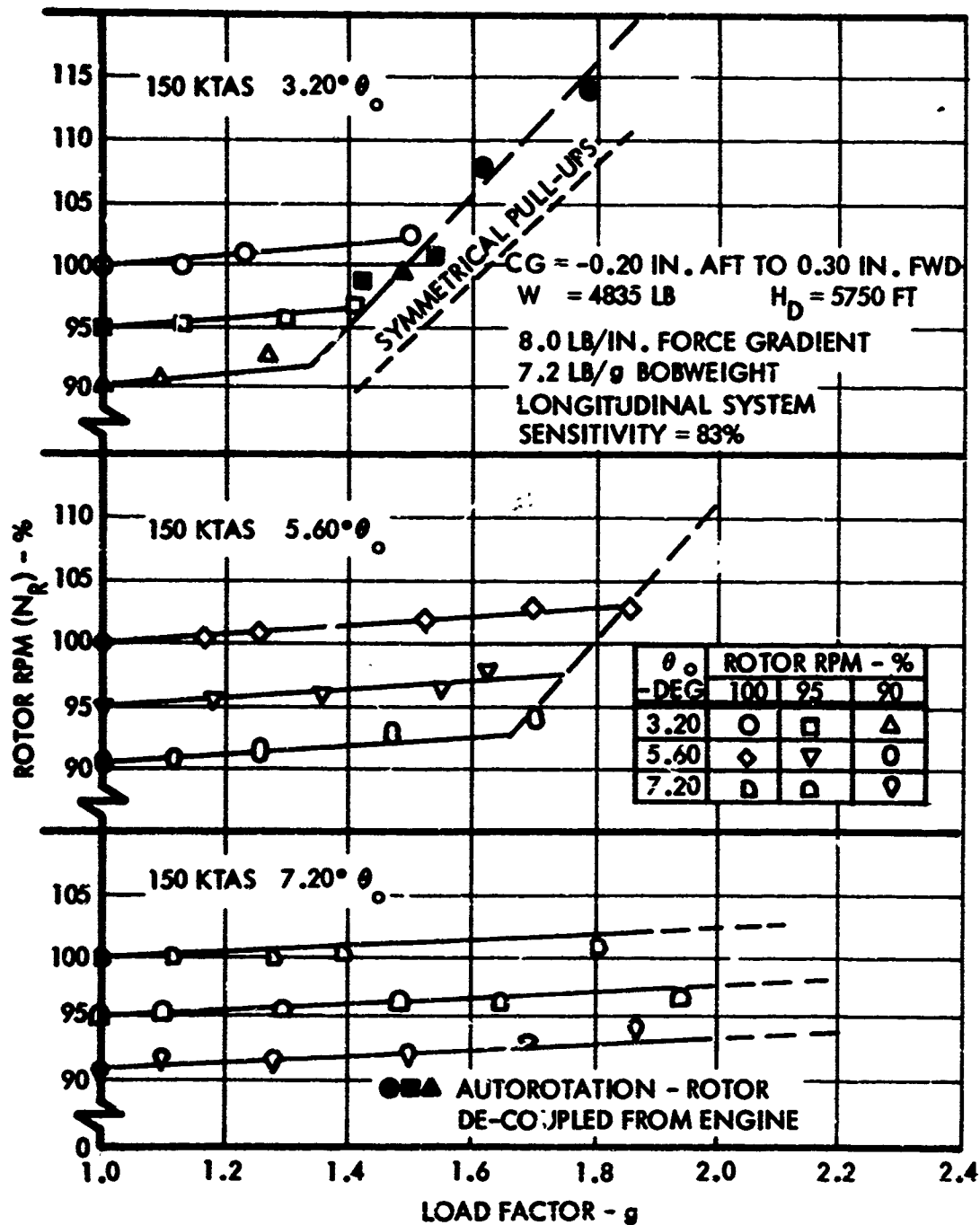


Figure 26. Variation of Rotor RPM with Load Factor in Steady Turns - Neutral CG.

maneuvering. At speeds beyond 200 knots, rotor power requirements are also fairly high even though collective blade angles are low. Moreover, excessive load factors are likely to occur before the angle of attack is sufficient to cause an overspeed.

It is also observed that unless this characteristic is considered in the design of high-performance compound vehicles, either by providing a large overspeed margin or by alternate means of preventing overspeed, it is probable that the maneuvering envelope will be compromised.

CYCLIC CONTROL TRIM REQUIREMENTS

Cyclic control trim requirements for level flight were evaluated throughout the level flight speed envelope as a function of control system sensitivity, collective blade angle, rotor RPM, and center of gravity.

As discussed previously, because of aircraft response characteristics, it was desirable to decrease the longitudinal control response and amplify the lateral control response for high-speed flight. Accordingly, the longitudinal control system geometry was modified to provide for evaluation of longitudinal system sensitivities of 83 and 66 percent of nominal, and the lateral system sensitivities of 154 and 200 percent of nominal.

The cyclic control tends to move aft and to the right with increasing level flight airspeed when using a fixed collective blade angle setting. The apparent instability, indicated by the aft motion of the cyclic stick, is the result of a trim shift due to the combined effects of changes in rotor downwash, angle of attack, and auxiliary thrust.

In hover, the rotor downwash contributes a negative increment to the angle of attack of the horizontal stabilizer causing a nose-up pitching moment increment. This incremental pitching moment decreases with increasing airspeed since the rotor is unloading and the "blow-back" of the rotor downwash field increases, with resultant lower downwash velocities at the horizontal stabilizer. The cyclic stick then moves aft due to the change of rotor downwash at the horizontal stabilizer with increasing airspeed. In addition, both the angle of attack (α) and the auxiliary thrust coefficient (C_{Δ}) decrease with increasing level flight airspeed. The nose-down pitching moment varies inversely with C_{Δ} but varies directly with α , i.e., a smaller C_{Δ} or larger α results in an increase of the nose-down moment.

In level flight, the longitudinal trim shift associated with rotor downwash and auxiliary thrust outweigh the change due to angle of attack, hence the pilot must use aft stick. However, it should be noted that at either a constant airspeed or C_{Δ} , the angle of attack stability indicated by $dC_m/d\alpha$ is positive, i.e., $dC_m/d\alpha < 0$. A more detailed discussion of these effects can be found in References 1 and 2.

The motion of the cyclic stick to the right is due to feathering moments produced as a result of loads in the rotor system which in turn produce a precessional moment on the control gyro. The geometry of the rotor system is such that at low collective blade angles, where the rotor lift is below 4000 pounds, the rotor is substantially underconed. Thus, as the drag of the advancing blade increases with increasing flight speed, a one-per-revolution chordwise bending moment causes a feathering moment to be produced which tends to reduce the blade's pitch. This feathering moment, transmitted through the pitch links causes a precessional moment on the gyro. The phasing of this moment is such that it manifests itself almost entirely as a lateral cyclic control requirement. A more detailed discussion of this effect on lateral cyclic control motion can be found in Reference 1.

During the early stages of testing, it was found that changing the longitudinal control system sensitivity affected the apparent stick position stability. This is because the total amount of control travel in the longitudinal axis remains unchanged with a decrease in system sensitivity, and thus larger control motions are required to provide trim moments over the airspeed envelope. Although in actuality it is a trim shift, this increase in control motion is sensed by the pilot as a decrease in stick position stability.

To partially compensate for this change in stick position stability, small metal tabs were added to the trailing edge tip of each control gyro arm. The purpose of this modification was to produce a nose-up precession of the control gyro with increasing airspeed as a result of aerodynamic forces acting on the tabs. This change produced the desired result, since forward control motion is required to counteract the moment produced by the tabs. Figure 27 indicates the control motion for tab settings of 0 degrees and -10 degrees with an aircraft neutral center of gravity. At the 0 degree setting, the tabs are parallel to the gyro arms and have very little effect on control motion. When the trailing edges of the tabs are bent downward to a -10-degree incidence with respect to the gyro arms, the longitudinal control motion becomes neutral to slightly negative.

The -10 degree tab setting also produced a right roll gyro precessional moment. This was an added benefit which resulted in an incremental shift of lateral control motion to the left, as shown in Figure 27. In addition, this configuration change also delayed the point of inception of the lateral trim shift to the right which occurs at high advancing tip Mach numbers. At 100% rotor RPM the pronounced trim shift to the right now begins at an advancing tip Mach number of approximately 0.920 instead of 0.90 as was experienced during previous testing.

Figure 28 presents the effect of changing system sensitivity on cyclic control motion with gyro tabs installed and with an aircraft neutral center of gravity. As previously stated, control motion tends to move

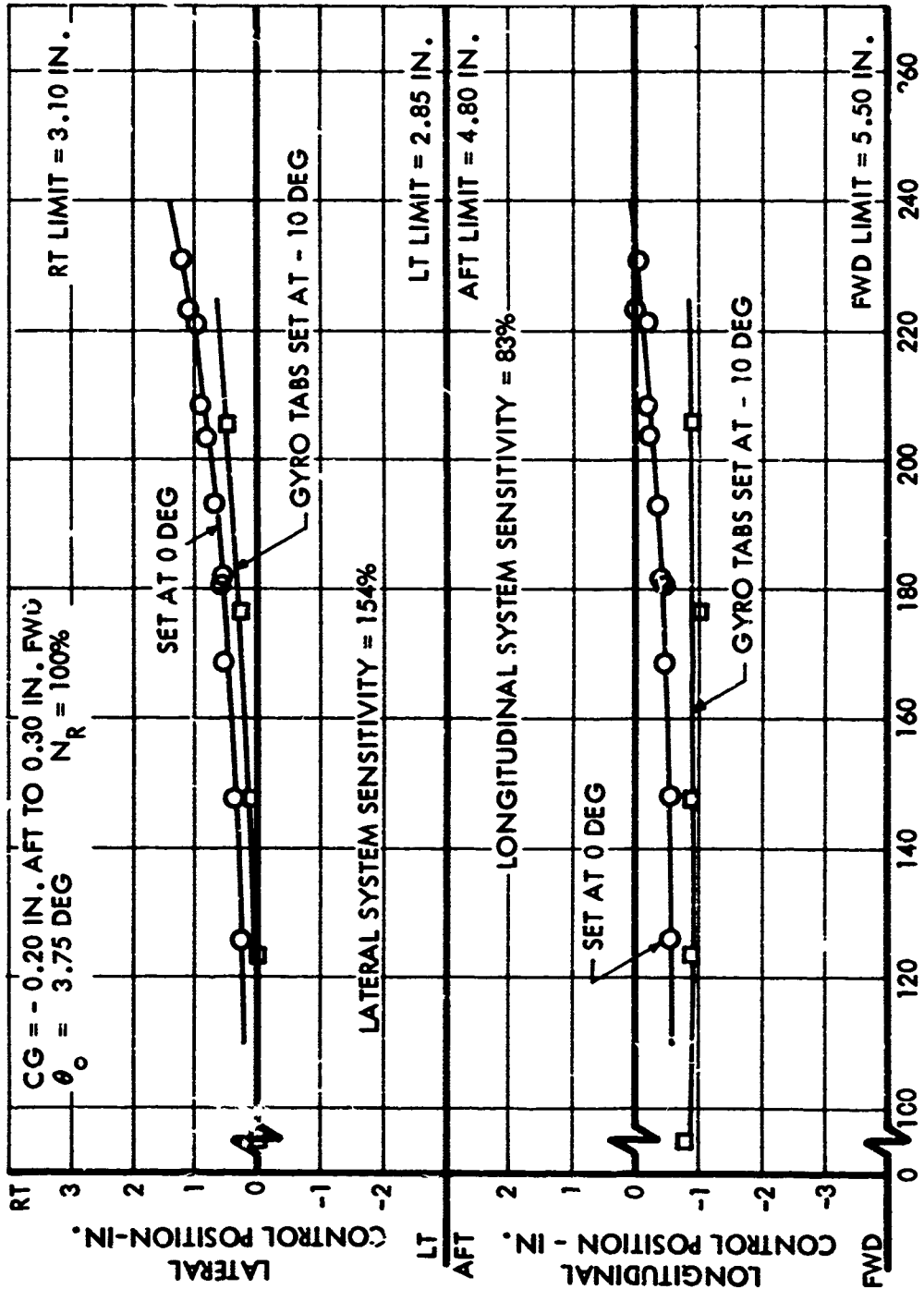


Figure 27. Variation of Cyclic Control Positions with True Airspeed - Effect of Control Gyro Tab Installation - Neutral CG.

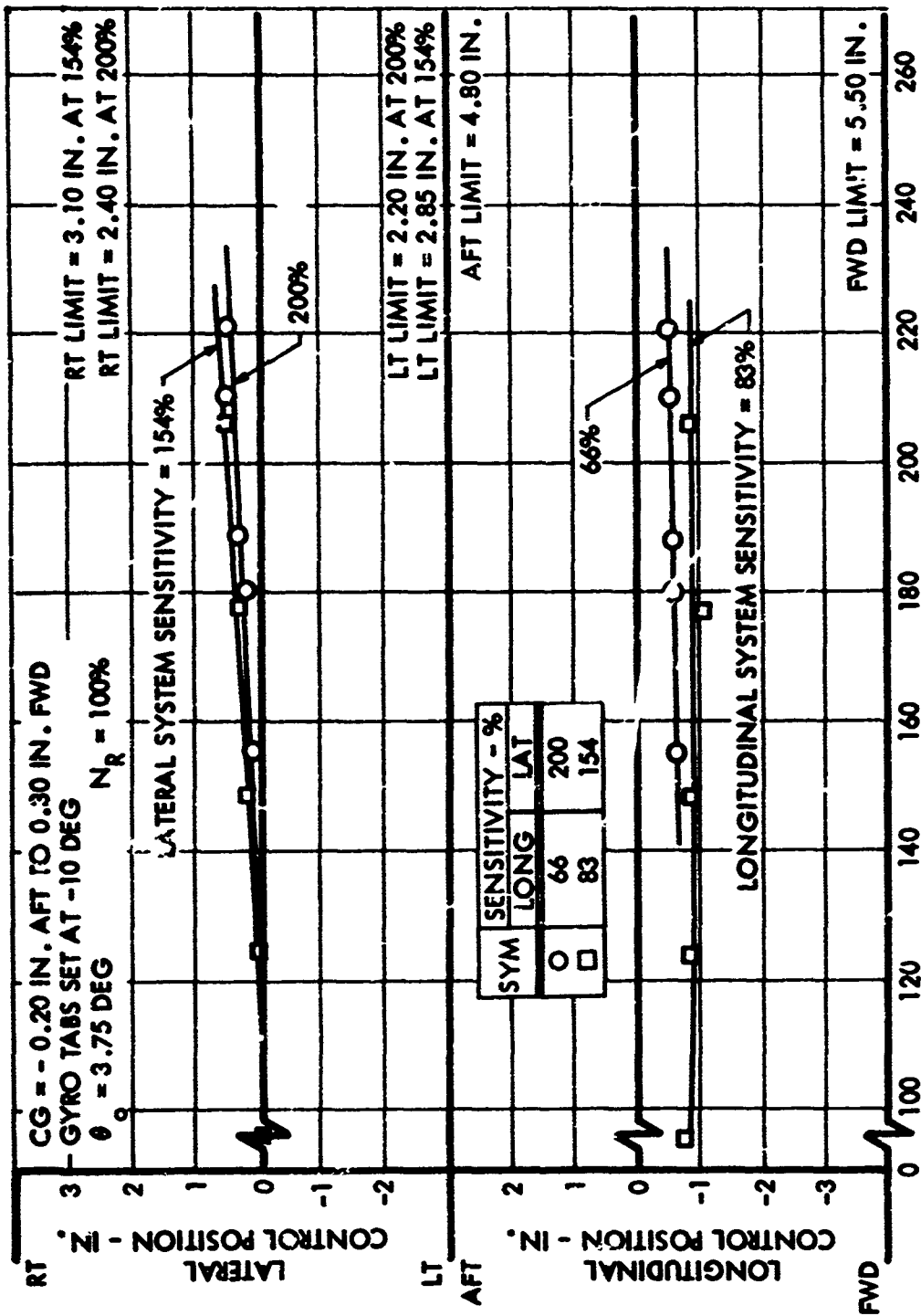


Figure 28. Variation of Cyclic Control Positions with True Airspeed - Effect of System Sensitivity - Neutral CG.

aft and to the right with increasing airspeed. A decrease in the longitudinal system sensitivity from 83 to 66 percent initially shifts the stick aft due to the basic linkage change without changing the total control travel, and also results in a slight decrease in the apparent stick position stability. This latter effect is due to the fact that larger incremental longitudinal control displacements are needed to produce the required trim moments at the 66-percent longitudinal system sensitivity. An increase in lateral sensitivity from 154 to 200 percent indicates an appropriate reduction in the amount of cyclic control required. This is due to the fact that increasing the lateral system sensitivity reduces the amount of total control travel available by an amount proportional to the increase in sensitivity. Therefore, approximately 30 percent less control motion is required when the lateral system sensitivity is increased from 154 to 200 percent.

The pilots report that the aircraft is easy to trim in all axes at high speeds. However, as described in a preceding section of this report, a single longitudinal system sensitivity is not considered adequate for operation at all speeds throughout the flight envelope particularly at neutral centers of gravity. Below 200 KTAS, with a 66 percent longitudinal system sensitivity, larger control inputs are required to maneuver, and this results in higher than desired control forces. The 100 percent system sensitivity is adequate for hover and low-speed flight, while the 83 percent system sensitivity seems most suitable in the intermediate speed range. A lateral system sensitivity of 200 percent is considered adequate over the entire speed envelope.

Figure 29 presents the variation of cyclic control motion with airspeed as a function of collective blade angle with an aircraft neutral center of gravity. Examination of these results indicates that cyclic control motion shifts aft and further to the right with increasing blade angle. Control motion remains aft and to the right with increasing airspeed.

As discussed in a previous section of this report, the longitudinal handling characteristics are further improved when the aircraft is flown with the center of gravity shifted forward. Tests were conducted with aircraft centers of gravity between 1.3 and 1.8 inches forward of the rotor mast. The static stability of the aircraft is improved under these conditions, and there is a general overall improvement in handling characteristics. Longitudinal damping remains strong and effective at all airspeeds. This configuration change permitted a significant expansion of the flight envelope.

The cyclic control trim requirements for this forward center of gravity condition are presented in Figure 30 for longitudinal system sensitivities of 100 and 83 percent and for a lateral system sensitivity of 200 percent. As expected, the longitudinal cyclic control trim setting shifts aft to counteract the nose-down moment due to the forward center of gravity.

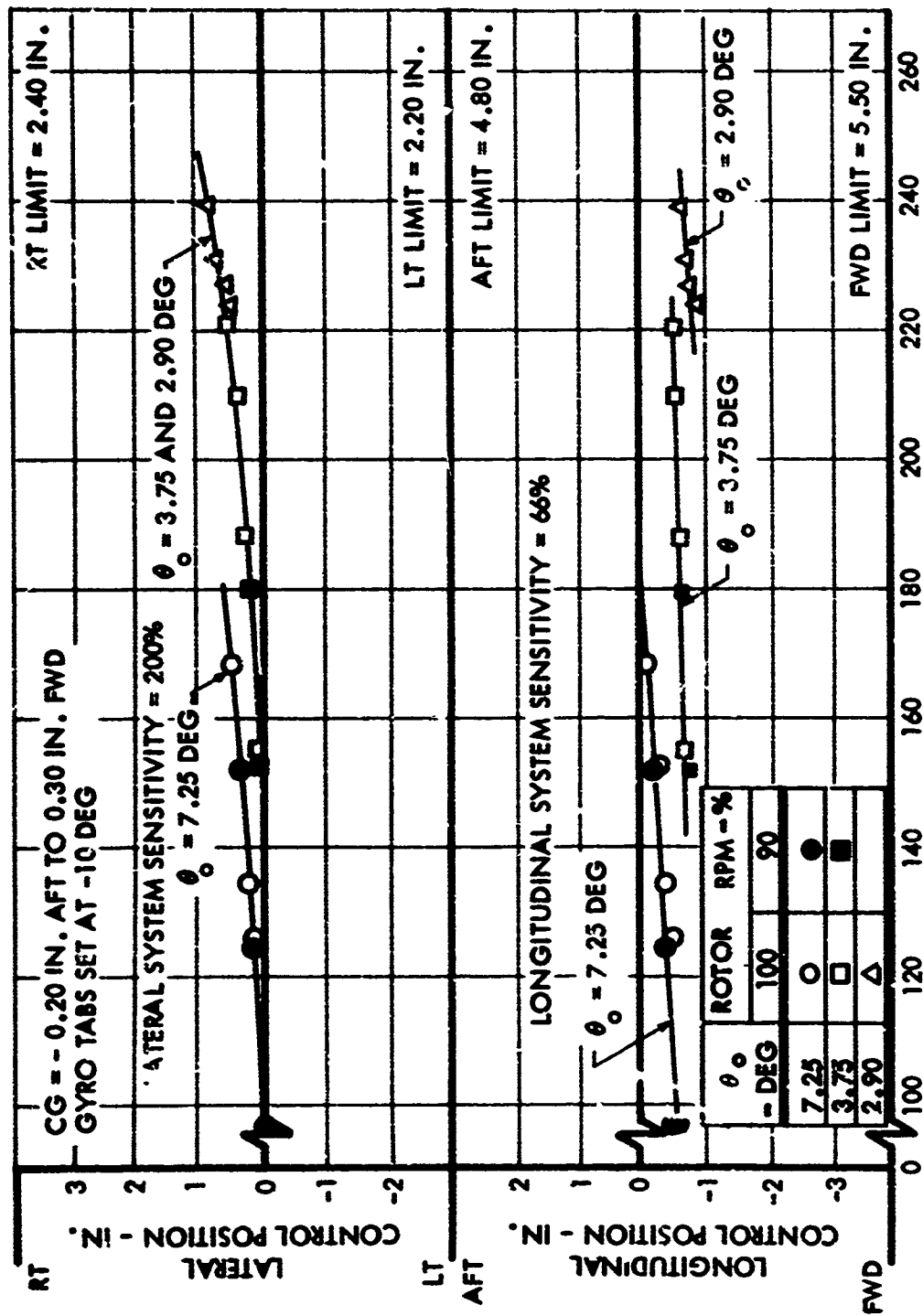


Figure 29. Variation of Cyclic Control Positions with True Airspeed - Effect of Collective Blade Angle and Rotor RPM Setting - Neutral CG.

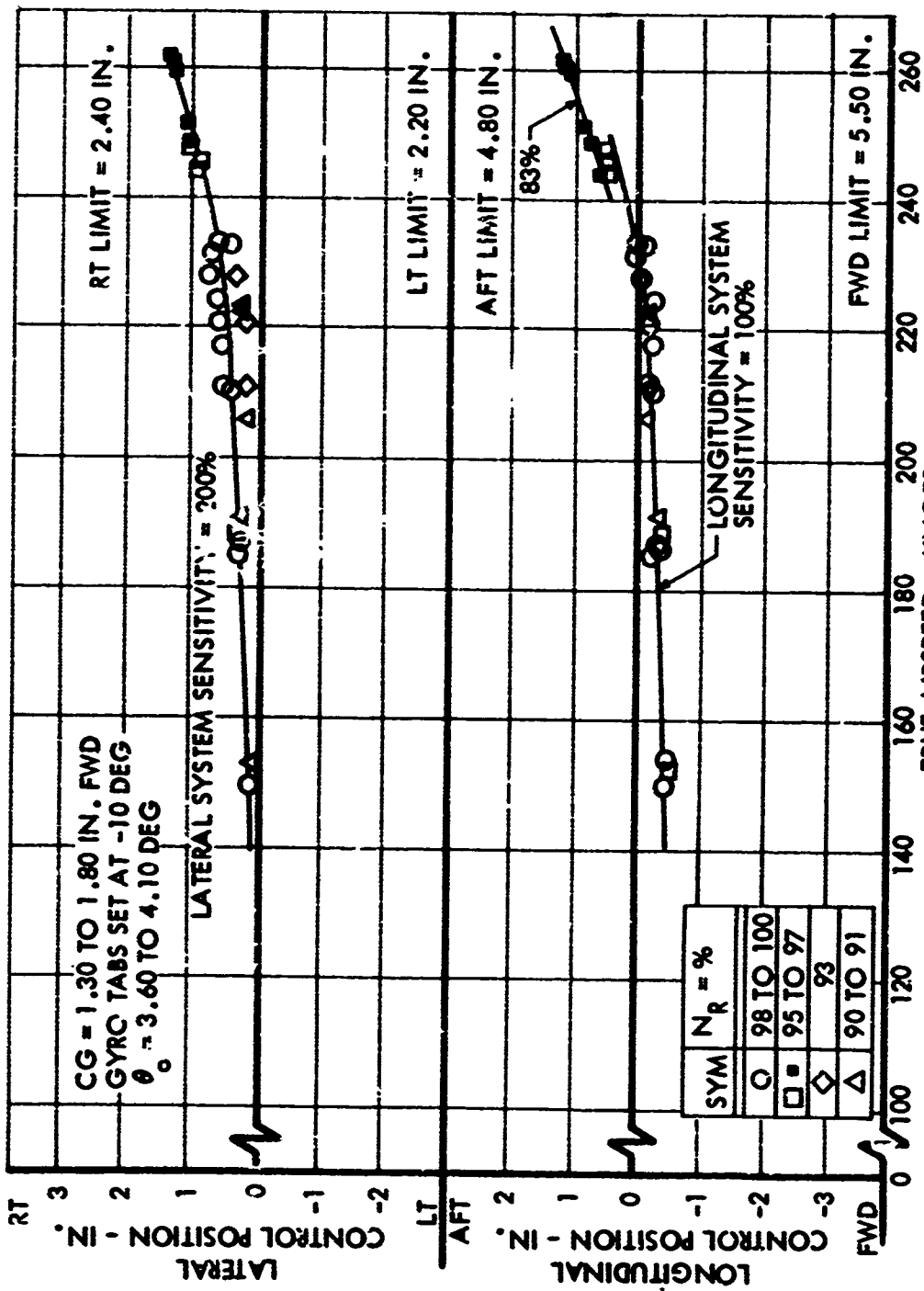


Figure 30. Variation of Cyclic Control Positions with True Airspeed - Effect of Longitudinal System Sensitivity - Forward CG.

The gradient with airspeed appears to be similar to that obtained with neutral centers of gravity with a 66-percent longitudinal system sensitivity. At true airspeeds in the vicinity of 230 knots, a noticeable change in the cyclic control position becomes apparent. The stick moves to the right at a more noticeable rate and also moves aft in the same manner. This change in trim characteristics is attributed directly to advancing tip Mach number effects.

Rotor RPM has no significant effect on cyclic control trim characteristics at true airspeeds below approximately 230 knots. However, above this speed, at 100 percent rotor RPM, advancing tip Mach numbers in excess of 0.90 are obtained and a definite cyclic control trim shift is experienced. At true airspeeds above 238 knots, the rotor RPM was gradually lowered from 100 percent to a value of 95.5 percent at 262.7 knots to minimize tip Mach numbers. This technique was found to be quite effective in controlling the undesirable characteristics associated with tip Mach number.

NAP-OF-THE-EARTH FLYING

Nap-of-the-earth flight demonstrations were performed to determine qualitatively and quantitatively the agility of the aircraft in close proximity to the terrain at both low and high speeds.

Three courses were selected in terrain suitable for performing the various types of maneuvers:

- Course 1 - A narrow winding canyon, where maneuvers were performed at 100 to 200 feet above the canyon floor, at equivalent airspeeds of 145 to 190 knots with the auxiliary thrust engine operating.
- Course 2 - An irregular 2.0-mile course over which terrain-following maneuvers were performed at 50 to 100 feet above the ground, at equivalent airspeeds of 125 to 190 knots with the auxiliary thrust engine operating.
- Course 3 - A level terrain over which excerpts from maneuvers described as the "Army Dozen" were performed at close proximity to the ground with and without the auxiliary thrust engine operating.

The terrain-following maneuvers were performed satisfactorily over the first two courses. However, the degree of aircraft maneuverability was limited by a rotor RPM overspeed condition caused by the rotor's entering autorotation during banked turns, symmetrical pull-ups, or a combination of both maneuvers. The rotor's tendency to overspeed is most pronounced in the airspeed range of 145 to 190 KEAS and makes it difficult to pull more than 2.0g for quick turns. Rotor speed was reported to be approximately 100 percent throughout most of the maneuvers.

Since data on rotor overspeed are somewhat limited, additional investigations are required before any definite conclusions can be drawn.

During these maneuvers, roll characteristics to the right were excellent. However, high roll rates to the left were generally accompanied by an increase in 4P vibration and a decrease in rotor speed. When the left cyclic input was held long enough, rotor RPM drooped below 100 percent and caused a lag in gas generator (N_1) acceleration. The pilot reported rotor speeds as low as 96 percent.

The Army Dozen maneuvers were performed over the third course with and without auxiliary engine thrust, and they were satisfactory with certain limitations encountered as described by the pilot in the following list of performed maneuvers:

- Confined area approach followed by a flare and landing - The research vehicle's favorable control and stability made it relatively easy to operate in confined areas. However, the steepness of the approach is limited by the power available for the flare.
- Pedal turns at 6- to 12-foot hover heights - Pedal turns to the left and right are smooth and easy to control. However, left pedal is limited by tail rotor torque which causes a slow recovery from a high-rate, right-pedal turn.
- Vertical climb to approximately 50 feet, stop in hover, peel off to the left or right - Vertical climb is power limited to under 50 feet; but from the maximum altitude attainable, it is easy to peel off either to the left or to the right.
- Hover pedal turn breaking into rapid sideward flight with quick stops into and out of the wind - This maneuver can be accomplished fairly rapidly to the right and into the wind. However, tail rotor torque and main rotor engine power limitations made it difficult to conduct this maneuver to the left and downwind, if the wind exceeded 10 knots.
- Quick stops or lateral flare maneuvers - These maneuvers can be accomplished easily in winds of at least 15 knots in either direction; however, heading control may be limited by tail rotor torque under some conditions. Downwind maneuvers must be conducted at a slow rate due to lack of power available.
- Slope Landings - Two side hill landings and takeoffs were performed on right side slopes (down to the right) of 4.2 and 7.2 degrees. These right side slope maneuvers were conducted without moving the cyclic control from the trim position required to hover. This was accomplished by slowly lowering the collective and letting main rotor lift support the aircraft's weight

as it adjusted to the degree of slope. Left side slope landings were not evaluated because of the vehicle's 22,000 inch-pound lateral center of gravity offset caused by the J-60 engine installation which would result in an unrealistic and an impractical loading for this test condition.

- Scramble takeoff (rapid, low-level, downwind takeoff) - This maneuver can be conducted rapidly into and out of the wind as a compound helicopter with the proper addition of auxiliary thrust.
- Cruise at a 200-foot altitude between 105 and 160 KEAS performing pull-up and break maneuvers - This maneuver cannot be conducted satisfactorily as a helicopter at airspeeds above 105 KEAS and is not very comfortable as a compound helicopter at airspeeds under 160 KEAS. However, when flying as a compound helicopter between 160 and 210 KEAS, this maneuver can be conducted satisfactorily and the vehicle is easily handled at a 50-foot altitude.
- High-speed, 180-degree heading reversal in a confined area - This maneuver can be conducted easily but is limited under some flight conditions by the rotor RPM overspeed characteristic.
- High-speed teardrop turn - This maneuver was satisfactorily conducted up to 180 KEAS. However, the maneuver can be limited by the rotor RPM overspeed characteristic under some flight conditions.
- High-speed S-turn - This maneuver was satisfactorily conducted at high airspeeds up to 180 KEAS.
- Hit-the-deck maneuvers from various altitudes - Favorable control effectiveness and stability make these maneuvers easy to accomplish at any airspeed; i.e., easy to push over and level off at close proximity to the ground.

It should be noted that all maneuvers conducted in hover and at very low airspeeds were performed without the auxiliary thrust engine operating.

STRUCTURAL LOADS

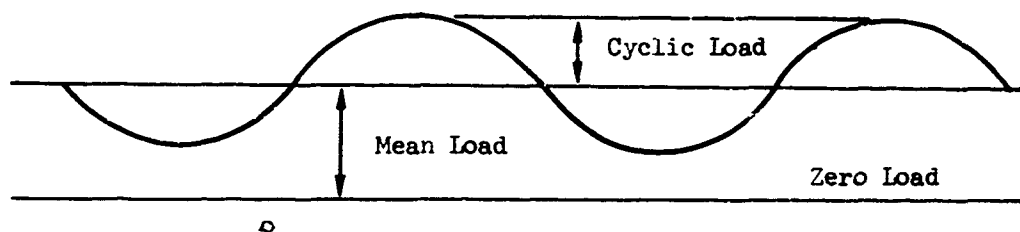
General

Structural loads were measured during all phases of the maneuverability testing. The 50-channel oscillograph, used to record the structural loads and control parameters, was run at normal paper speed for each of the prescribed test conditions. During the time that the pilot was setting up for the next test condition, the oscillograph was run at a slow paper speed, one-tenth the normal rate. From these continuous oscillograph records, the structural loads were monitored for all flight conditions, including any inadvertent condition. As a safety precaution, these

records were examined prior to each flight to determine the magnitude of loads encountered on the previous flight.

Measurements taken during the testing include the main rotor hub and blade loads, main rotor pitch link axial loads, control gyro arm loads, wing bending, main rotor lift, horizontal stabilizer loads, and tail rotor loads.

In this report, the load measurements are divided into two components: cyclic load and mean load. The sketch below indicates the meaning of these components.



A review of all structural data indicates that station 7.0 is the most critical fatigue section of the main rotor. Assuming a stress concentration factor of 3, the estimated endurance limit stress is 26,000 psi. The strain gage calibration was effected in terms of bending moment rather than stress because the bending moment curve along the span of hub and blade is predictable. Bending moments are then readily convertible into stresses from the known structural section properties along the span of the hub and blade. The conversion of bending moment to stress at station 7.0 is as follows:

Flapwise bending moment at station 6.0 x 1.42 = stress at station 7.0

Chordwise bending moment at station 6.0 x 0.152 = stress at station 7.0

Main Rotor Blade Loads

Three main rotor blade configurations were flown during the maneuverability program. These three blade configurations were identified as Part Number 6260-1100-01 (standard XH-51A blades), Part Number 6261-1100-01 (Model 286 prototype blades with XH-51A cuff fittings), and Part Number 6260-1100-01 (XH-51A blades with 20-pound anti-nodal weights).

Initial flights in this program were made with 6260* standard XH-51A main rotor blades while waiting for approval to fly the 6261* Model 286 prototype main rotor blades. During these initial tests, the Model 286 type of tail rotor also was being tested. The test conditions flown with the standard XH-51A blades were within conditions that had been tested during the previous program and reported in Reference 1. Therefore, no main rotor loads data from these initial tests are included in this report.

6261-1100-01 Model 286 Prototype Blades with XH-51A Cuff Fittings

The natural frequency of the second flapwise bending mode of these blades is lower than that of the 6260 blades. These 6261 blades were used to attempt to reduce the sharp rise of the response in the second bending mode at three per revolution of the rotor associated with high tip Mach number of the advancing main rotor blade at the higher forward speeds. Tests were conducted at various speeds, rotor RPM's, and collective blade angles to determine their effect on these blades and also to determine the optimum rotor RPM and collective blade angles for the higher speeds. The rotor RPM was reduced during these tests to lower the advancing blade tip Mach number at a given forward speed.

Variation of hub flapwise and chordwise loads at station 6 with equivalent airspeeds up to 194 knots for 100 percent RPM is shown in Figure 31. Changes in RPM from 100 percent had a negligible effect on rotor loads; thus, loads for other RPM's are not shown.

At the higher speeds, the overall cyclic flapwise bending blade loads at station 6 were higher than with the 6260 original XH-51A main rotor blade loads. Use of the 6261 blades resulted in a reduced amplitude of the three-per-revolution component of flapwise cyclic bending loads as was expected, but the two-per-revolution component loads increased at a higher rate and thus increased the overall cyclic loads. These components of the flapwise loads are shown in Figure 32. Cabin vertical vibration was also higher with the 6261 blades than with the 6260 blades.

When the collective blade angle was lowered at higher speeds, the helicopter encountered a rotor plane oscillation at a frequency of approximately three cycles per second or every two revolutions of the main rotor (one-half per revolution). Because of the rotor plane oscillation, higher flapwise cyclic blade loads, and increased vibration, these 6261 main rotor blades were removed to install the 6260 main rotor blades.

For a more complete description of this phenomenon, see the section of this report entitled Rotor Plane Oscillations.

* Abbreviated notation.

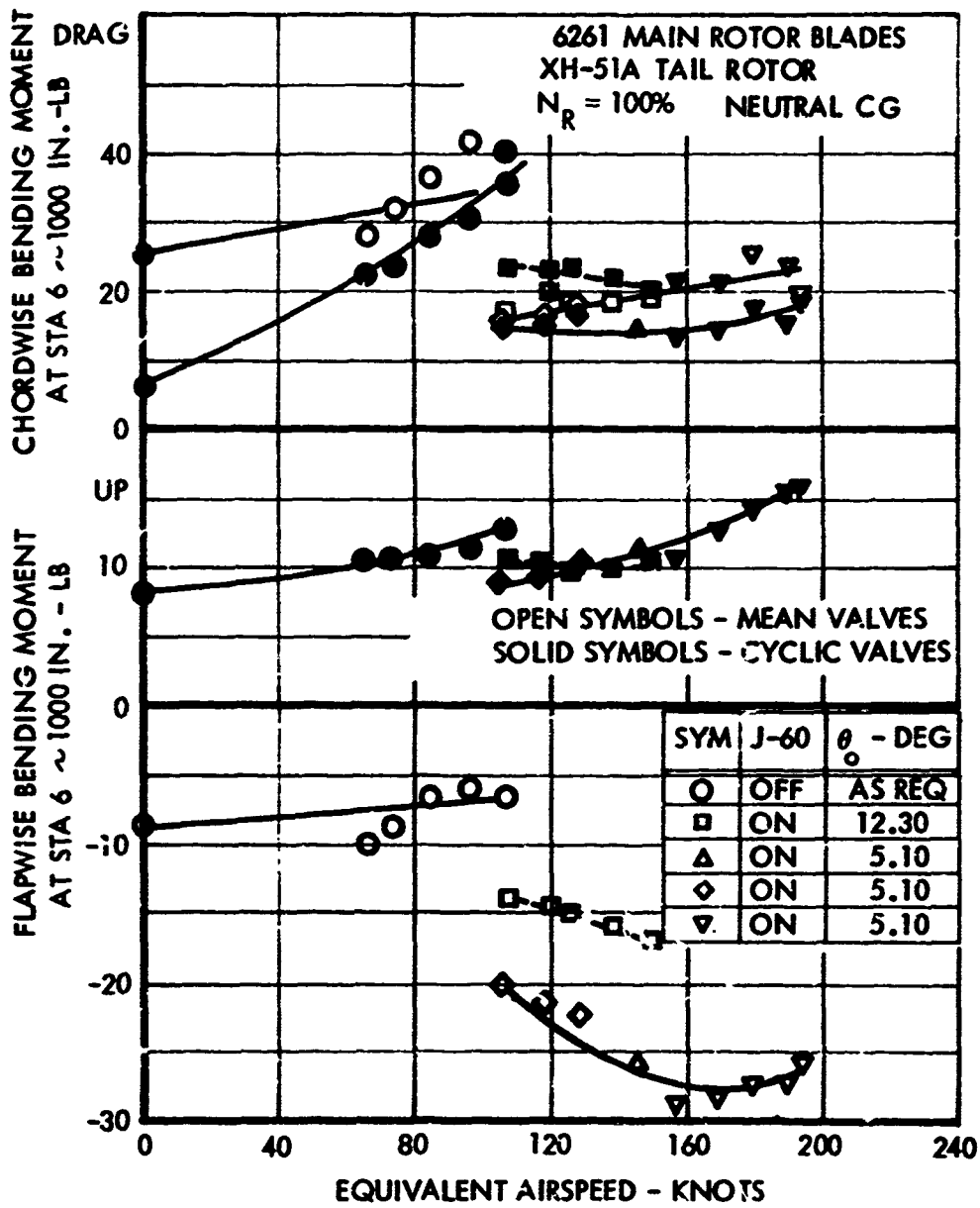


Figure 31. Main Rotor Hub Loads as a Function of Equivalent Airspeed.

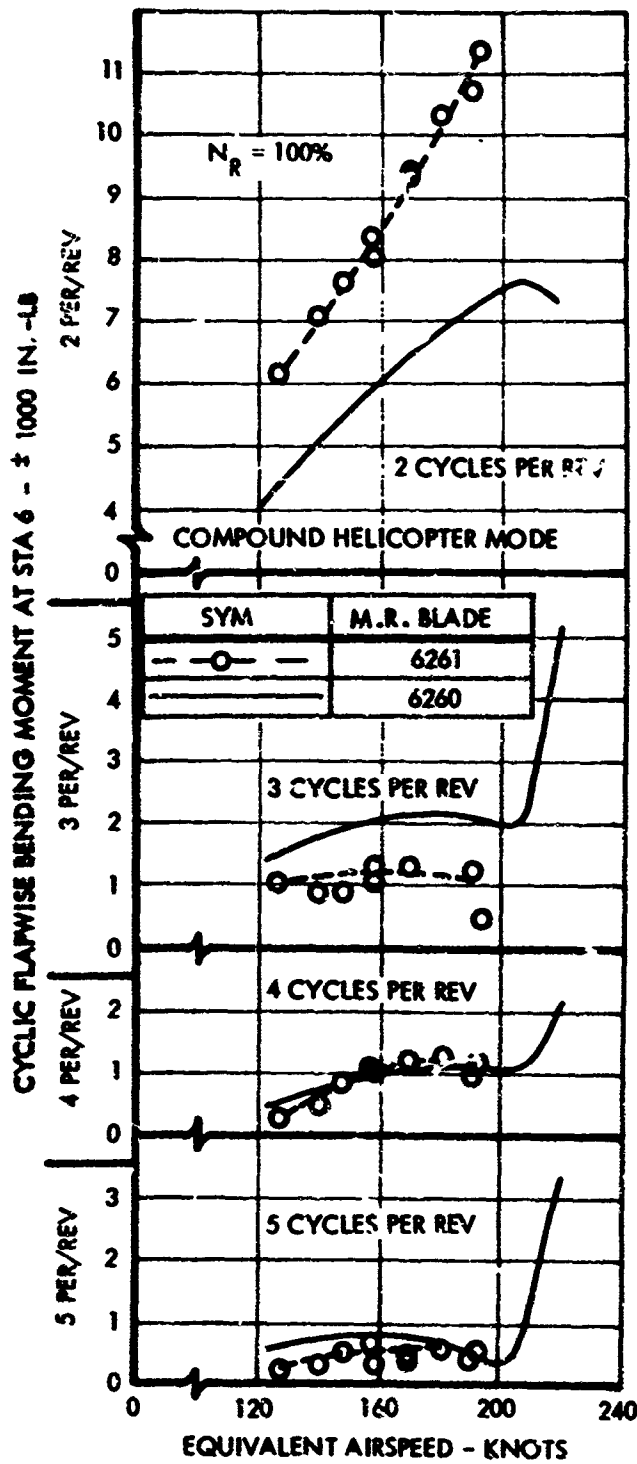


Figure 32. Harmonic Components of Cyclic Flapwise Bending Moment at Sta. 6 as a Function of Equivalent Airspeed.

6260-1100-01 Standard XH-51A Main Rotor Blades

With the 6260 standard XH-51A main rotor blades reinstalled, the rotor RPM and collective blade angle were varied to determine their effect on blade hub loads and vibration. These blades were installed because they were not tested at lower RPM settings during the initial flights described above, or during the previous program that was reported in Reference 1.

The RPM was varied from 92 percent to 104 percent at several speeds. The main rotor blade loads were not noticeably affected by this RPM variation. However, the vibration level increased at lower RPM. The collective blade angle was varied from 3.4 to 5.6 degrees. Blade loads were slightly higher at the lower blade angles, but cabin vibration was not noticeably affected by the blade angle changes.

6260-1100-01 Main Rotor Blades with 20-Pound Anti-Nodal Weights

To obtain a complete comparison of the various main rotor blades which were available, 6260 blades with external, 20-pound anti-nodal weights were installed. These blades had a reduced second flapwise bending natural frequency similar to the 6261 prototype Model 286 blades but with a slightly different weight and blade stiffness distribution.

Tests were made varying the RPM from 90 percent to 104 percent and the collective blade angle from 3.0 to 12.0 degrees. The results obtained were essentially similar to those obtained for the 6261 blades. The loads were relatively unaffected by RPM changes, and the flapwise cyclic loads increased with a decrease in collective blade angle. Also, the flapwise load level was increased by the increased response to two-per-revolution loads. The vibration level was higher than it was with the standard XH-51A blades.

Rotor plane oscillation was also encountered with these blades at higher speeds at increased collective blade angles. The oscillation frequency was approximately two cycles per second or every third revolution of the main rotor (one-third per revolution) as compared with the three-cycle-per-second oscillation encountered with the 6261 blades at lower blade angles.

After the test data from the three configurations were compared, the 6260-1100-01 blades were selected for further testing because they had the lowest overall flapwise cyclic loads and the lowest vibration and because they had not encountered a rotor plane oscillation in the operating range tested at that time.

6260-1100-01 Standard XH-51A Main Rotor Blades

Level Flight Conditions

With the 6260 main rotor blades reinstalled, structural loads were further investigated as the RPM and forward speed were varied. Main rotor hub flapwise and chordwise bending moments at Station 6 were plotted versus equivalent airspeed (Figure 33). This curve shows the increase in cyclic loads as the speed was increased to 221.5 KEAS (245.0 KTAS) with the center of gravity at 0.3 inch forward of the mast and with the rotor RPM at 98 percent. These curves also show the loads up to the maximum speed obtained of 234 KEAS (262.7 KTAS) with the center of gravity at 1.5 inches forward and the rotor RPM at 95.5 percent. Data from reference 1 are also included for comparison. These curves show an increase in cyclic loads as forward speed and the advancing main rotor tip Mach number increase.

The overall flapwise cyclic bending at Station 6, shown in Figure 33, increased with speed to a maximum value of 25,000 inch-pounds at 234 KEAS. This cyclic flapwise bending of 25,000 inch-pounds at Station 6 converts to a cyclic stress of 35,600 psi at station 7. The cyclic chordwise moment at Station 6, as shown in Figure 33, was 43,000 inch-pounds; this converts to a stress of 6,500 psi at Station 7. The sum of the two results in a maximum possible cyclic stress of 42,100 psi. To assess the effects on main rotor hub fatigue life of the stresses which are above the estimated endurance limit of 26,000 psi, a conservative cumulative damage analysis was performed. This analysis was limited to test time above a speed of 208 KEAS where the flap and chord loads resulted in a combined stress equal to the estimated endurance limit. Review of test data resulted in the following time distribution for various speeds:

<u>Speed Range - KEAS</u>	<u>Time in This Speed Range - Minutes</u>
210 - 220	6
220 - 230	2
230 - 234	0.5

The cumulative damage analysis indicated that about five percent ($\sum \frac{n}{N} = .05$) of the hub fatigue life was used in the high-speed flying. This is considered acceptable for a high-speed research vehicle.

Harmonic analyses were run on the waveform of the flapwise bending moment at Station 6 to determine the magnitude of the various components. The various frequencies were then plotted versus equivalent airspeed, as shown in Figure 34. Also, the various frequencies were plotted versus

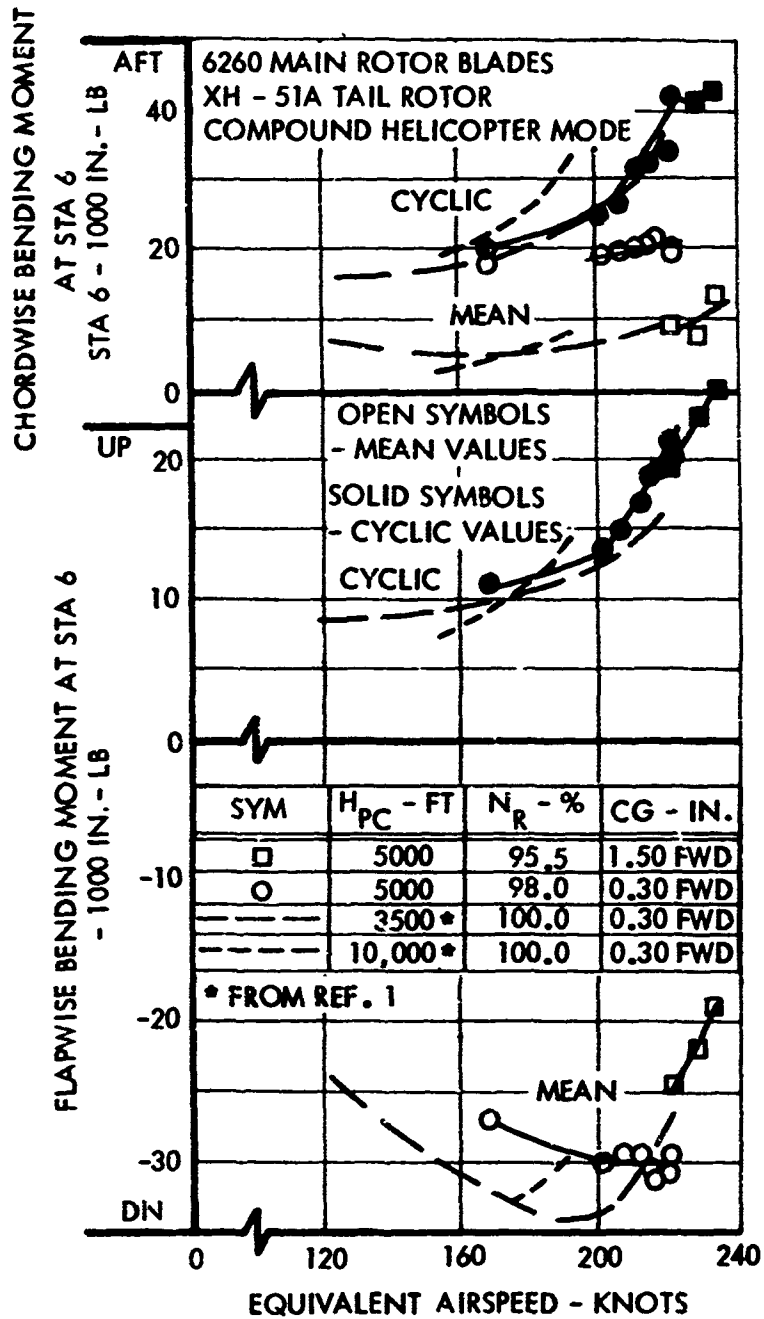


Figure 33. Main Rotor Hub Loads as a Function of Equivalent Airspeed.

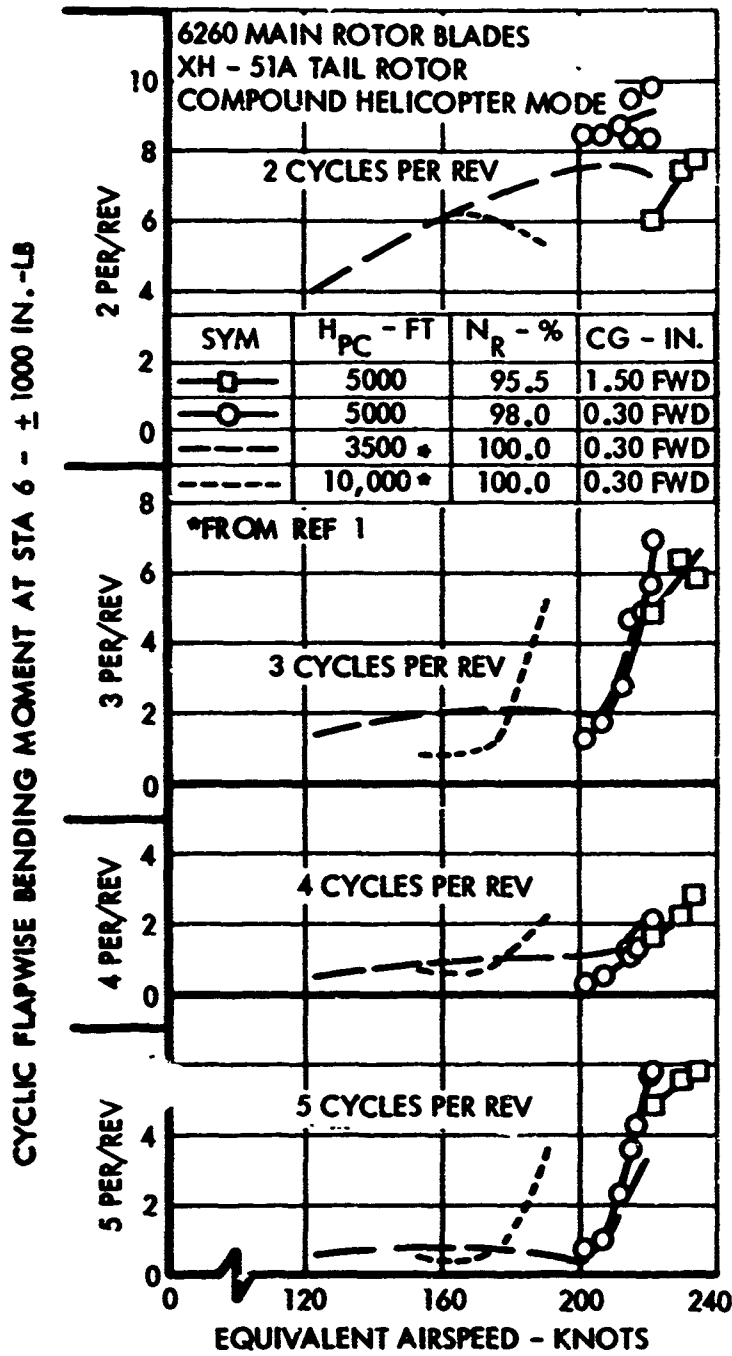


Figure 34. Harmonic Components of Cyclic Flapwise Bending Moment at Sta. 6 as a Function of Equivalent Airspeed.

the advancing main rotor blade tip Mach number as it was increased from 0.925 to 0.937 with the center of gravity at 0.3 inch forward and with the rotor RPM at 98 percent. These curves also show the harmonics up to the maximum advancing tip Mach number of 0.942 with the center of gravity at 1.5 inches forward with the rotor RPM at 95.5 percent (Figure 35). This 0.942 Mach number of the advancing blade tip is well above the critical Mach number for a 12-percent-thick blade section. These curves show the same sharp rise in the three- and five-per-revolution components as the data presented in Reference 1.

The one-per-revolution pitch and roll components of the Number 1 blade flapwise bending moment at Station 6 were plotted versus equivalent airspeed (Figure 36). This curve shows that a significant portion of the overall cyclic bending moment at the maximum speed of 234 KEAS was due to the resulting one-per-revolution roll and pitch moment. The pitch component increased rapidly at speeds above 220 KEAS. The line for 0.3 inch forward center of gravity at high speed represents data corrected for shifting the test center of gravity from 1.5 inches to 0.3 inch forward and an approximate correction for jet engine thrust difference for the descent at the maximum speed point.

Main rotor blade loads in the outer portion of the blade also were monitored during the test program. They exhibited the same characteristics as the blade root loads but were less critical for both maximum loads and fatigue.

Rotor plane oscillations were encountered with these blades at speeds above 215 KTAS at reduced RPM. The conditions where oscillations occurred were low collective blade angle and rotor RPM's between 90 and 95 percent. As RPM was lowered, the oscillation occurred at a lower airspeed. This prevented obtaining maximum speed at 90 percent RPM as planned (see Rotor Plane Oscillations, page 73).

Maneuvering Conditions

Main rotor loads were measured during the stability testing that was conducted to expand the maneuvering envelope. Flapwise and chordwise bending moments at Station 6 are plotted versus load factor for each of the maneuvers that define the outer boundaries of the maneuvering envelope (Figure 37). Windup turns were used to obtain the load factor at 175 and 200 KEAS, and the rest of the maneuvers were symmetrical pull-ups. The moments shown are the maximum obtained at any time during the maneuver.

Cyclic flapwise and chordwise loads during the symmetrical pull-ups are somewhat higher than those in windup turns. This increase in rotor loads is due to the higher angular accelerations normally encountered in a pull-up maneuver.

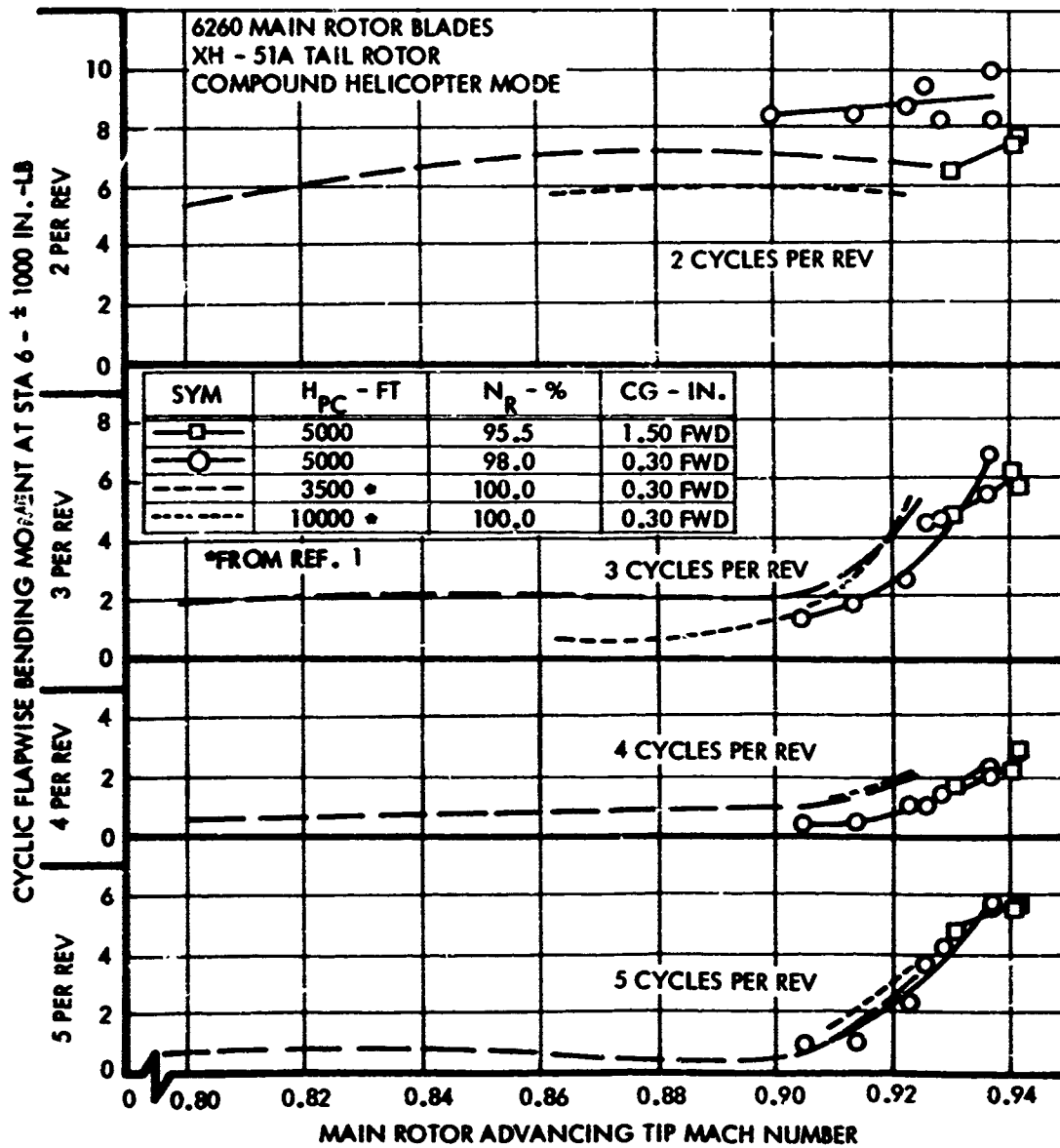


Figure 35. Harmonic Components of Cyclic Flapwise Bending Moment at Sta. 6 as a Function of Main Rotor Advancing Tip Mach Number.

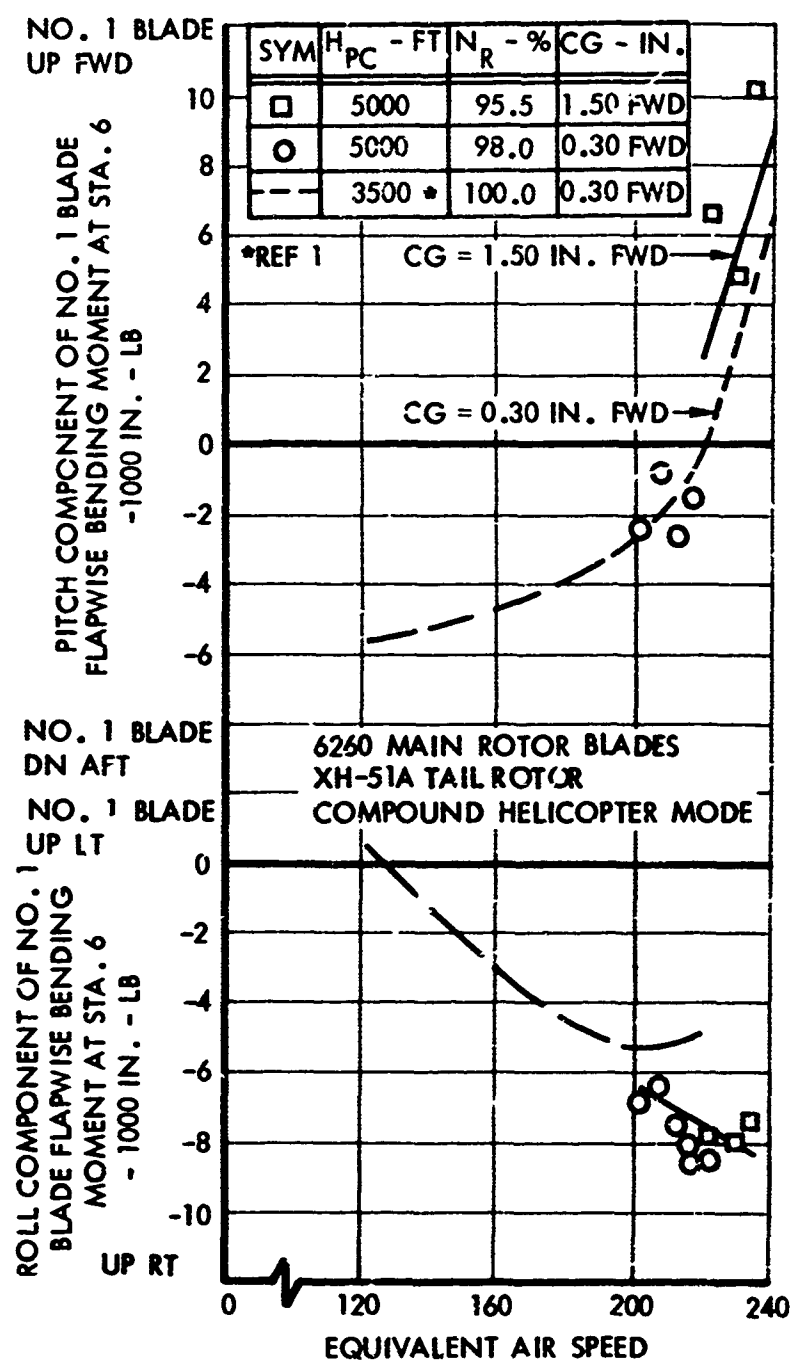


Figure 36. Roll and Pitch Components of Cyclic Flapwise Bending Moment at Sta. 6 as a Function of Equivalent Airspeed.

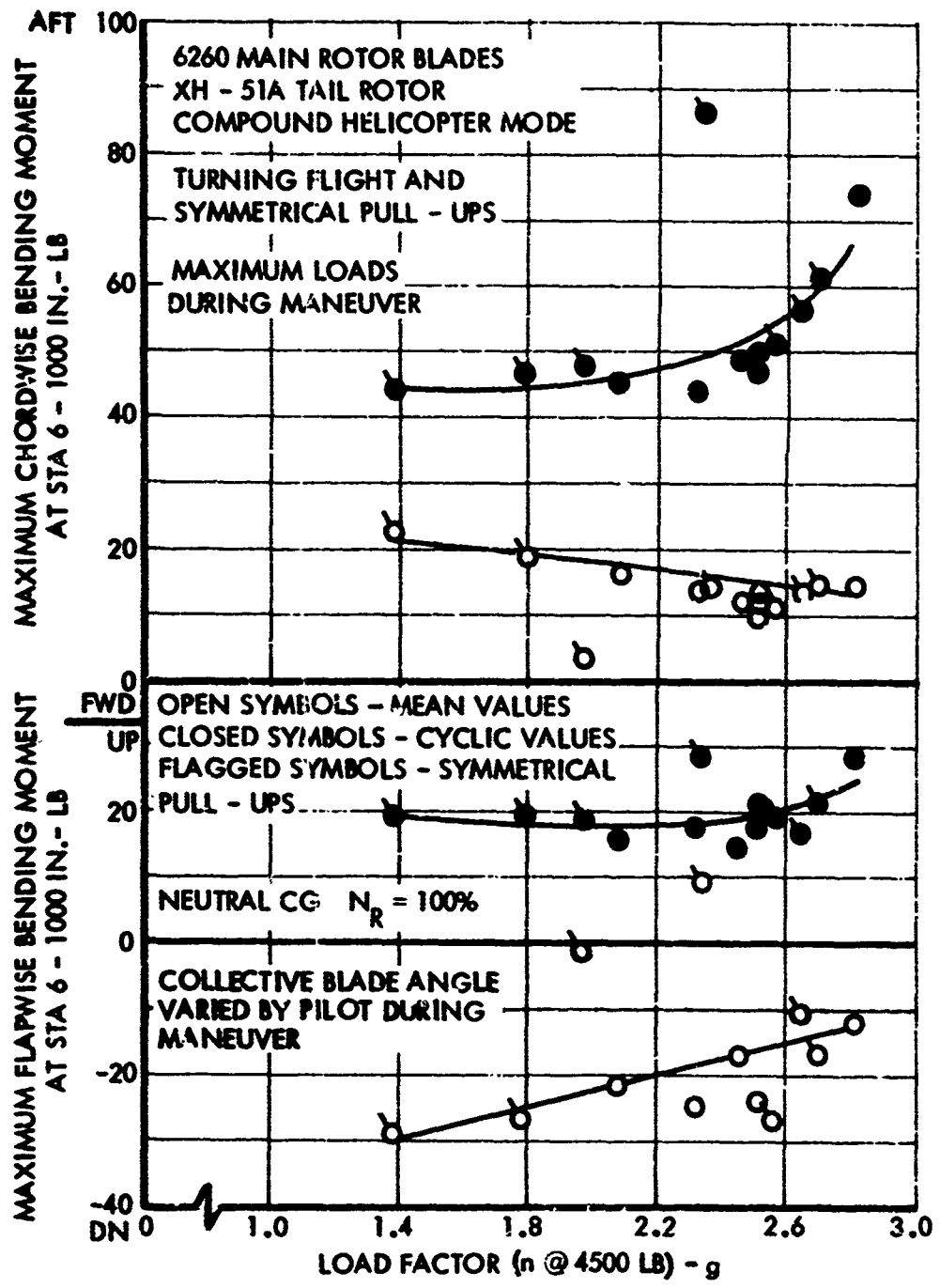


Figure 37. Maximum Main Rotor Blade Loads as a Function of Load Factor.

Pitch angular acceleration was calculated by differentiating the pitch rate and is plotted versus cyclic flapwise bending moment at Station 6 (Figure 38). This curve shows the increment of cyclic flapwise bending moment due to angular acceleration during the symmetrical pull-up maneuvers that define the outer boundaries of the maneuvering envelope.

Main rotor loads at or near the maximum load factor when the angular acceleration is at or near zero are plotted versus load factor (Figure 39). This curve shows that the cyclic flapwise bending at Station 6 is not significantly affected by steady load factor but that chord load is a function of load factor.

Data obtained in steady turns at various load factors corroborate the above observations. Flapwise cyclic loads are relatively unaffected by load factor, whereas chordwise cyclic loads appear to be essentially a direct function of load factor. Rotor lift and right wing bending moment at Station 25 were plotted versus load factor to illustrate the lift-sharing relationship between the wing and rotor for various speeds (Figure 40). The wing carries the largest portion of total aircraft lift at the higher speeds as load factor is increased.

The maneuvering envelope obtained during the program is presented in Figure 7.

Gyro Arm Bending

Control gyro arm cyclic chordwise bending loads are plotted versus main rotor RPM for various speeds up to the maximum speed of 234 KEAS in Figure 41. The loads are plotted versus equivalent airspeed in Figure 42.

When the rotor RPM was reduced, the gyro arm cyclic chordwise bending loads tended to increase, indicating that the gyro arm was at its natural frequency in the 94 to 97 percent RPM range. This RPM range was avoided during the early testing, but when the speed extension testing was being performed at a reduced rotor RPM, the airspeed was limited for operation at 90 to 94 percent RPM due to rotor plane oscillation. A rotor RPM less than 97 percent was desirable for reducing the advancing main rotor blade tip Mach number effect; therefore, the RPM was reduced gradually in small increments from 97 percent down to 95.5 percent as the speed was increased to 234 KEAS. The gyro arm chordwise loads were checked after each flight and plotted in Figure 41. The cyclic chordwise bending increased as the rotor RPM approached 95.5 percent RPM at the higher speeds, but the damping was sufficient to keep the loads from getting excessive. The maximum cyclic chord load at 234 KEAS was 1560 inch-pounds. This load produces a stress of 4550 psi in the titanium gyro arm section and 1930 psi in the aluminum hub section.

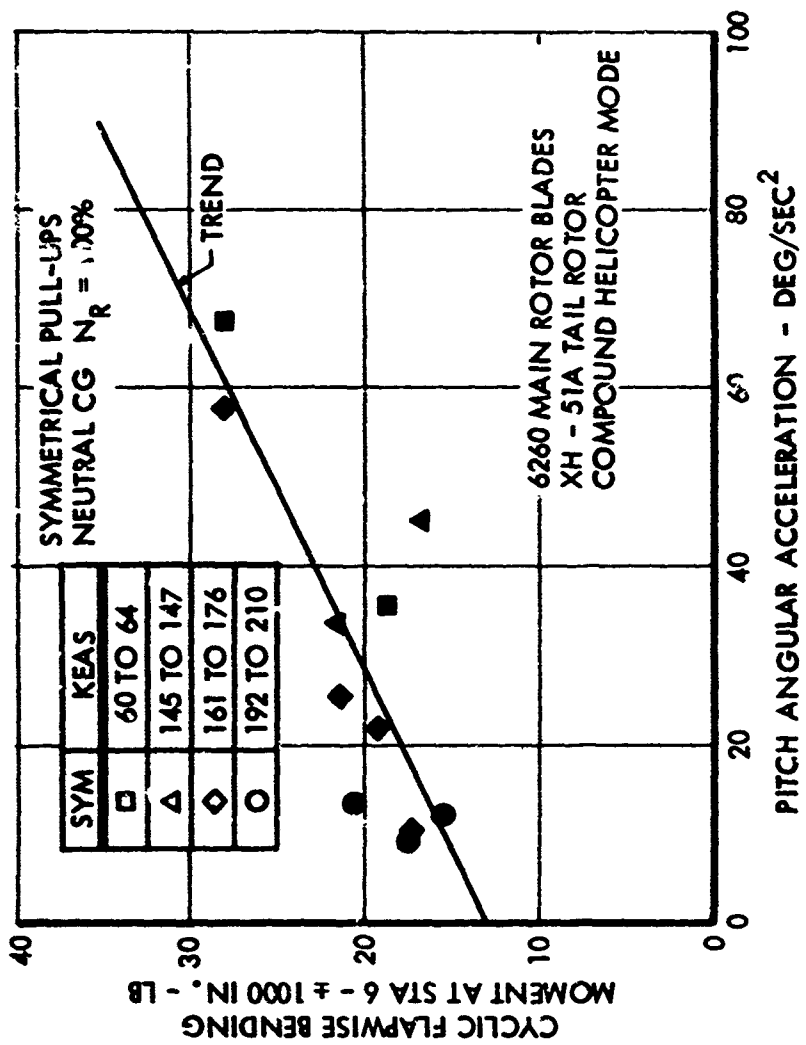


Figure 38. Flapwise Bending Moment at Sta 6 as a Function of Pitch Angular Acceleration.

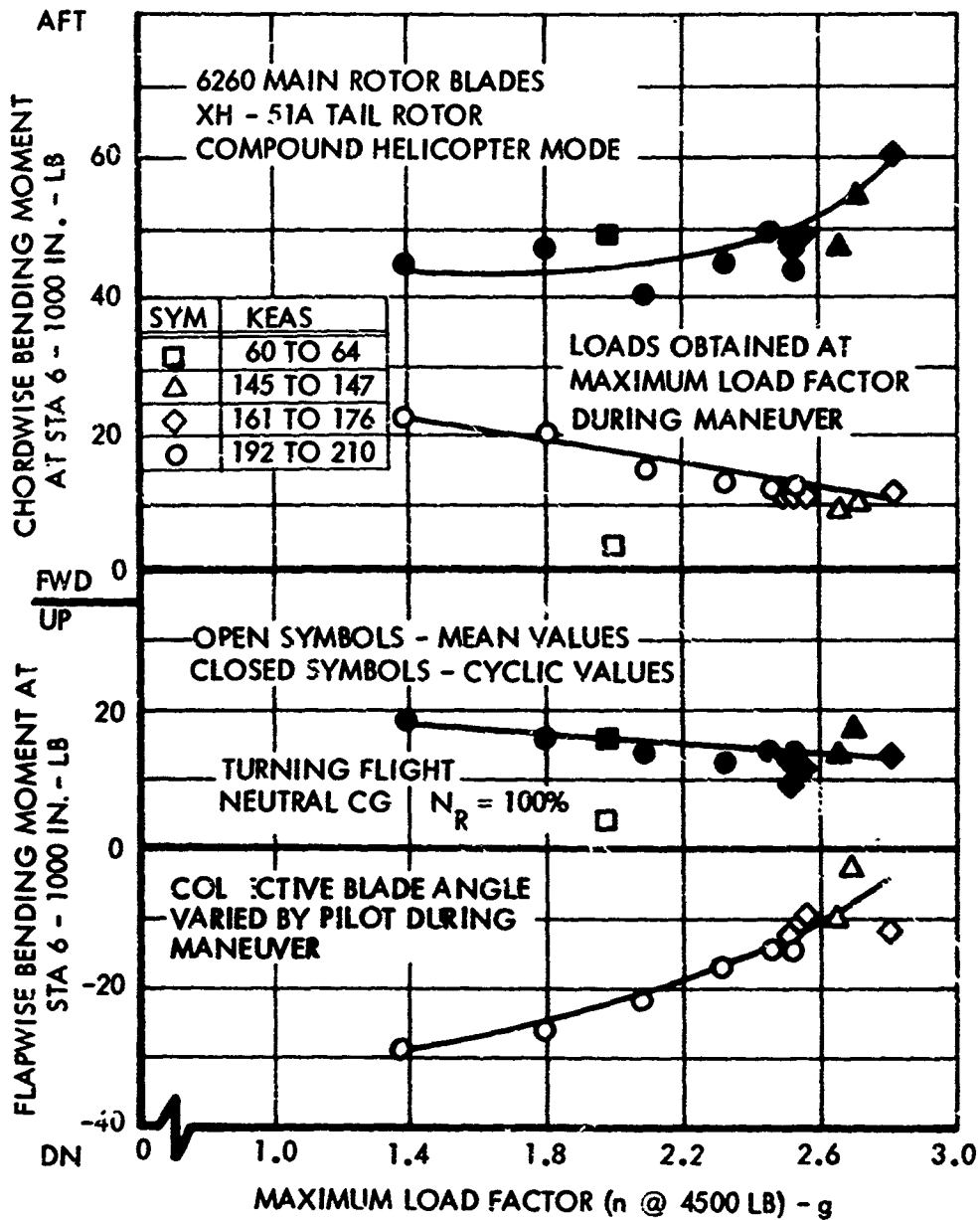


Figure 39. Main Rotor Blade Loads as a Function of Maximum Load Factor.

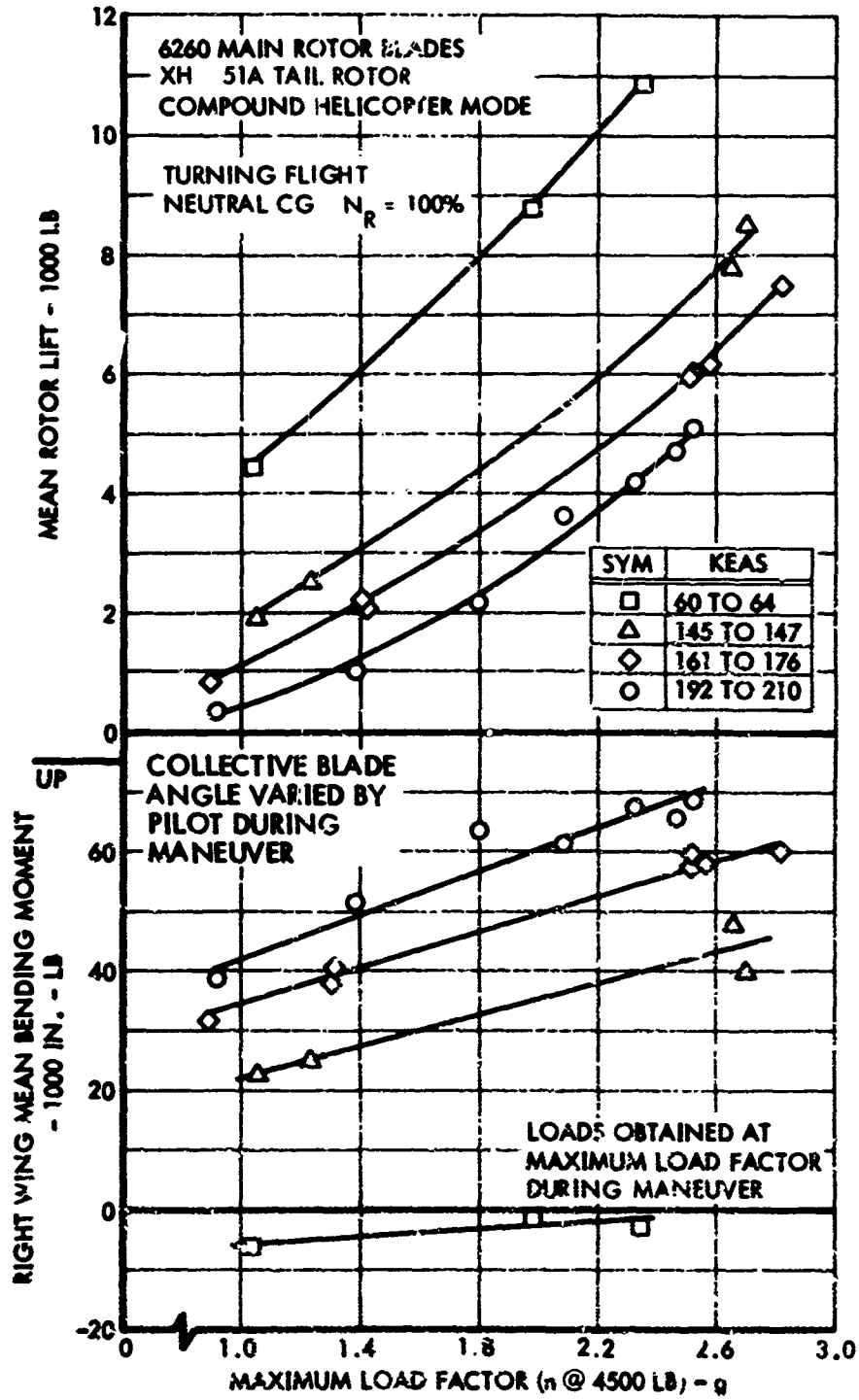


Figure 40. Right wing Bending Moment and Rotor Lift as a Function of Maximum Load Factor.

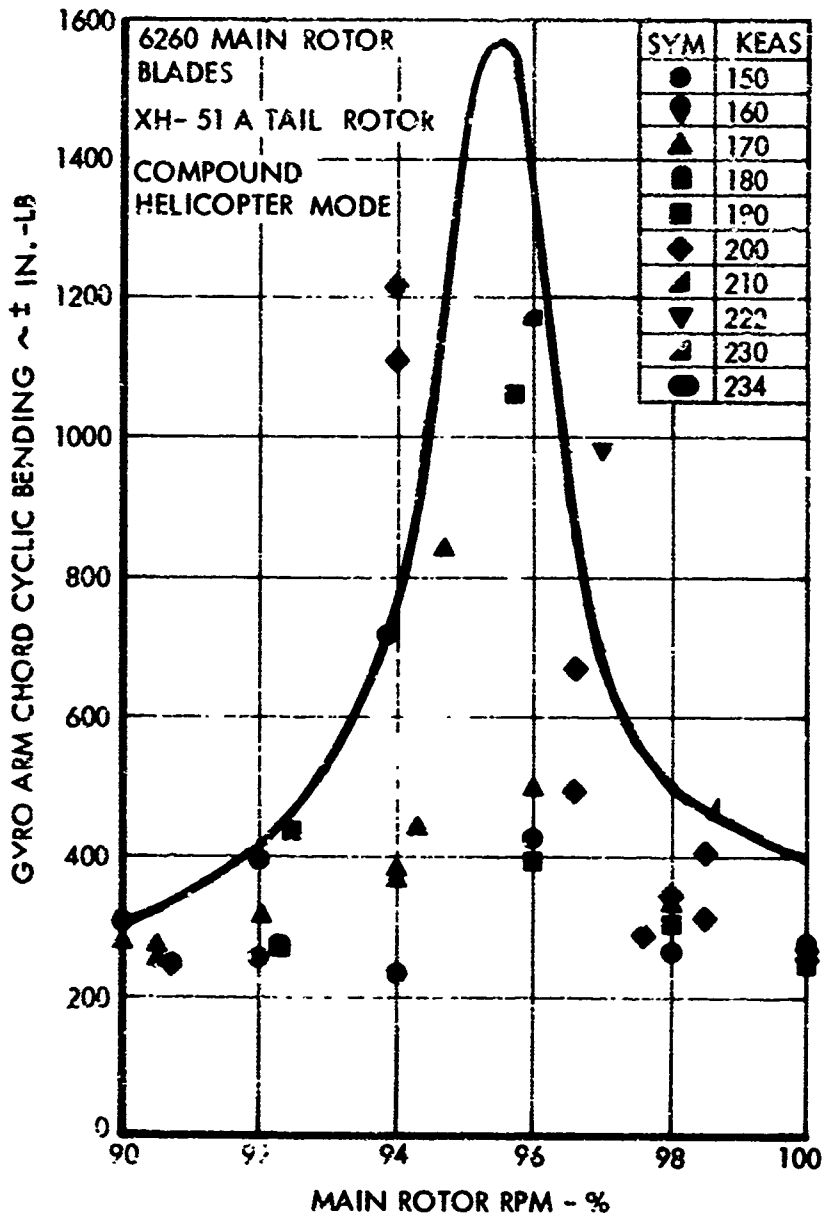


Figure -1. No. 1 Gyro Arm Chord Cyclic Bending Moment as a Function of Main Rotor RPM.

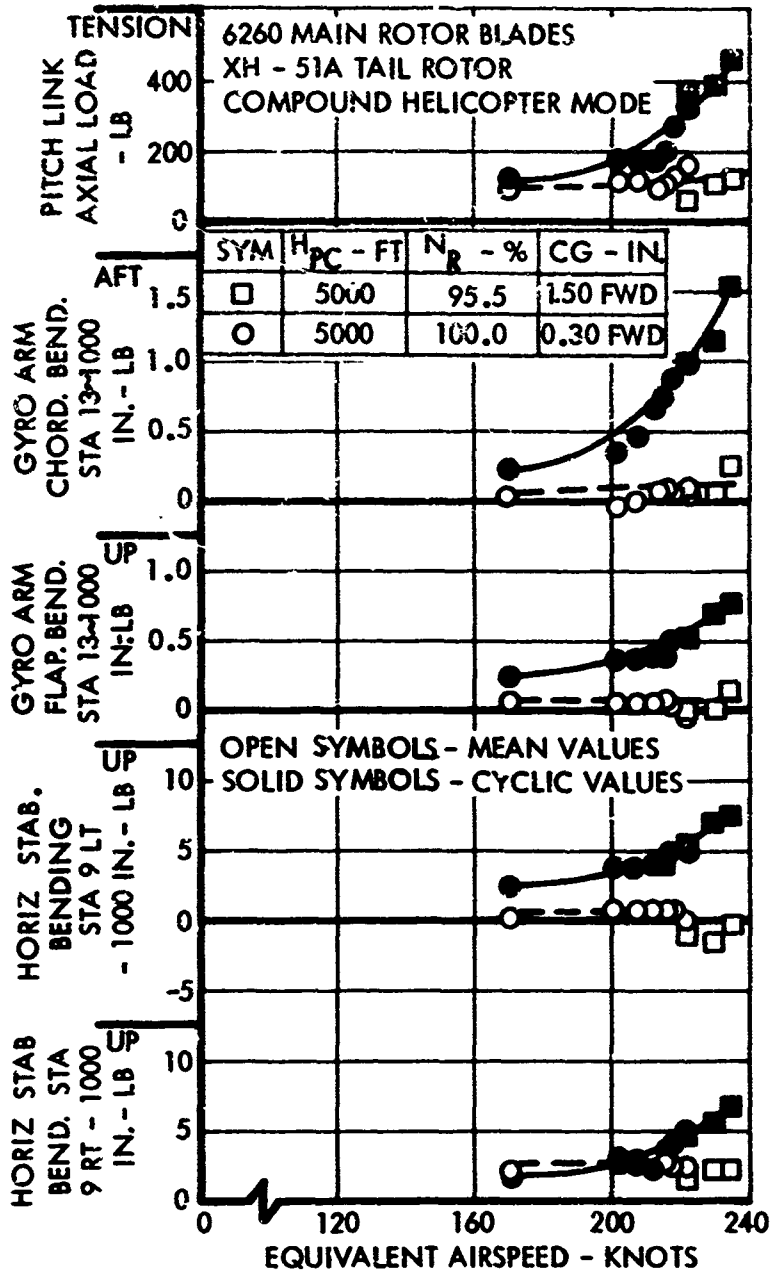


Figure 42. Horizontal Stabilizer, Gyro Arm, and Pitch Link Loads as a Function of Equivalent Airspeed.

Maximum cyclic load in the gyro arm flapwise bending was 783 inch-pounds at 234 KEAS. This load produces a stress of 8100 psi in the titanium gyro arm section and 2300 psi in the aluminum hub section.

Assuming that the flap and chord loads are in phase, the maximum possible stresses in the titanium are 12,650 psi and 4250 psi in the aluminum. The titanium stresses are well below the endurance limit for titanium, however, the 4230 psi stress in aluminum is slightly above the estimated endurance limit of 4000 psi. This stress exceeding the endurance limit of the aluminum hub occurred only at the highest speed point. For the next lower speed of 230 KEAS, the combined stresses are 3500 psi. The total time spent above 230 KEAS is less than one-half minute. The gyro arm loading frequency in flap is at four-per-revolution of the main rotor (24 CPS) so that the total number of cycles exceeding the endurance limit is less than 720, which would result in negligible fatigue damage.

Vibration

Vibration level in the cabin was measured as the speed was increased to 234 KEAS (Figure 43). This curve shows the sharp rise in vibration, especially the cabin longitudinal vibration, as the speed approaches 205 KEAS (≈ 0.9 Mach number of the advancing blade tip). This increase in vibration is due to the rise in three- and five-per-revolution cyclic moments of the main rotor as shown in Figure 34. This excessive vibration was one of the main factors limiting further high-speed exploration.

Rotor Plane Oscillations

In the early testing with the standard XH-51A 6260 blades, rotor plane oscillations were not encountered at speeds up to about 215 KTAS throughout the normal collective blade angle range and for rotor RPM settings from 90 to 100 percent. However, as the speed was increased at rotor RPM's below about 95 percent and with low collective blade angles, oscillations were encountered. The attempt to obtain maximum speeds with rotor RPM reduced to about 90 percent was limited by these rotor plane oscillations. Sufficient data were not obtained at various RPM and airspeed combinations to firmly establish the boundary. However, it appears that the airspeed limit for rotor plane oscillation would increase about 8 to 10 knots for each 1-percent increase in RPM. See Figure 5 (RPM/airspeed envelope diagram) for the actual RPM/airspeed boundary obtained.

It was found that airspeed strongly affected rotor plane oscillations. For a given rotor configuration with the RPM and collective blade angle at settings which would produce an oscillation at some airspeed, increasing airspeed increased the severity of the oscillation.

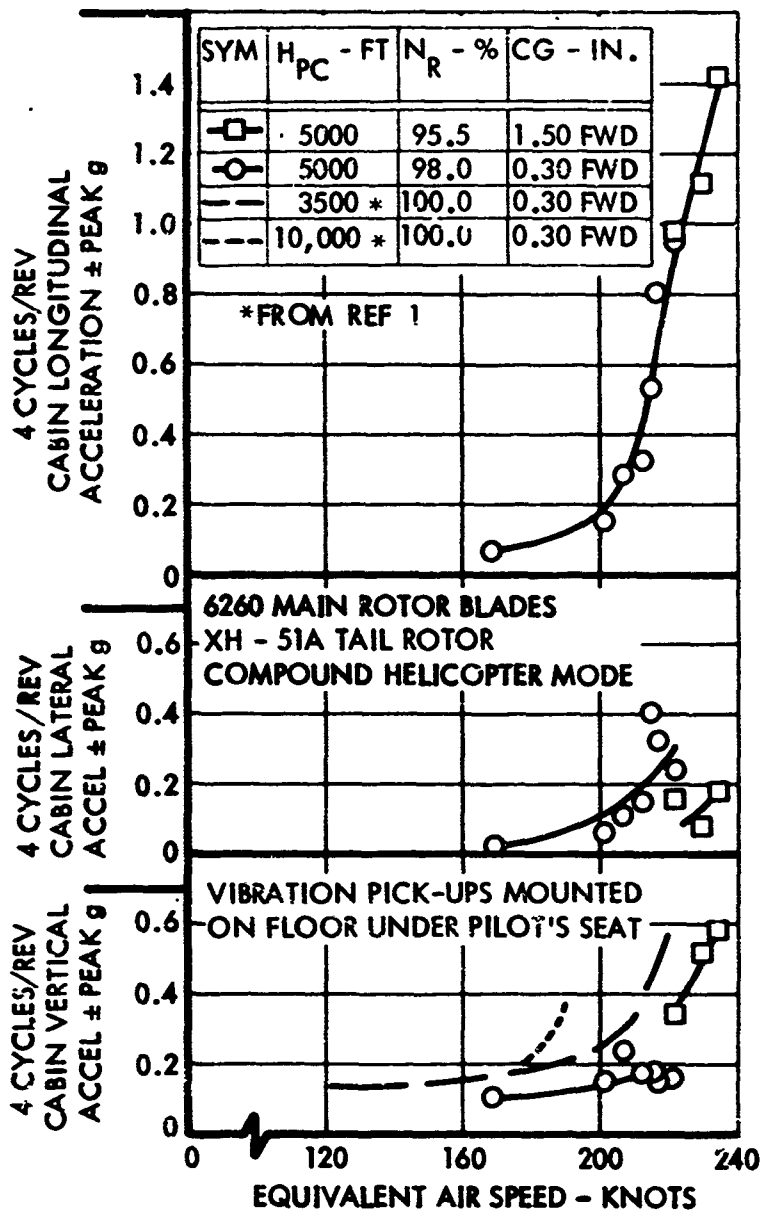


Figure 43. Cabin Vibration as a Function of Equivalent Airspeed.

The most severe rotor plane oscillation encountered was during an auto-rotation entry at 23 KEAS and 93 percent RPM. The body frequency was about halfway between one-half and one-third per revolution of the main rotor. The maximum amplitude of excursion in cg vertical acceleration at this frequency was about 1.5g. Pilot control motions induced by the oscillation contributed some to the rotor plane oscillation severity.

As described previously, no additional rotor configurations were tested during this program. The rotor plane oscillation phenomenon was observed in both configurations and was strongly related to the first in-plane natural frequency of the blades. Generally, the oscillation occurred when the in-plane frequency was a value such that subtracting one from the frequency, to convert from the rotating system to the nonrotating system, would result in a frequency of body motion that was an even fraction of rotor rotation, such as one-half or one-third per revolution. However, this did not always happen and some of the body motions encountered were at an odd fraction of rotor rotational frequency.

With 6261 Model 286 prototype blades installed, rotor plane oscillation was encountered at 96 to 98 percent rotor RPM and low collective blade angle with the body motion at one-half per revolution. With 6260 standard Xh-blade blades plus 20-pound anti-nodal weights installed, rotor plane oscillation with a body motion at one-third per revolution was encountered at 98 to 100 percent RPM and high collective blade angles. The 6260 blade with added weights had a lower chordwise natural frequency. Collective blade angle has an effect on the blade in-plane natural frequency so that increasing the collective blade angle reduces the natural frequency. This contributed to the different frequencies of body motion noted above.

An analytical study of the phenomena is presently under way. It is expected that further tests to resolve the problem will be conducted incorporating configuration changes suggested by the results of this analysis.

Horizontal Stabilizer Loads

Structural loads of the horizontal stabilizer obtained during build up to the maximum speed of 234 KEAS are shown in Figure 10. The maximum cyclic loads obtained are 6900 inch-pounds for the right side and 7600 inch-pounds for the left side. These loads are well above the estimated endurance limit of 4000 inch-pounds. A conservative cumulative damage analysis was accomplished for the left stabilizer using the same time estimates obtained for the main rotor hub as described on Page 60. Results of this analysis indicated that about six percent of the stabilizer fatigue life was used in the high-speed flying. This is acceptable for a high speed research vehicle.

Pitch Link Loads

The maximum cyclic pitch link axial load was only 470 pounds, as compared to an estimated endurance limit of 1400 pounds. The loads obtained during buildup to maximum speed are shown in Figure 42.

Miscellaneous Loads

Miscellaneous loads and positions that were measured up to the maximum speed of 234 KEAS are shown in Figure 44. These measurements include collective blade angle, rotor lift, and right wing bending moment.

Tail Rotor Loads

Three tail rotor configurations were flown during the maneuverability program. These three tail rotor configurations were identified as Part Number 541618-1 Assembly - 6.3-foot-diameter rotor with Model 286 blades and 15 degrees delta-3; Part Number 541618-1 FT 1494 Assembly - 6.0-foot-diameter rotor with 37 degrees delta-3; and Part Number 540571-3 Assembly - 6.0-foot diameter standard XH-51A rotor with 15 degrees delta-3.

Structural loads in the 6.3-foot-diameter Model 286 tail rotor were measured at speeds up to 200 KEAS. This tail rotor was evaluated because it had a first antisymmetric loading frequency that was further removed from three-per-revolution frequency of the tail rotor. A sizeable reduction was anticipated in blade flap bending loads as compared with the standard XH-51A blade as shown in Figure 38 of Reference 1. The reduced loads were realized; however, excessive teetering and undesirable force feedback to the rudder pedals were encountered at higher speeds.

As a result of the excessive teetering and undesirable force feedback to the rudder pedals, the tail rotor was modified to reduce the diameter from 6.3 feet to 6.0 feet to help alleviate the force feedback. In addition, delta-3 was increased from 15 to 37 degrees to alleviate the excessive teetering.

The reduced diameter and increased delta-3 tail rotor blades were reinstalled. Loads obtained with this tail rotor were reduced even more; however, at the higher speeds, the pilot still reported undesirable random low-frequency oscillations with directional kicks and rudder pedal force feedback. It was considered that further investigation of this phenomenon was not significant to this contract; therefore, the 6-foot-diameter 286 tail rotor was removed, and the 6-foot-diameter XH-51A tail rotor installed.

Tests were then conducted at various RPM's from 90 to 100 percent at various forward speeds. Tail rotor flapwise bending moment at station 16.8, tail rotor collective blade angle, tail rotor teeter angle, tail

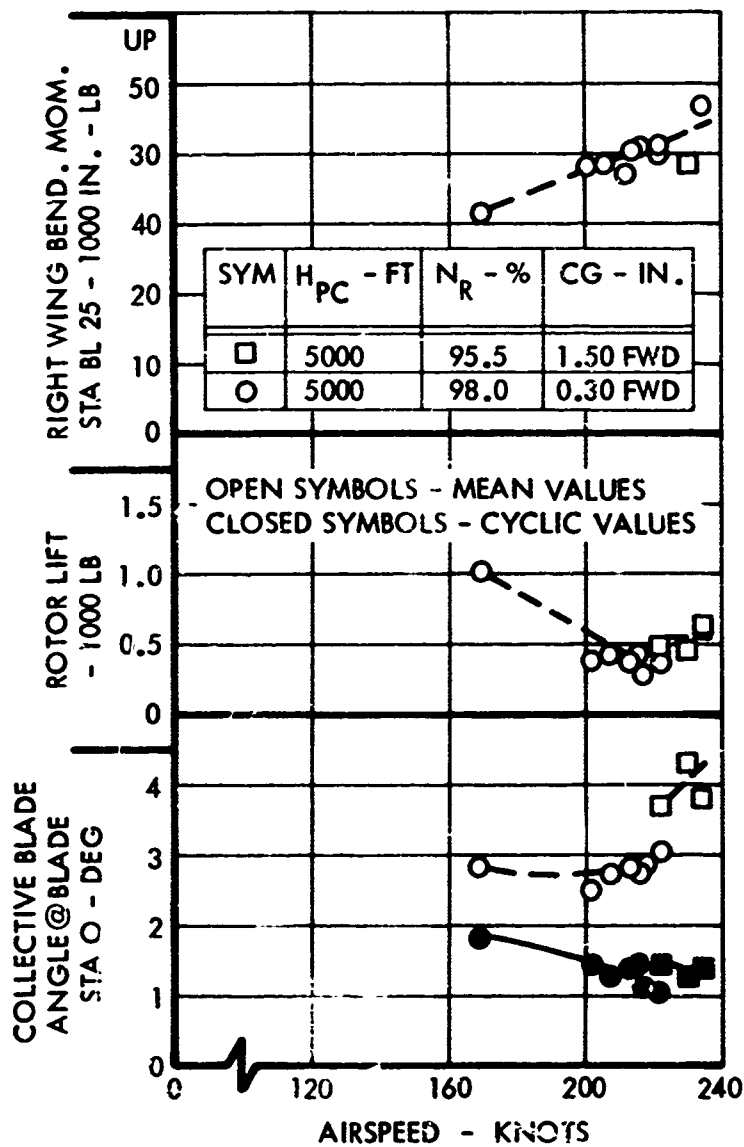


Figure 44. Collective Blade Angle, Rotor Lift, and Right Wing Bending Moment as a Function of Equivalent Airspeed.

rotor shaft horsepower, and tail rotor pitch and axial loads are plotted versus calibrated airspeed for speeds up to 234 KEAS (Figure 45).

Analysis of the previous XH-51A tail rotor loads and structural properties showed that Station 16.8 was the most critical station. Therefore, only flapwise bending at Station 16.8 was instrumented and measured during these tests. Maximum cyclic load at Station 16.8 was 1240 inch-pounds at 98 percent RPM at 221.5 KEAS. The cyclic load with the RPM reduced to 95.5 percent at 234 KEAS was only 1050 inch-pounds. The 1240 inch-pound cyclic load is only slightly over the 1060 inch-pound estimated endurance limit for this section.

This estimated endurance limit of 1060 inch-pounds was raised from the 760 inch-pounds used in Reference 1 by taking advantage of fatigue test data that were obtained for Federal Aviation Agency certification of the Model 286 helicopter, which has a similar tail rotor blade construction. The 760 inch-pound endurance limit was based on an allowable endurance limit stress of 15,000 psi.

Nap-Of-The Earth Testing

Maximum main rotor hub loads obtained during the terrain-following portion of the nap-of-the-earth testing were during the high-speed run at 192 KEAS. During these tests, the maximum cyclic flapwise bending moment at Station 6 was 30,500 inch-pounds. This cyclic flapwise bending moment converts to a stress of 13,200 psi at Station 7. The cyclic chordwise bending moment at Station 6 was 52,000 inch-pounds; this converts to a stress of 7,900 psi at Station 7. The sum of the two results is a maximum possible cyclic stress of 21,100 psi at the corner of the hub at Station 7.

During the Army Dozen portion of the nap-of-the-earth testing (except for side hill landings), the maximum cyclic flapwise bending moment of 22,300 inch-pounds converts to a stress of 31,700 psi at Station 6, and the chordwise bending moment of 120,000 inch-pounds converts to a stress of 18,200 psi at Station 7. The sum of the two results is a maximum possible cyclic stress of 49,900 psi at the corner of the hub at Station 6.

Side Hill Landing

Two side hill landings and takeoffs on a right slope (down to the right) of 4.2 and 7.0 degrees were conducted during the Army Dozen nap-of-the-earth testing. The cyclic main rotor flapwise and chordwise bending moments at Station 6 are as follows.

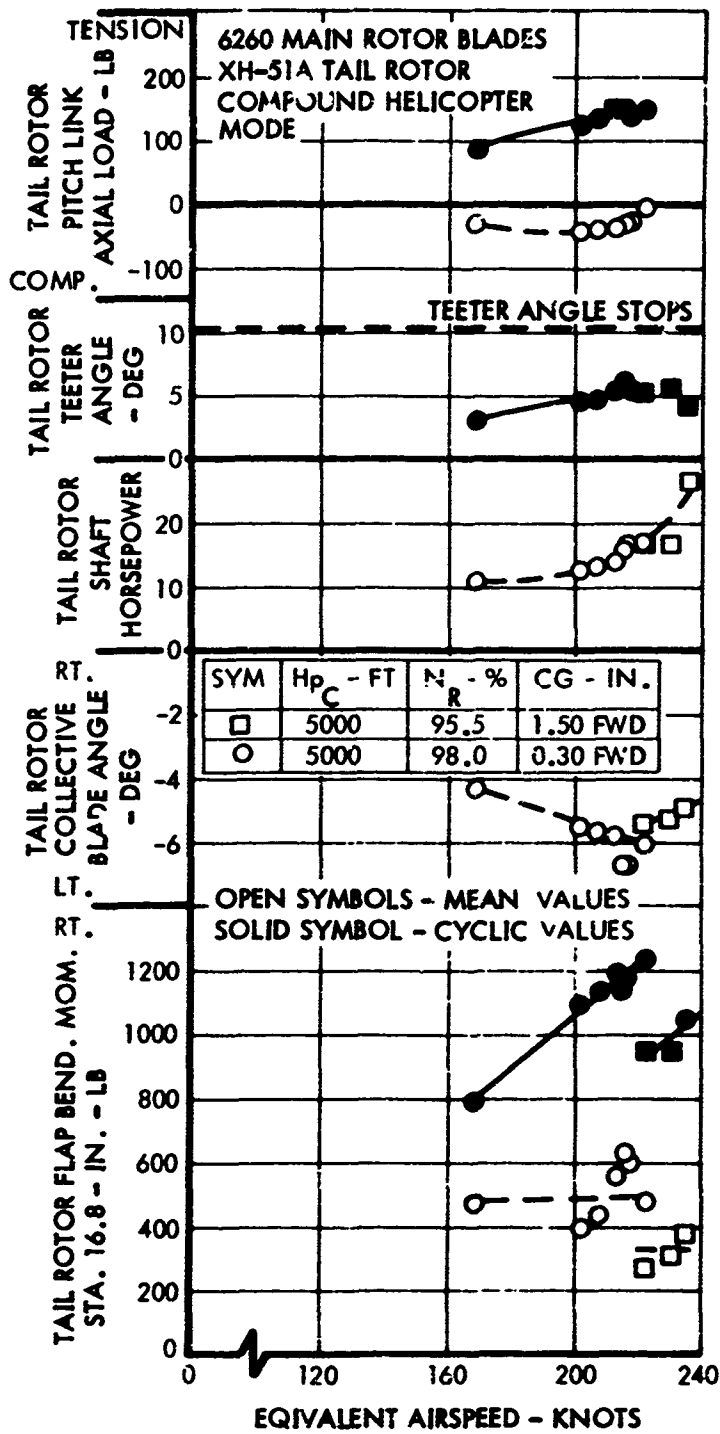


Figure 45. Tail Rotor Loads, Control Positions, and Horsepower as a Function of Equivalent Airspeed.

	<u>Chord Bend at 6</u>	<u>Flap Bend at 6</u>
Landing on 4.2-degree slope	30,600 in.-lb	12,300 in.-lb
Takeoff on 4.2-degree slope	39,400 in.-lb	15,200 in.-lb
Landing on 7.0-degree slope	23,100 in.-lb	18,100 in.-lb
Takeoff on 7.0-degree slope	26,300 in.-lb	14,500 in.-lb

The maximum stress was 29,200 psi during the landing on the 7.0-degree slope.

ROUGH AIR OPERATION

GENERAL

The compound helicopter was flown in turbulent atmospheric conditions at different airspeeds in the range from 125 to 200 KEAS. An instrumented fixed-wing airplane (Beechcraft Baron) was flown in formation with the helicopter to obtain comparative data on CG vertical acceleration for the two types of aircraft.

The flights were made at an average pressure altitude of 1500 feet with the course along the edge of a mountain range so that the ground clearance varied from around 100 feet to over 500 feet. The horizontal separation between the two aircraft was held at about 100 feet. Records were taken only when both aircraft were in rough air over the selected course. The time distribution of recorded and analyzed data for each speed is shown below. Data for the Beechcraft Baron were not obtained at 200 KEAS since this speed was above its level-flight speed capability.

<u>Speed- KEAS</u>	<u>Time in Rough Air - Airplane</u>	<u>Seconds helicopter</u>
125	101.4	101.4
130	294.5	294.5
158	194.1	194.1
177	123.0	123.0
200	-	95.3
Total Time - Sec. =	713.0	808.3
- Min. =	11.9	13.5

The average helicopter weight was 5100 pounds, and the average airplane weight was 4000 pounds.

VERTICAL ACCELERATION DUE TO GUSTS

A time-history showing a comparison of CG accelerations obtained in the two aircraft for a time span of 120 seconds is shown in Figure 46. The equivalent airspeed for this test was 130 knots. The CG vertical

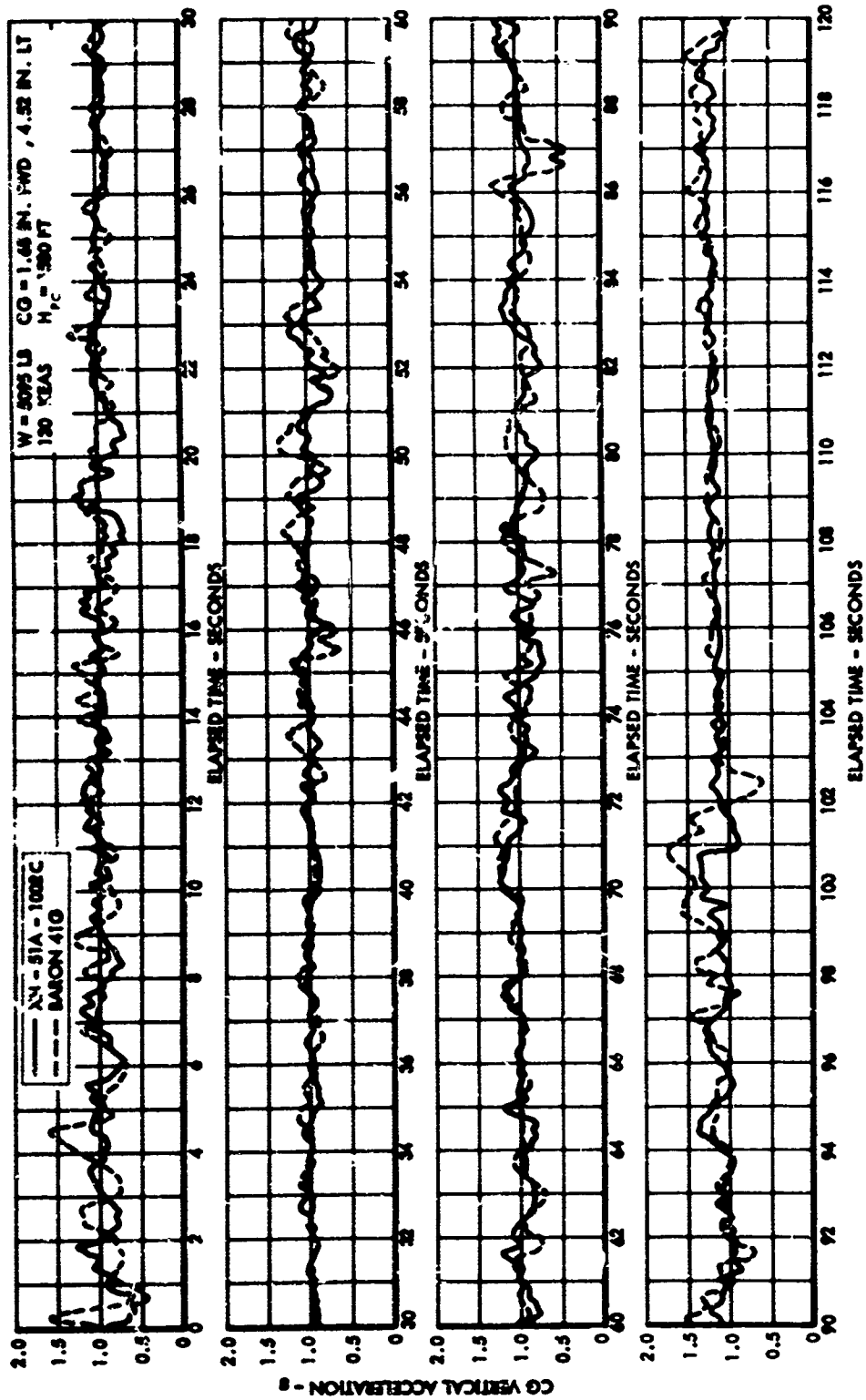


Figure 46. Comparison of CG Vertical Acceleration in Gusts.

acceleration shown is the response of the aircraft to a gust input after fairing out the structural response at approximately 8 cps of the airplane and one per revolution response of the helicopter at 6 cps due to a slight unbalance in the rotor

A statistical analysis of the gust response of the two aircraft was made using the "mean-crossing peak count method" as described in Reference 4 to obtain peak counts of CG vertical acceleration. In this procedure, only one count is made between two successive mean crossings. Either the highest maximum or the lowest minimum is counted. The positive and negative deviations from the mean 1-g level were counted separately. The counting started at the level of $\pm 0.05g$ and was stepped up and down in increments of $\pm 0.1g$, disregarding all maxima and minima in the $\pm 0.05g$ band. The results are shown as number of exceedances plotted in the center of the corresponding g increment.

A comparison of CG vertical acceleration exceedances for the XH-51A compound and the Beechcraft Baron is shown in Figure 47. The data represent a flight time of 4.9 minutes at 130 KEAS. Figure 48 shows a similar comparison for a flight time of 11.9 minutes at various equivalent airspeeds from 125 to 177 knots, the maximum speed where airplane data were obtained. Even though the times involved are quite short and therefore represent only a small statistical sample, it is evident for both the airplane and the helicopter that there was no significant change in the shape and slope of the load factor distribution curves. Therefore, it is reasonable to presume that if a considerably longer sample had been obtained over the same course, there would be no significant change in distribution, just a greater count at each g level and possibly a higher peak g value.

The compound helicopter load factor increments for the total time averaged about three-fourths of the airplane load factor increments. The airplane shows a nearly symmetric response for both positive and negative load factor increments. The helicopter had slightly less response in the negative direction as compared to its positive response, especially at higher load factors.

Pilot comments on flying the compound helicopter in rough air are given below:

"The compound helicopter's flight through rough air at a forward center of gravity is very comfortable and it is more stable than most airplanes. In the 150 to 200 KEAS range, it can be trimmed for hands-off flight and gusts will not disturb the flight path for long periods of time.

"With a neutral center of gravity the helicopter has a sharp momentary nose-down pitch at the peak of a gust that gives an unstable feeling, especially at high speed. However,

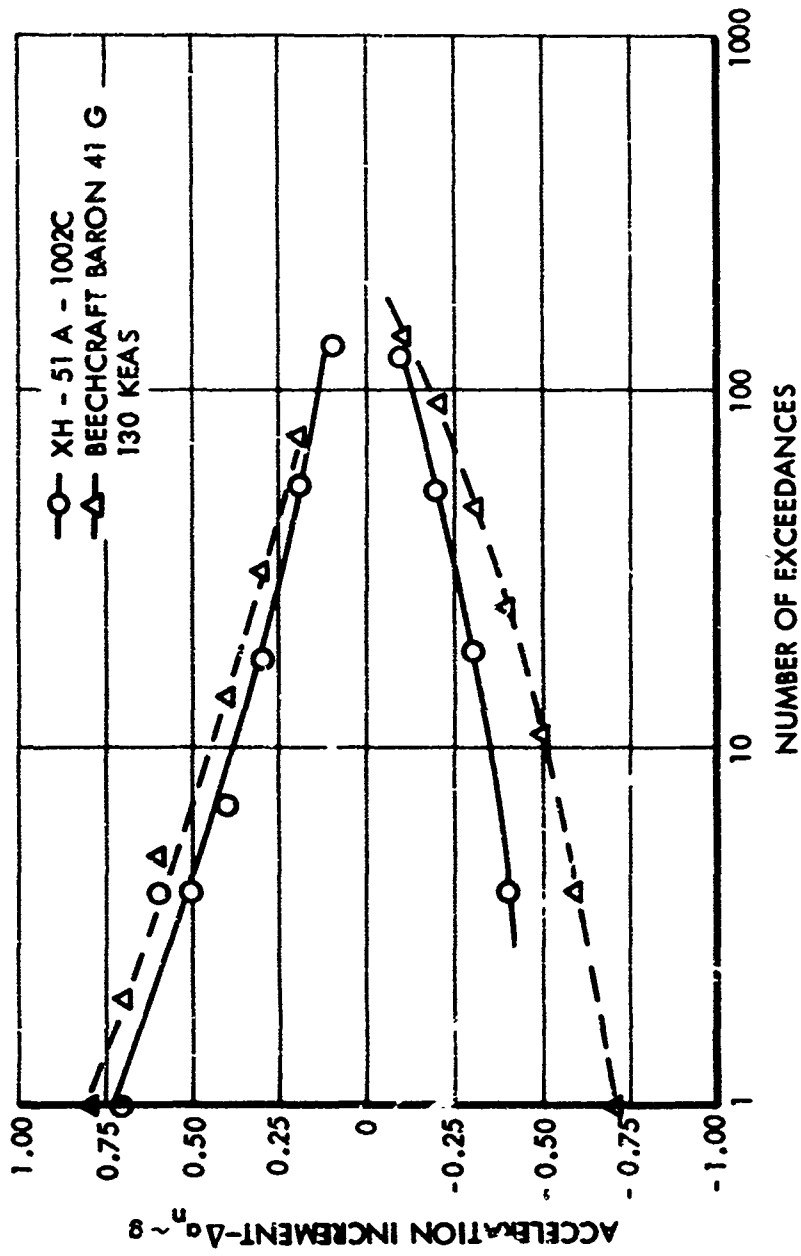


Figure 47. Exceedance of CG Acceleration Increments in Rough Air for a Test Time of 4.9 Minutes.

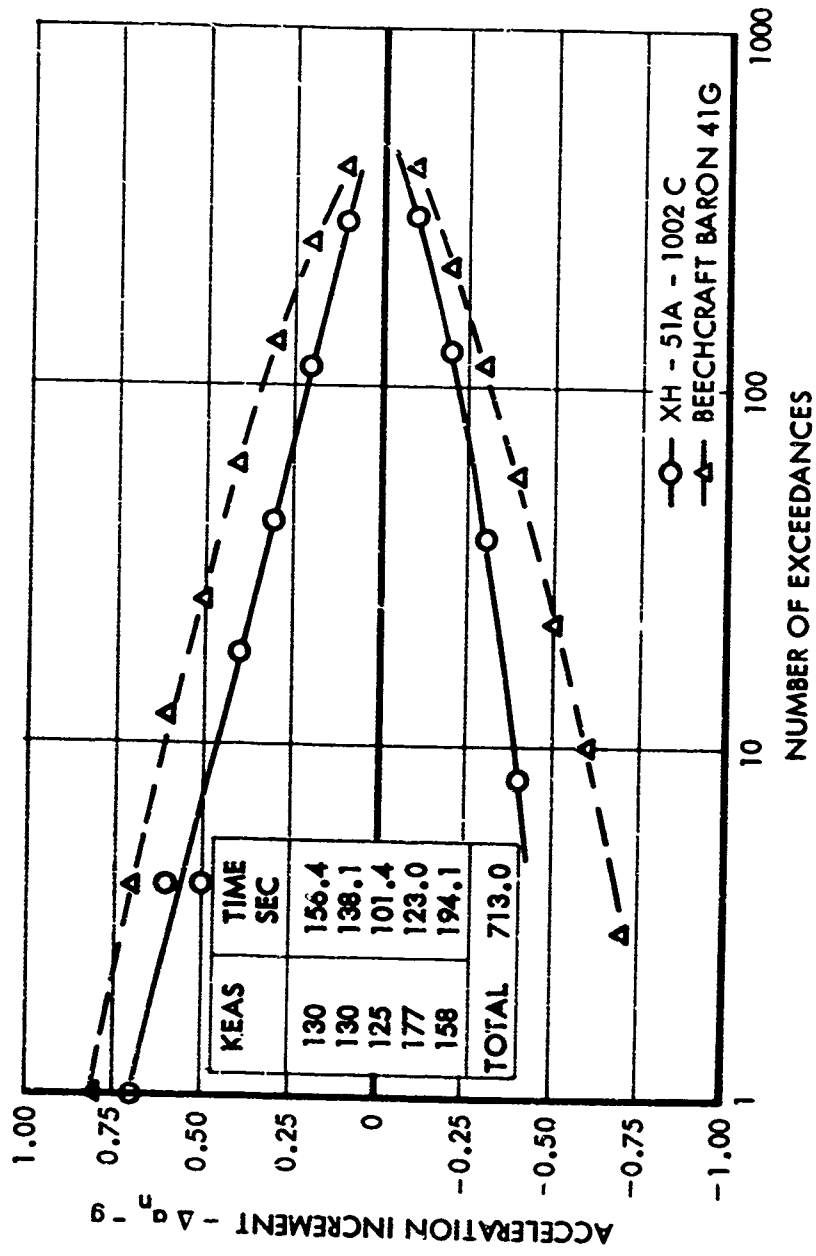


Figure 4d. Exceedance of CG Acceleration Increments in Rough Air for a Test; Time of 11.9 Minutes.

in rough air with the Beechcraft Baron alongside, the airplane was bouncing around much more than the compound helicopter was."

The load factor count for the helicopter for the full time of 13.5 minutes is shown in Figure 4. These data include one test at 200 KEAS. The general shape and slope of the distribution curves are similar to those obtained for shorter times. This further corroborates the contention that the relative load factor distribution obtained is a reasonable representation for any time period for the same type of terrain and terrain clearance.

DERIVED GUST VELOCITIES

Gust velocities were derived from the CG vertical acceleration peaks for both the airplane and the compound helicopter. The gross air minus g peaks were added together and calculations were made to convert from peak count to nautical miles to reach or exceed a given gust velocity. The results obtained for both aircraft are shown in Figure 5. The two sets of data are in close enough agreement that a single training represents both. The good agreement obtained indicates that both vehicles experienced essentially the same gust environment. Derived gust velocities in the 20 to 24-feet per second range were obtained about every 15 miles, indicating that the atmosphere encountered was quite turbulent. A comparison is made with data obtained with an OV-10A airplane during training missions at an altitude range of 1000 to 2000 feet (Reference 3, Figure 3). Assuming that the OV-10A data include the sum of positive and negative gusts, the environment for the XH-51A compound helicopter contained gusts with a derived gust velocity of 12 feet per second about 50 times more frequently than did the OV-10A environment. At higher gust velocities, the ratio was even greater.

The airplane-derived gust velocities were calculated using the generally accepted equation for airplanes shown in paragraph 2.1 of Reference 5. The compound helicopter-derived gust velocities were calculated using an equation which combined the airplane equation with an equation for computing helicopter rotor gust load factors as shown in Reference 6. The gust alleviation factor was computed for the airplane parameter of the compound helicopter assuming that the aircraft was strictly an airplane and that the wing supported the entire weight. The same gust alleviation factor (0.84) was arbitrarily applied to the helicopter rotor portion of the equation. The good agreement obtained in the derived gust velocities of the two aircraft indicates that this assumption of alleviation factor was reasonable. The derived gust velocities for the rotor of the compound helicopter were also computed using a method independently developed by Lockheed. The results obtained were essentially identical to those obtained using the reference equation.

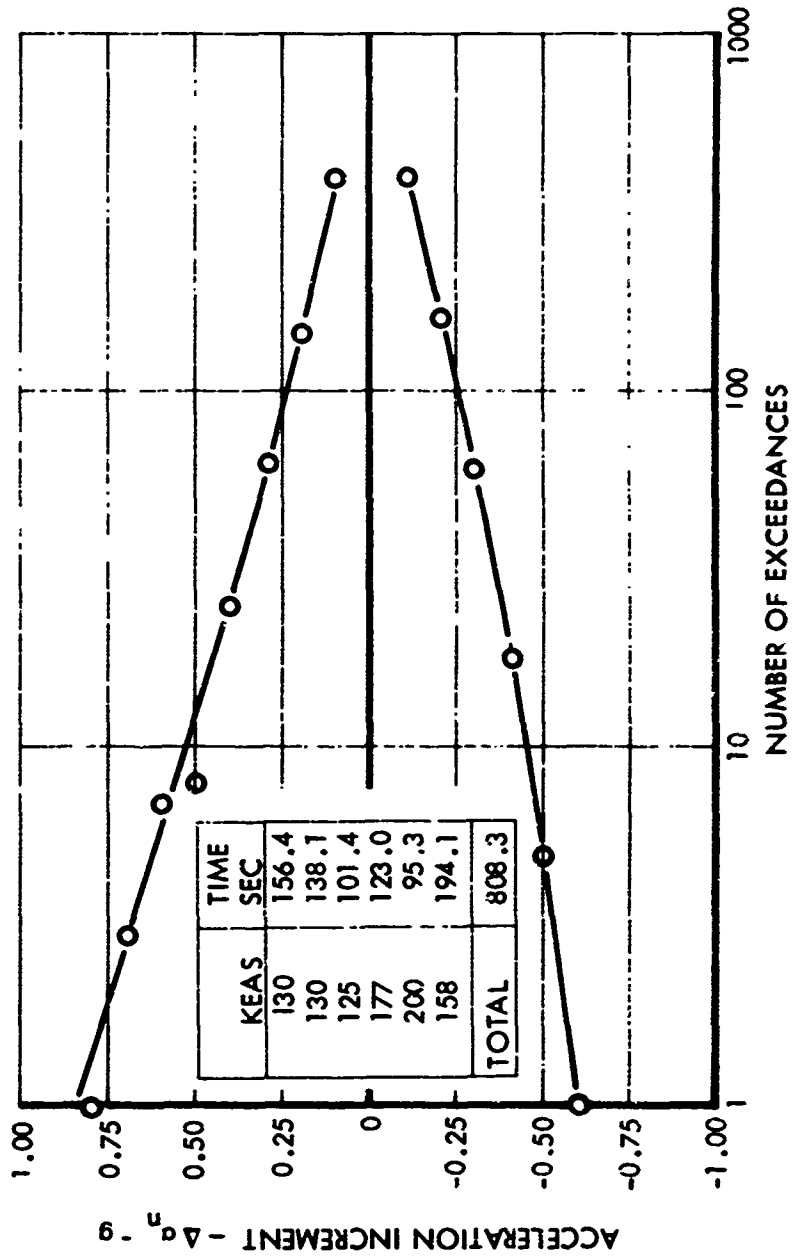


Figure 49. Exceedance of CG Acceleration Increments in Rough Air for a Test Time of 13.5 Minutes.

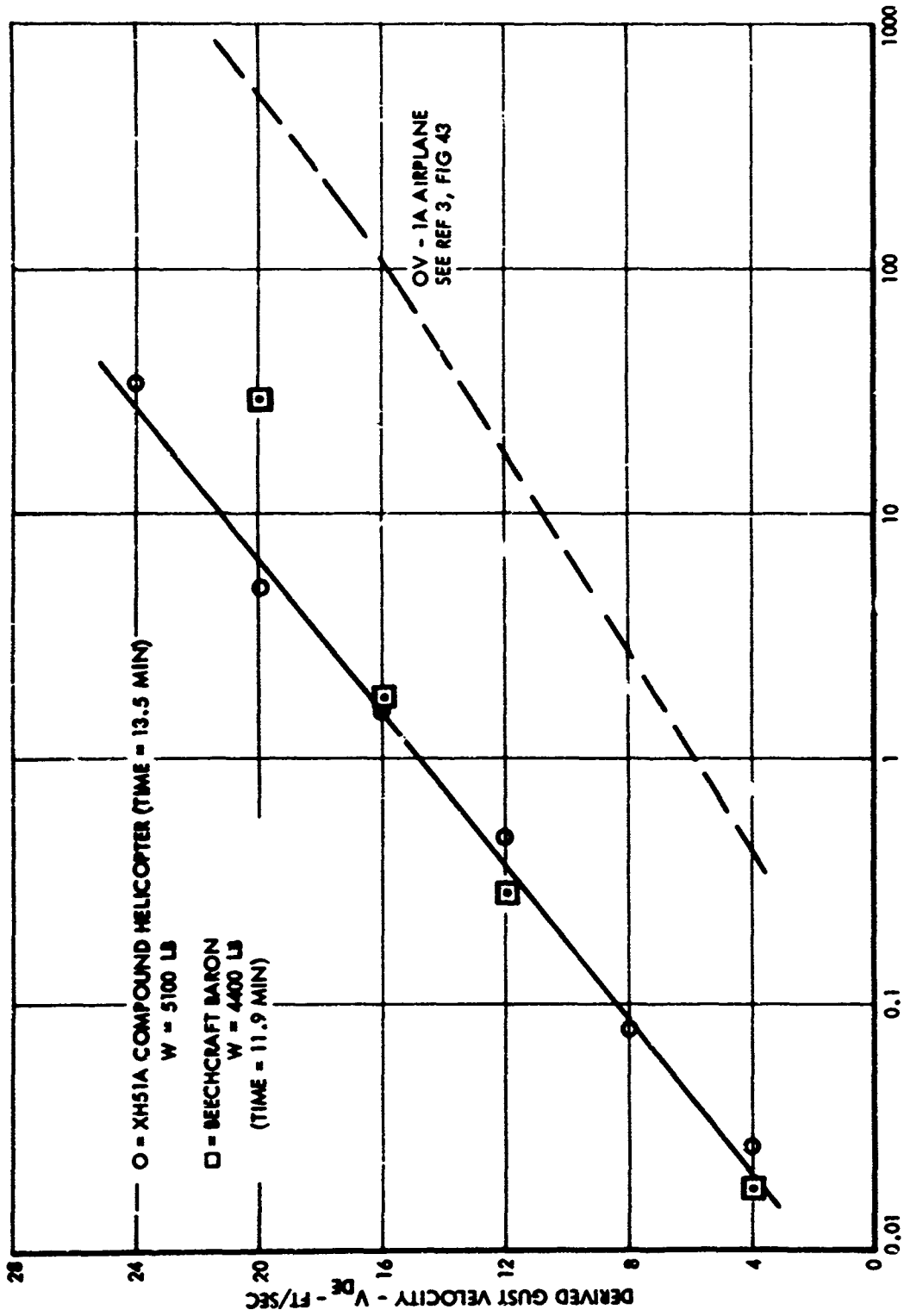


Figure 50. NAUTICAL MILES TO REACH OR EXCEED DERIVED GUST VELOCITY
Distance to Reach or Exceed a Given Gust Velocity.

MAIN ROTOR LOAD MEASUREMENTS

Main rotor chordwise and flapwise bending moment measurements on the hub at Station 6 were obtained during the flights in rough air. Time-histories of these measurements for speeds of 130 and 200 KEAS are shown in Figures 51 and 52. Also shown are CG acceleration, pilot control positions, and derived gust velocity. The chordwise cyclic moments are at one-per-revolution frequency and appear to be essentially a direct function of load factor. The flapwise cyclic moments have a high two-per-revolution component of load in addition to the one-per-revolution loads. The mean flapwise load is a function of load factor, but the cyclic component is not directly related to load factor. As explained previously in the Structural Loads portion of the Agility and Maneuverability section, the cyclic component is mainly a function of angular acceleration in pitch.

Statistical analysis of the flapwise and chordwise bending moments has been performed using the range-pair count method as described in Reference 4. A range pair consists of a pair of ranges of opposite sign where the range is defined as the difference between two successive extreme values of the variable load. A positive range goes from a minimum to a maximum and a negative range goes from a maximum to a minimum. One half of a range is called the cyclic value. In the following data presentation, only cyclic values are shown. Each range pair to be counted consists of a positive increment exceeding a prescribed threshold value combined with the next negative increment exceeding the same prescribed magnitude. Load variations below the prescribed value are disregarded. The prescribed threshold value, the exceedance of which is being counted, is increased in steps up to the maximum load expected, starting with a low threshold value. New exceedance counts are obtained for each threshold level. By this counting procedure, the frequently occurring low loads are counted when the threshold level is low, while large-amplitude mean load variations at low frequency are counted when the threshold level is high.

The gust loading spectrum of chord bending at Station 6 for the total time of 13.5 minutes is shown in Figure 53. A steady flight spectrum for the same speeds and time distribution is also shown. The maximum chordwise loads in the rough air encountered are about 40 percent greater than the maximum level flight loads.

Gust loading spectra for flap bending at Station 6 are shown in Figure 54. Spectra are shown for 4.9 minutes at 130 KEAS and for the total time of 13.5 minutes. Also shown are level flight spectra for comparable times and speeds. The curve for 4.9 minutes at 130 KEAS and the curve for total time have essentially the same slope and distribution. This further verifies the load factor count data and indicates that even though the total sample obtained is fairly small, it is large enough to produce reasonably valid statistics on load factor and rotor blade load distribution in rough air.

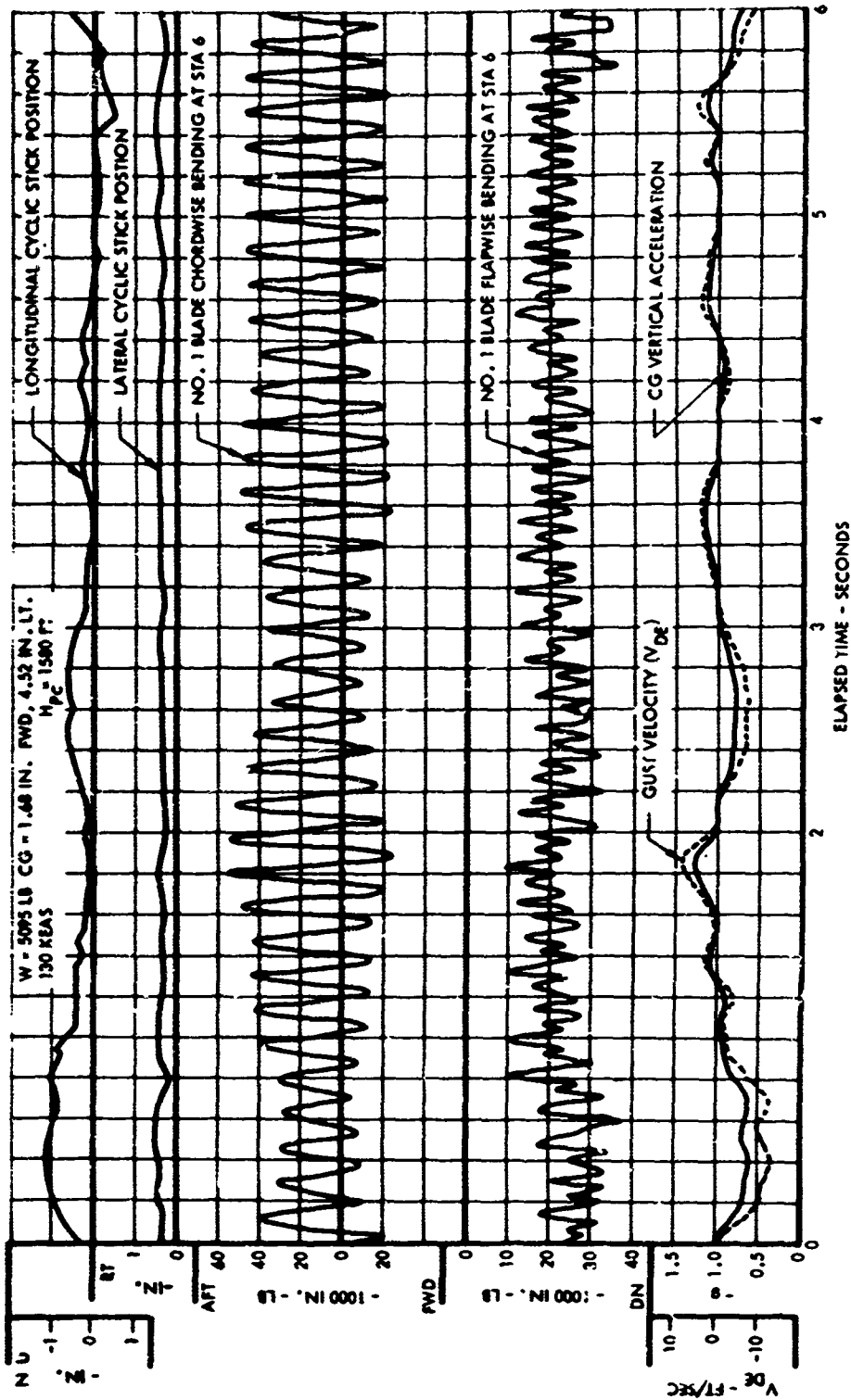


Figure 51. Time History of Blade Loads and CG Vertical Acceleration in Turbulence at 130 KEAS.

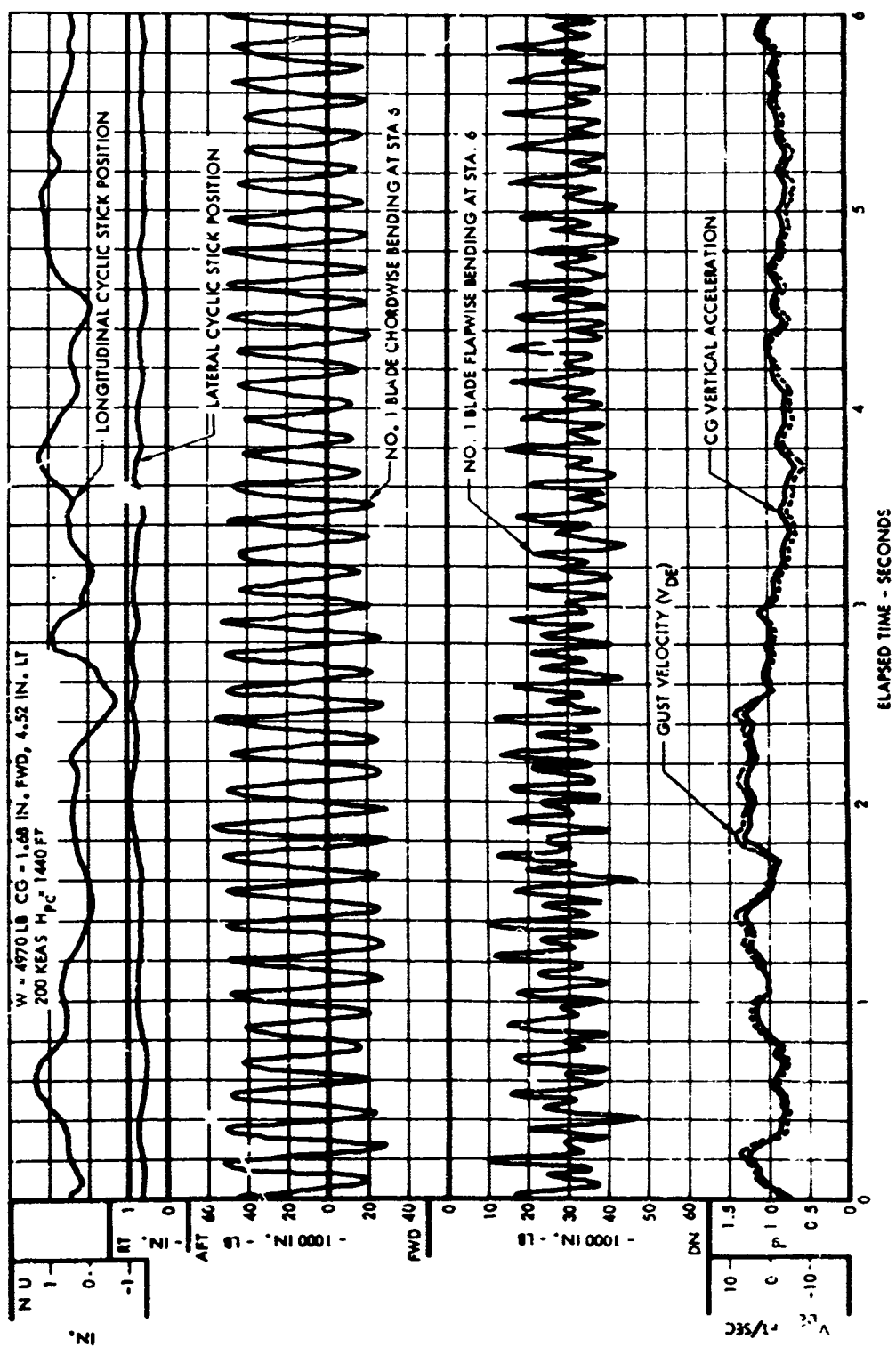


Figure 52. Time History of Blade Loads and CG Vertical Acceleration in Turbulence at 200 KEAS.

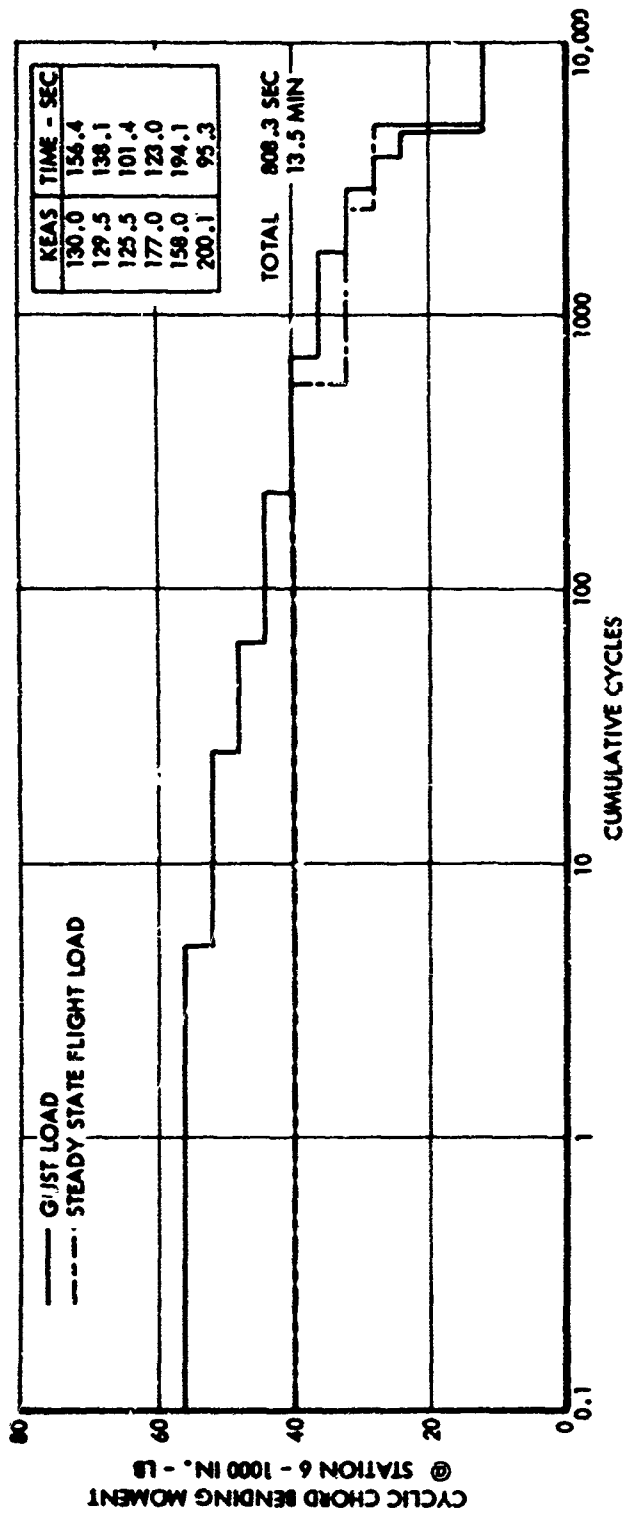


Figure 53. Gust Loading Spectrum - Chordwise Bending Moment at S.a. 6.

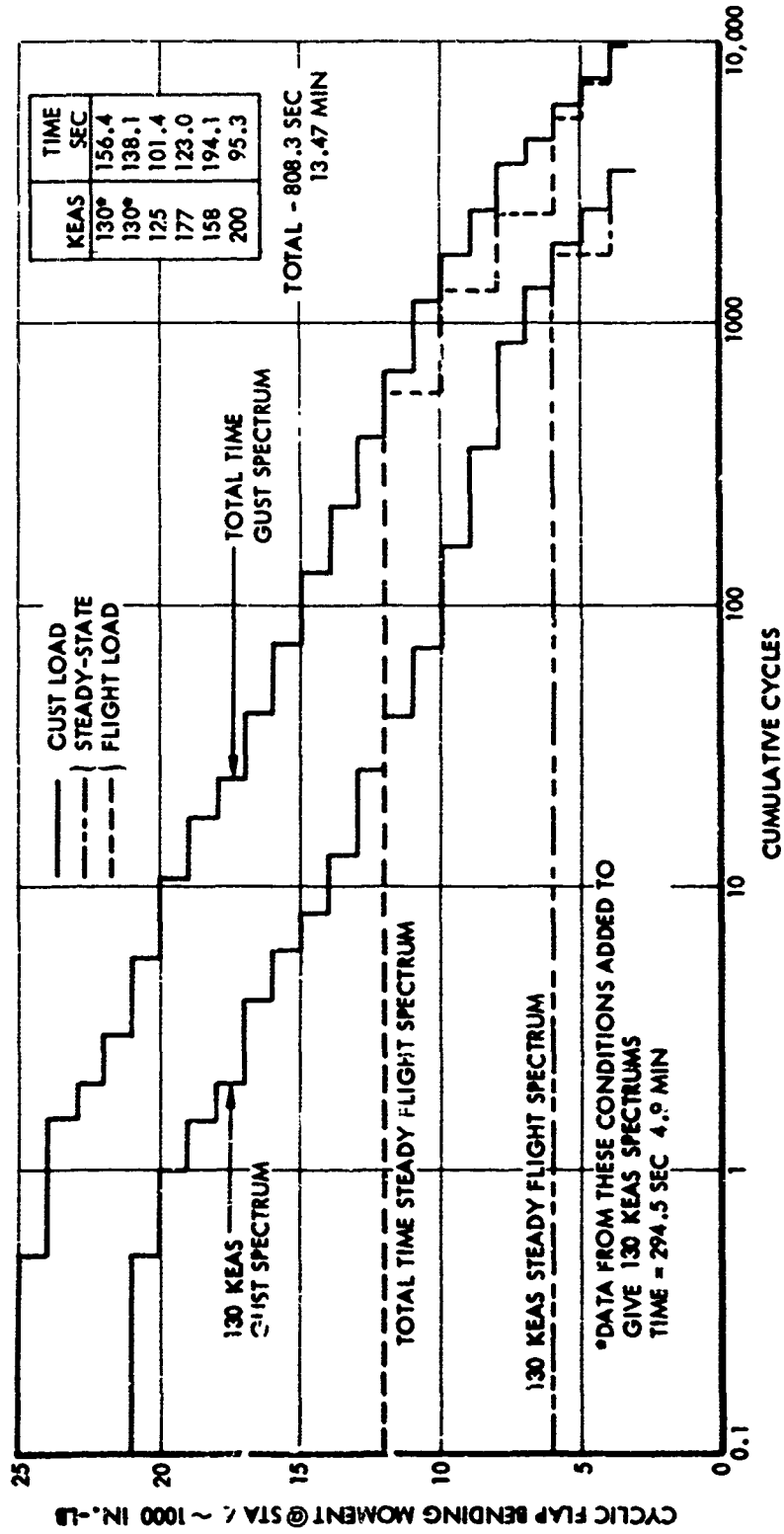


Figure 54. Gust Loading Spectrum - Flapwise Bending Moment at Sta 6.

The maximum flapwise loads encountered in rough air are about double the maximum steady flight loads. Thus, the flap bending loads are relatively more sensitive to rough air than are the chord bending loads. From a fatigue stress standpoint, the flapwise loads are significantly greater in importance, since the hub stresses due to chord moment are quite small compared to those due to flap moment.

For the total time spectra, the load count due to gusts is greater at all load levels than the count for steady flight. However, to get an approximate assessment of the effect of rough air on main rotor fatigue life, the relation between the rough air loads and the loading levels corresponding to endurance limit stresses has to be obtained. Using the known section properties of the critical area of the hub and an endurance limit stress conservatively estimated at 26,000 psi, the endurance limit loads would be a flap moment of about 14,000 in.-lb in combination with a chord moment of 44,000 in.-lb.

For the total time gust spectra of 13.5 minutes, the endurance limit flap moment of 14,000 in.-lb is exceeded for 130 cycles out of a total number of one-per-revolution cycles of about 4800, or less than 3 percent of the total cycles. Referring to Figure 50, which compares the gust environment of these tests with the gust environment for typical low altitude mission flying obtained with an OV-1A airplane, a factor of 50 is a reasonable value for reducing the test rough-air spectrum to one that would simulate typical mission flying. Therefore, for 1000 hours of flight time where 21,300,000 cycles of one per revolution are obtained, the number of cycles of load due to rough air which would exceed the endurance limit load could be estimated as follows:

$$\text{Cycles} = \frac{130 \times 21,300,000}{4800 \times 50} = 11,600$$

The number of cycles which exceeds the endurance limit per 1000 hours of flight time will certainly have some effect on fatigue life, but the reduction in fatigue life does not appear to be very severe. In fact, it would appear that the proportion of fatigue damage that rough air would cause in a gyro controlled rigid-rotor helicopter main rotor is probably less than the damage that would occur in an airplane designed for the same mission and flying in the same environment.

HOVERING AND HOVER MANEUVERS

GENERAL

All hover maneuvers discussed in these sections were performed with a longitudinal/lateral system sensitivity of 83/154 percent, respectively. In addition they were all performed without the J-60-2-2 auxiliary thrust engine operating. The increased gross weight and the tail rotor torque limits of the compound helicopter restricted this investigation.

HOVERING OVER A SPOT

A steady hover over a spot was performed for 5 minutes. The aircraft had no tendency to wander, and it was possible for the pilot to remove his hands and feet from the controls for short periods.

SIDEWARD FLIGHT

Sideward flight characteristics were evaluated at speeds of 10, 20, and 30 knots to the right and left. A pace vehicle, incorporating an anemometer, was used to establish the steady-state speeds. The variation of the cyclic control and rudder pedal positions in sideward flight are presented in Figure 55. The results indicate that control margins are adequate at sideward flight speeds up to 30 knots in either direction. The positive position gradient for the lateral cyclic control, shown in Figure 55, is less than that obtained for the conventional XH-51A helicopter. This is due primarily to using a lateral system sensitivity of 154 percent which reduces the control travel required for a given trim moment by 35 percent. The wing did not appear to have an adverse effect on sideward flight characteristics.

Sideward flight was easily accomplished. However, there is a transition zone from about 8 to 18 knots in left sideward flight that can be objectionable. This is shown by the shaded area in Figure 55. In this region the pilot senses a near neutral directional stability, which is manifested as an uncertainty in the pedal position required. The scope of this research program did not permit a more detailed investigation of this area. At either side of this speed range, the aircraft handles very well. High pedal forces are apparent in left sideward flight due to the 36-pound-per-inch pedal force gradient. Like the conventional XH-51A helicopter, tail rotor torque limits the maximum speed in right sideward flight. The

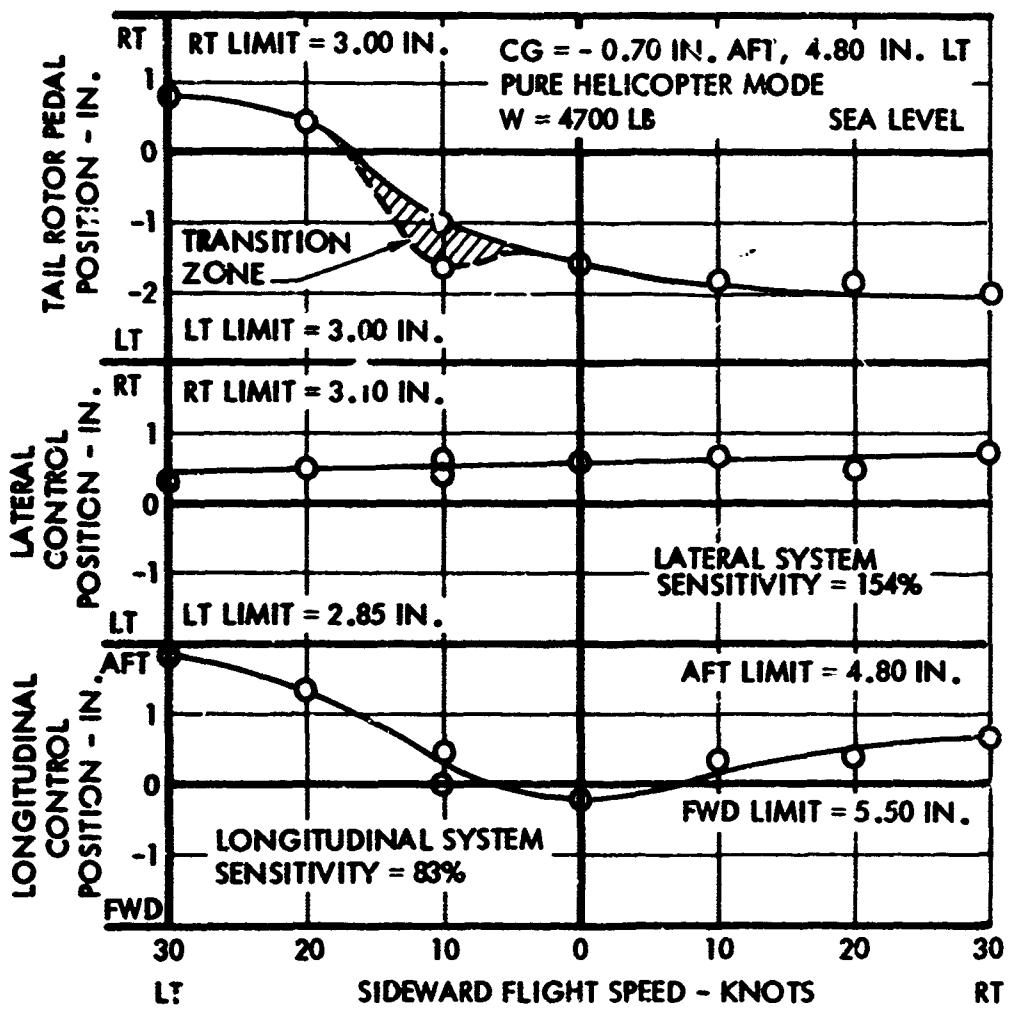


Figure 55. Control Position Variation During Sideward Flight.

results, as shown in Figure 55, are quite similar to those obtained in sideward flight for the conventional XH-51A helicopter, when the differences in gross weight and longitudinal/lateral system sensitivities are considered.

During the sideward flight testing, the maximum cyclic load of the tail rotor flapwise bending at station 16.8 was only 605 inch-pounds. This maximum load, which occurred during the 20-knot right sideward flight, is well below the 1060 inch-pound estimated endurance limit. The maximum tail rotor cyclic teetering angle was only 2.0 degrees. This cyclic teetering angle is well below the teeter stops which are at 10.5 degrees.

REARWARD AND LOW-SPEED FORWARD FLIGHT

Rearward and low-speed forward flight evaluations were conducted at air-speeds up to 30 knots with the same pace vehicle used for sideward flight. Figure 56 presents the control positions required for rearward and forward flight from a trimmed hover condition. These data indicate that adequate control margins remain in all axes. Control motion is positive from 30 knots rearward to the forward flight transition speed.

Rearward flight was stable and smooth with the exception of a 4P vibration at 20 to 30 knots. Longitudinal forces were high because of the large control displacement from trim required for rearward flight. These high forces are due to the 8-pound-per-inch longitudinal feel spring. 4P vibration was also higher during the forward flight transition. Tail rotor loads did not change significantly from hover to the 30-knot rearward or the 30-knot forward speed.

The results obtained in forward and rearward flight are also similar to those obtained with the conventional XH-51A helicopter, when the differences in gross weight and longitudinal/lateral system sensitivities are considered.

TURN ON A SPOT

Turn-on-a-spot tests were conducted to evaluate hover control response. The rudder pedals were displaced in 1/2-inch increments up to a maximum of 2 inches to the right and 1.5 inches to the left of the hover trim position. The steady-state yawing control response is approximately 72.0 degrees per second per inch of pedal input. Right pedal displacement was limited to 2 inches from trim because of tail rotor teeter stop limitations. When the teeter stops were contacted, the tail rotor blade cyclic flapwise bending moments at station 16.8 reached a maximum of 5950 inch-pounds, well above the 1060 inch-pounds estimated endurance limit. A count of the number of cycles at each amplitude of the cyclic flapwise bending moment at station 16.8 in combination with a cumulative damage

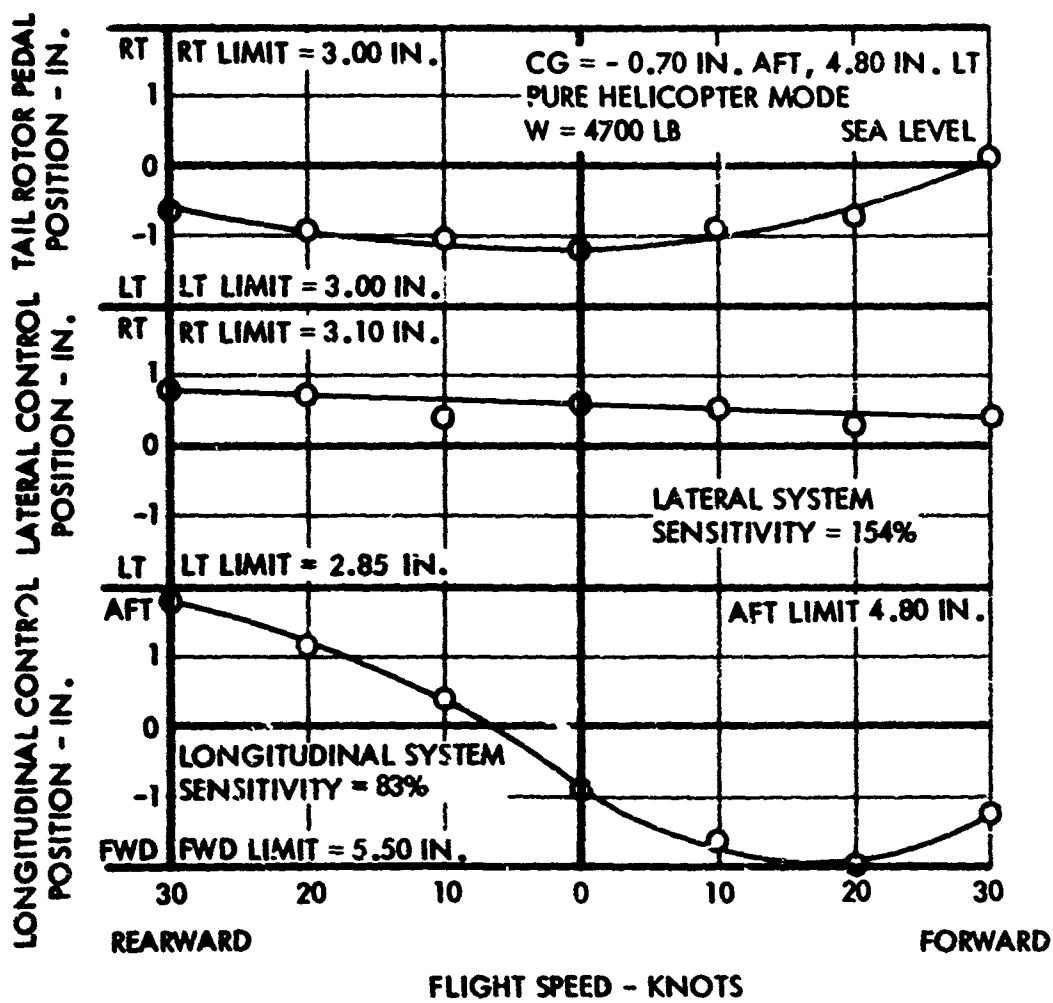


Figure 56. Control Position Variation During Hover, Rearward, and Low-Speed Forward Flight.

analysis indicated that the fatigue life of the tail rotor blades may have been approached, so the blades were replaced.

Left pedal inputs were limited to 1.5 inches from trim because of tail rotor torque limitations. Although it was easy to execute turns on a spot in either direction, it was difficult to stop a right turn on a desired heading without exceeding the tail rotor torque limit. As in sideward flight, the wing did not have any appreciable effect on the results.

CROSSWIND HOVER

Crosswind hover maneuvers were conducted in winds of 12 to 15 knots to simulate real-life conditions. Station-keeping capabilities with head winds, tail winds and quartering winds were evaluated along with acceleration and deceleration in sideward flight to new hovering locations. The pilot reported that the maneuvers were easily accomplished and that no limiting conditions were encountered.

AUTOROTATION

ROTOR RPM DECAY CHARACTERISTICS

Simulated failures of the PT6B-9 main rotor engine from a level flight condition were conducted to evaluate the power-off rotor RPM decay characteristics over the airspeed envelope as a function of initial rotor RPM and collective blade angle. Nominal true airspeeds of 55 to 200 KTAS were evaluated in combination with initial rotor speed settings of 100, 95 and 90 percent and collective blade angles from 1.45 to 7.50 degrees. The auxiliary thrust level of the J-60 engine was maintained at its trim value, and no corrective action was taken except the use of cyclic control to maintain constant airspeed.

The results of these tests are shown in Figure 57; they indicate that the power-off decay rate increases with increasing airspeed, collective blade angle, and initial RPM setting.

Because the compound helicopter is operated with very little lift on the rotor at high speed, the power requirements of the rotor are correspondingly low. This results in lower RPM decay rates in the event of engine failure.

The RPM decay rates are less at lower initial RPM settings; this is only partially relieving since the underspeed margins are reduced accordingly, and the minimum power-off RPM of 89 percent is reached sooner.

As flight speed is reduced, the decay rates diminish rapidly. This indicates the desirability of reducing auxiliary thrust soon after a main engine failure occurs. A pull-up maneuver produces two beneficial effects. First, the higher angles of attack reduce the main rotor power requirements. Second, forward speed is lost at a greater rate. Each of these factors tends to prevent rotor underspeeds.

No difficulty is encountered in establishing steady decay rates at a constant airspeed. The longitudinal trim shift which accompanies a simulated power failure is small and is controlled, with no difficulties encountered in maintaining aircraft attitude and airspeed control.

Because of these characteristics, autorotations could be made at flight speeds above 200 knots. This phase of the program is discussed more fully in the following section.

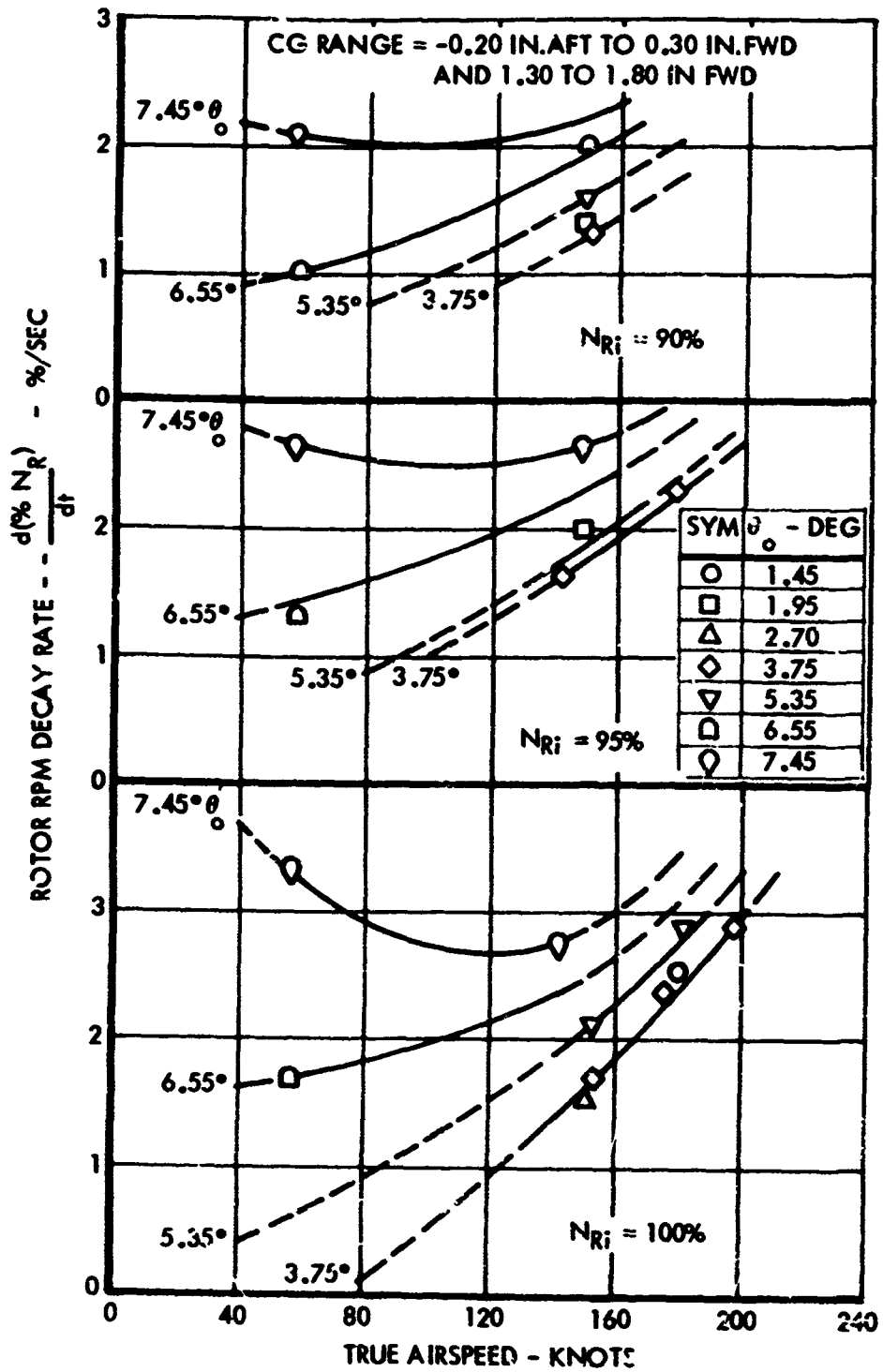


Figure 57. Power-C_f Rotor RPM Decay Rate as a Function of True Airspeed - Normal Acceleration = 1.0g.

AUTOROTATION ENTRIES

Simulated Failure of the PT6B-9 Main Rotor Engine

Autorotation entries were evaluated in progressive increments over the airspeed envelope up to and including a true airspeed of 232 knots at an initial rotor speed of 100 percent and a forward center of gravity. Entries were also performed over the airspeed envelope up to and including a true airspeed of 212 knots with an initial rotor RPM of 100 percent and a neutral center of gravity. Entries at reduced initial RPM settings of 95 and 90 percent were conducted up to and including maximum true airspeeds of 165 and 180 knots, respectively, with neutral centers of gravity.

All entries were performed at a collective blade angle of approximately 4.00 degrees at blade station zero. This blade angle is the optimum setting, since the same position is used for high-speed level flight; thus, the need for any manipulation of the collective control is eliminated.

The basic autorotation entry technique consisted of immediate spoiler deployment upon sensing (or simulating) the main rotor engine failure, followed by entry into a right climbing turn to increase rotor angle of attack and to assist in decelerating the aircraft to lower airspeeds. Rotor RPM was controlled by varying load factor in the turn. Auxiliary thrust was reduced to idle immediately after spoiler deployment to further aid in deceleration of the aircraft to lower airspeeds. When the lower airspeeds were reached, a power recovery to level flight was performed. (In the event of an actual main rotor engine failure, auxiliary thrust can be modulated to maintain flight and permit selection of a suitable landing site.) Variations of this method were performed by the pilots and consisted mainly of entering the right turn before spoiler deployment, followed by reducing the auxiliary thrust or vice versa. An alternate at high speed consists of using a symmetrical pull-up in lieu of a climbing turn. This not only results in a more rapid reduction in flight speed but also should permit the attainment of the proper angle of attack in a shorter period of time. Additional autorotation testing is required to determine all of the advantages and disadvantages of this procedure.

During a simulated main rotor engine failure, the helicopter noses down slightly and yaws to the left. These trim changes are easily handled and do not require any unusual piloting techniques. When the spoilers are deployed, the aircraft again noses over slightly. This results in a small rotor RPM loss which is easily regained during the rest of the maneuver.

Figure 56 is a time history of an autorotation entry at a true airspeed of 228.5 knots, at a longitudinal system sensitivity of 100 percent, and with a center of gravity approximately 1.5 inches forward of the rotor mast. The spoilers were deployed 1.0 second after entry, and auxiliary thrust was reduced 1.8 seconds after spoiler deployment. Rotor RPM dropped to a

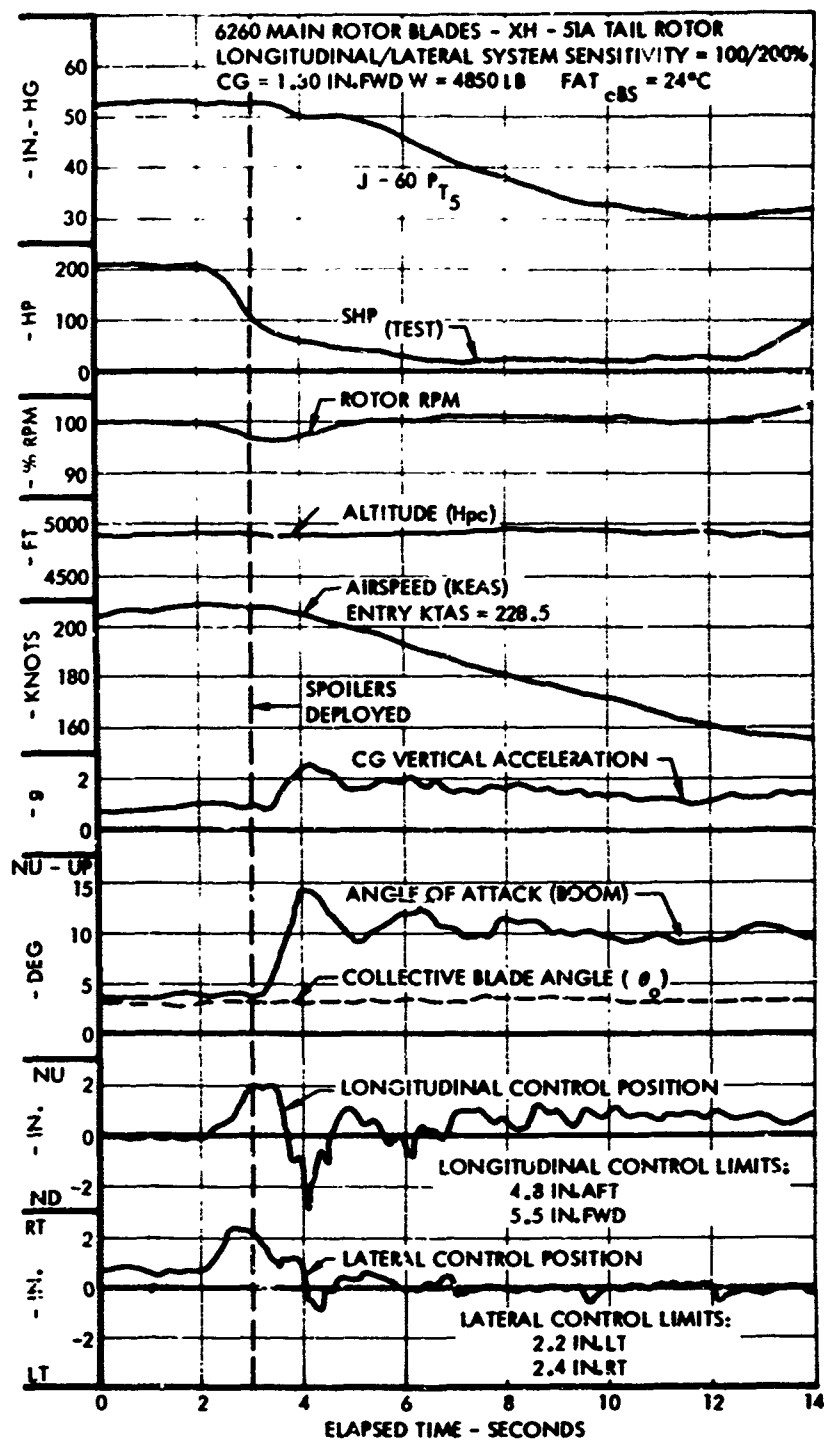


Figure 58. Time History of Autorotation Entry at 228.5 KTAS - Forward CG.

minimum of 96.5 percent, but an increase in load factor brought it back up to 100 percent well before the power recovery was initiated. At this point, the aircraft had decelerated from 208 to 158 KEAS in a period of 10.5 seconds. Aside from the initial control inputs to build up the load factor, the longitudinal and lateral trim shifts were approximately 0.80 inch aft and 0.70 inch left, respectively.

The autorotation entry at a maximum true airspeed of 232.0 KTAS is presented in Figure 59. The longitudinal system sensitivity was 100 percent, at an initial rotor RPM of 100 percent and a center of gravity 1.5 inches forward of the rotor mast. Auxiliary thrust was reduced 1.0 second after entry, and the spoilers were deployed 1.3 seconds later. This maneuver was a satisfactory demonstration of a high-speed autorotation entry. However, the combination of low load factor upon entry into the turn and the delay in spoiler deployment allowed the rotor RPM to decrease to 93 percent approximately 2.5 seconds after initiation of the autorotation entry. This combination of high airspeed and low rotor RPM is outside of the RPM/airspeed envelope and resulted in rotor plane oscillation. This condition damped out as the aircraft was decelerated to a lower airspeed, from which a normal recovery to powered flight was performed. Rotor plane oscillation is a phenomenon encountered at high airspeeds with low to intermediate rotor RPM settings and is not directly related to high speed autorotation entries. See Rotor Plane Oscillations for a complete discussion of this condition (page 73).

Simulated Failure of J-60-P-2 Auxiliary Thrust Engine

Eighteen simulated power failures of the J-60 auxiliary thrust engine were conducted over a true airspeed range of 160 to 226 knots to evaluate the effect of J-60 engine power loss on flight characteristics. While maintaining a fixed collective blade angle, the rate of simulated auxiliary thrust loss was varied and did not appear to have any effect on handling characteristics.

The nose-down trim change associated with thrust loss became more noticeable with increasing airspeed, but was easily controlled. If no immediate corrective action was taken, a mild right sideslip together with the nose-down trim shift occurred. However, control of the aircraft was still easily maintained.

Simulated Simultaneous Failure of Both Engines

The location of the J-60 auxiliary thrust engine throttle control on the collective twist grip and the PT6B-9 main rotor engine N_1 control mounted on the console quadrant lever precluded simulating the simultaneous failure of both engines. However, several autorotation entries were made in which simultaneous failure was approximated. There were no recovery control problems during this limited investigation of simultaneous engine failure.

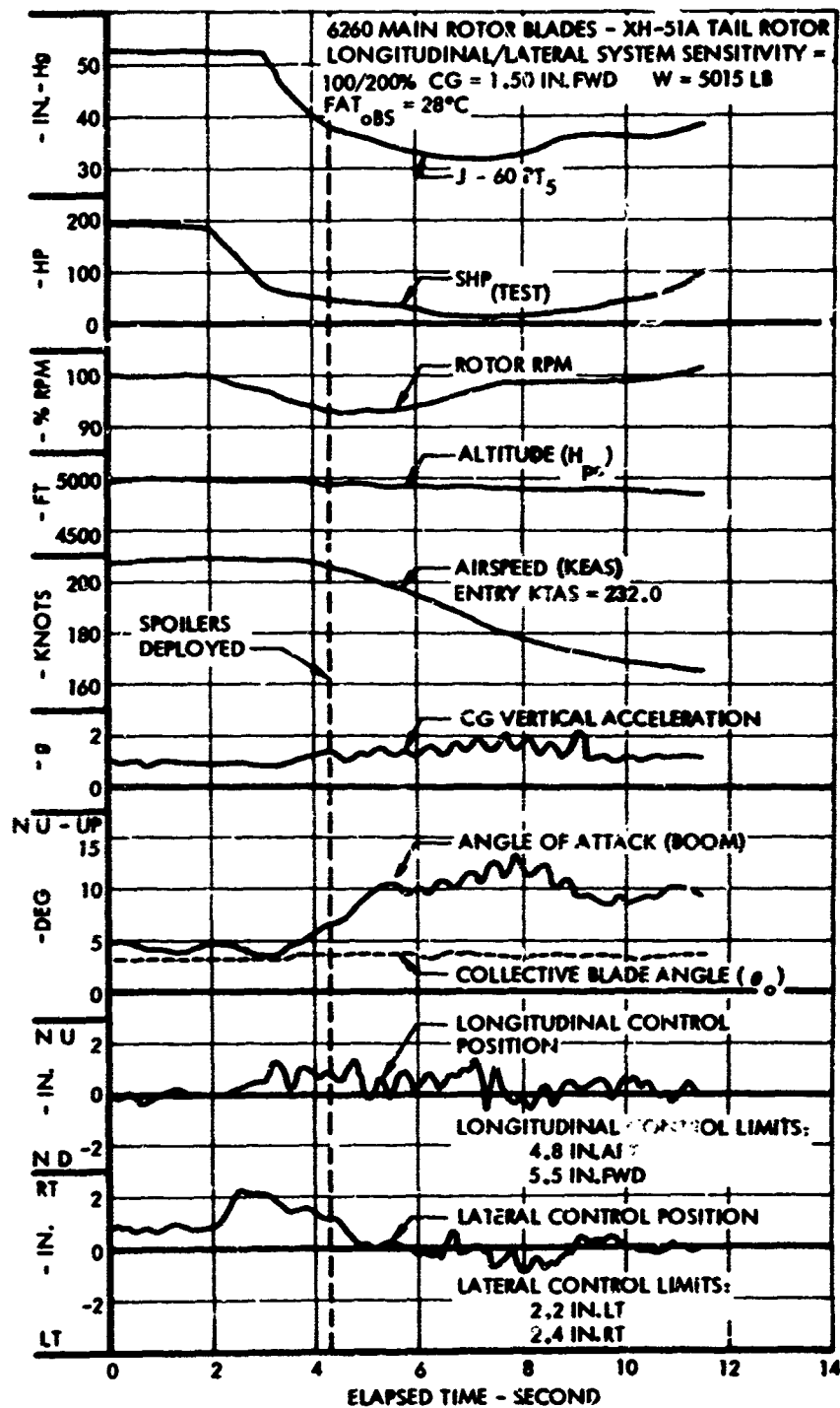


Figure 59. Time History of Autorotation Entry at 232.0 KTAS - Forward CG.

Structural Loads

Structural loads were measured during the transition from powered flight to autorotation and during autorotation for various speeds as the entry speed was increased from 212 to 232 KTAS. The main rotor hub cyclic loads at station 6 and the stress at station 7 during autorotation entry for the three highest speed conditions are as follows:

<u>Autorotation Entry</u>	<u>Flap Bend Mom. @ 6</u>	<u>Chord Bend Mom. @ 6</u>	<u>Stress @ 7</u>
221.5 KTAS	22,800 in.-lb	34,000 in.-lb	37,600 psi
228.5 KTAS	29,600 in.-lb	68,000 in.-lb	52,300 psi
232.0 KTAS	26,000 in.-lb	51,300 in.-lb	44,900 psi

The maximum combined cyclic stress on the main rotor hub at station 7, as derived from flapwise and chordwise bending moment at station 6, was 52,300 psi at the 228.5 KTAS autorotation entry. This stress was due to the high load factor of 2.81g that set the high-load-factor high-speed point on the V-N diagram. The combined cyclic stress, at station 7, at the maximum speed of 232 KTAS was 44,900 psi. These combined stresses are well above the estimated endurance limit of 26,000 psi but the number of stress cycles which exceeds the endurance limit is four or less per maneuver, hence very few cycles are accumulated in this condition, and the degradation of fatigue life is minimal. As mentioned previously, the high-speed autorotation entry at 232 KTAS was a satisfactory autorotation entry. However, the combination of high airspeed and low rotor RPM after entry resulted in a rotor plane oscillation that produced a combined cyclic stress of 68,200 psi in the main rotor hub at station 7. The loads obtained in autorotation after the initial entry maneuver were generally about the same or less than those obtained in powered flight at comparable airspeeds.

LEVEL FLIGHT PERFORMANCE CHARACTERISTICS

AIRSPEED SYSTEM CALIBRATION

The ship's airspeed system calibration was checked and extended to a speed of 219 KCAS by the pacer aircraft method. These data were obtained by pacing the compound helicopter with a North American P-51D Mustang whose airspeed system had been calibrated by the altimeter depression method.

The results shown in Figure 60 are identical to those obtained using the altimeter depression method during previous test programs (Figure 4 of Reference 1). Extrapolation of these data to the maximum attained calibrated airspeed of 235 knots was considered to be valid because of the linearity and repeatability of the data.

POWER REQUIRED

The level flight performance objectives of this program were to evaluate the power requirements and lift sharing characteristics of the XH-51A compound helicopter over the airspeed envelope as a function of collective blade angle and rotor RPM setting. These objectives were met by conducting the testing at a constant weight to density ratio of 5875 pounds for the following test conditions, at neutral centers of gravity.

<u>θ_0 ~ DEG</u>	<u>ROTOR RPM (N_R) ~ %</u>
3.75	100, 95, and 90
5.40	
7.25	

The weight-to-density ratio of 5875 is consistent with the test weights and the atmospheric conditions encountered during the other phases of testing discussed in this report. The scope and span of the maneuverability program did not permit evaluation of other weight-to-density ratios.

A collective blade angle of 3.75 degrees is the optimum setting for high-speed flight in the XH-51A compound helicopter at takeoff gross weights from 5165 to 5275 pounds. At collective blade angles above 3.75 degrees the rotor provided the largest portion of the lift and the wing is not being used effectively. Moreover, the maximum attainable airspeed is lowered due to vibration and structural loads. At collective blade angles

below 3.75 degrees, the wing supplies a larger than desirable amount of the lift. Indeed, the rotor becomes completely unloaded at an airspeed below the maximum attainable. Thus, it is not desirable to use a collective blade setting below 3.75 degrees because the wing will not be used efficiently with a resultant loss of high-speed flight capability.

Figure 61 presents the variation of engine shaft horsepower with airspeed for a weight-to-density ratio of 5875 pounds at 100 percent rotor RPM and collective blade angles of 3.75, 5.40, and 7.25 degrees. As expected, the power required rises with increasing blade angle for a given airspeed, and the change is most pronounced at the low and intermediate airspeeds. At true airspeeds above 180 knots the incremental change in power required with blade angle becomes less and tends to approach some mean variation with airspeed.

As stated previously, a collective blade angle of 3.75 degrees is near optimum for operation in the high-speed flight regime. At these higher speeds, the incremental change in engine shaft horsepower required with airspeed can be attributed almost solely to drag effects on the main rotor. The induced power required decreases with airspeed and the degree of rotor unloading. Parasite and profile power increase with airspeed and are influenced by compressibility and reverse flow effects. A small portion of this increase in power is due to the tail rotor. The variation of tail rotor horsepower over the airspeed envelope at 100 percent rotor RPM is presented on the lower half of Figure 62 as a function of collective blade angle setting. These data indicate that with the 3.75-degree collective blade angle, the increase in tail rotor power required at the greater airspeeds is due to parasite and profile drag effects of the tail rotor. At high airspeeds, the tail rotor is providing very little antitorque control, since the major portion of directional trim is provided by the cambered vertical fin. In addition, Figure 62 also indicates that the tail rotor power is a minimum at a collective blade angle setting of 5.40 degrees. At a given airspeed, the combined net torque of the auxiliary thrust engine and main rotor is a minimum at the 5.40 degree collective setting and the lowest amount of antitorque control is needed. At a collective blade angle setting greater or less than 5.40 degrees the net torque is higher with a resultant increase in tail rotor power required.

Since main rotor profile power varies almost directly with rotor RPM, lowering the rotor RPM at a given airspeed and collective blade angle causes a reduction in engine shaft horsepower required. Also, induced power decreases at the lower RPM settings under these conditions because rotor lift is reduced. These results are shown in Figure 63 as a function of engine shaft horsepower required at collective blade angles of 3.75, 5.40, and 7.25 degrees. Rotor lift characteristics are fully discussed in a succeeding section.

The upper half of Figure 62 indicates that for a given airspeed and collective blade angle setting the tail rotor power required decreases as

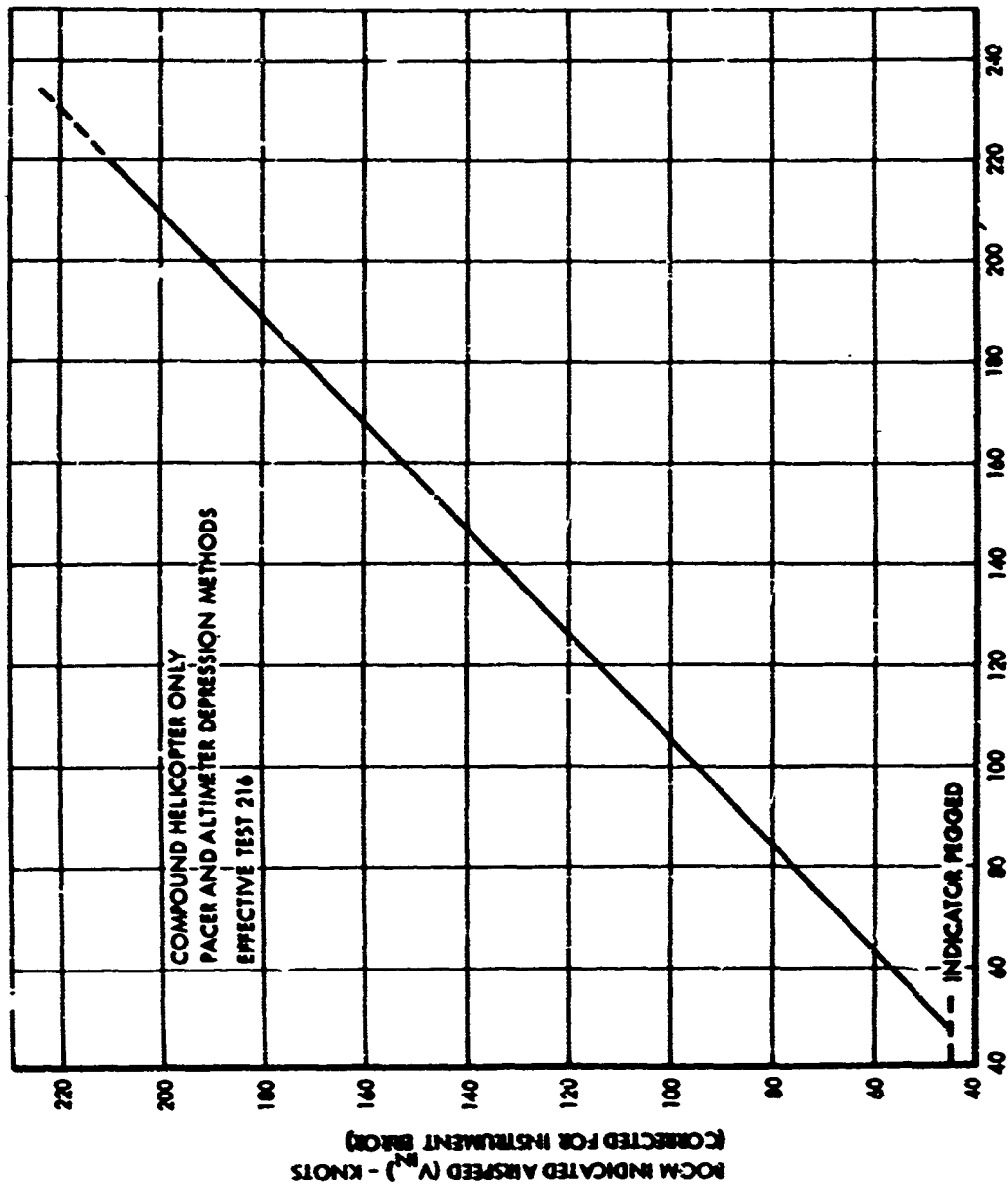


Figure 60. Airspeed Calibration - Boom System

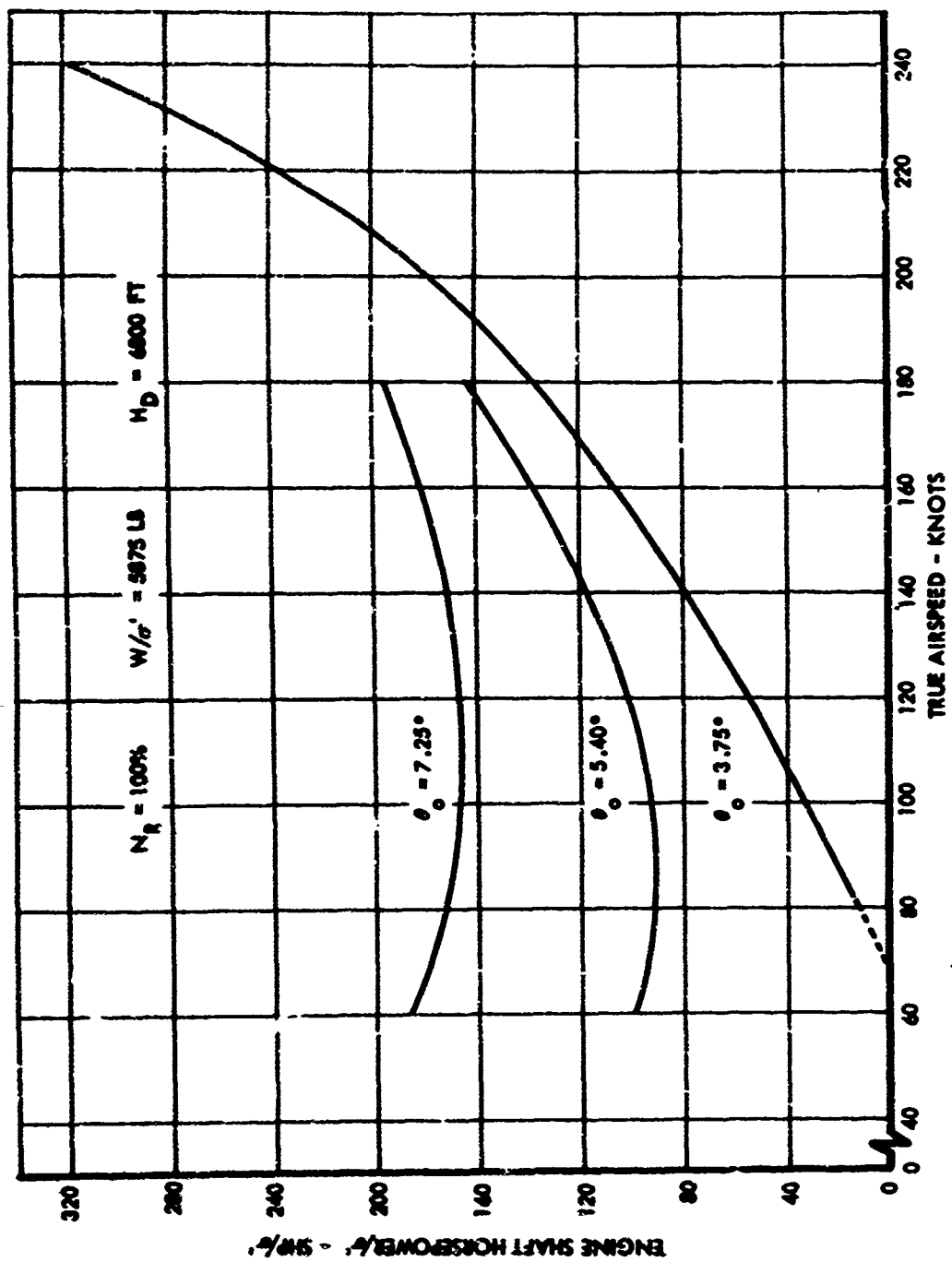


Figure 61. Engine Shaft Horsepower Required for Level Flight - Effect of Collective Blade Angle - Neutral CG.

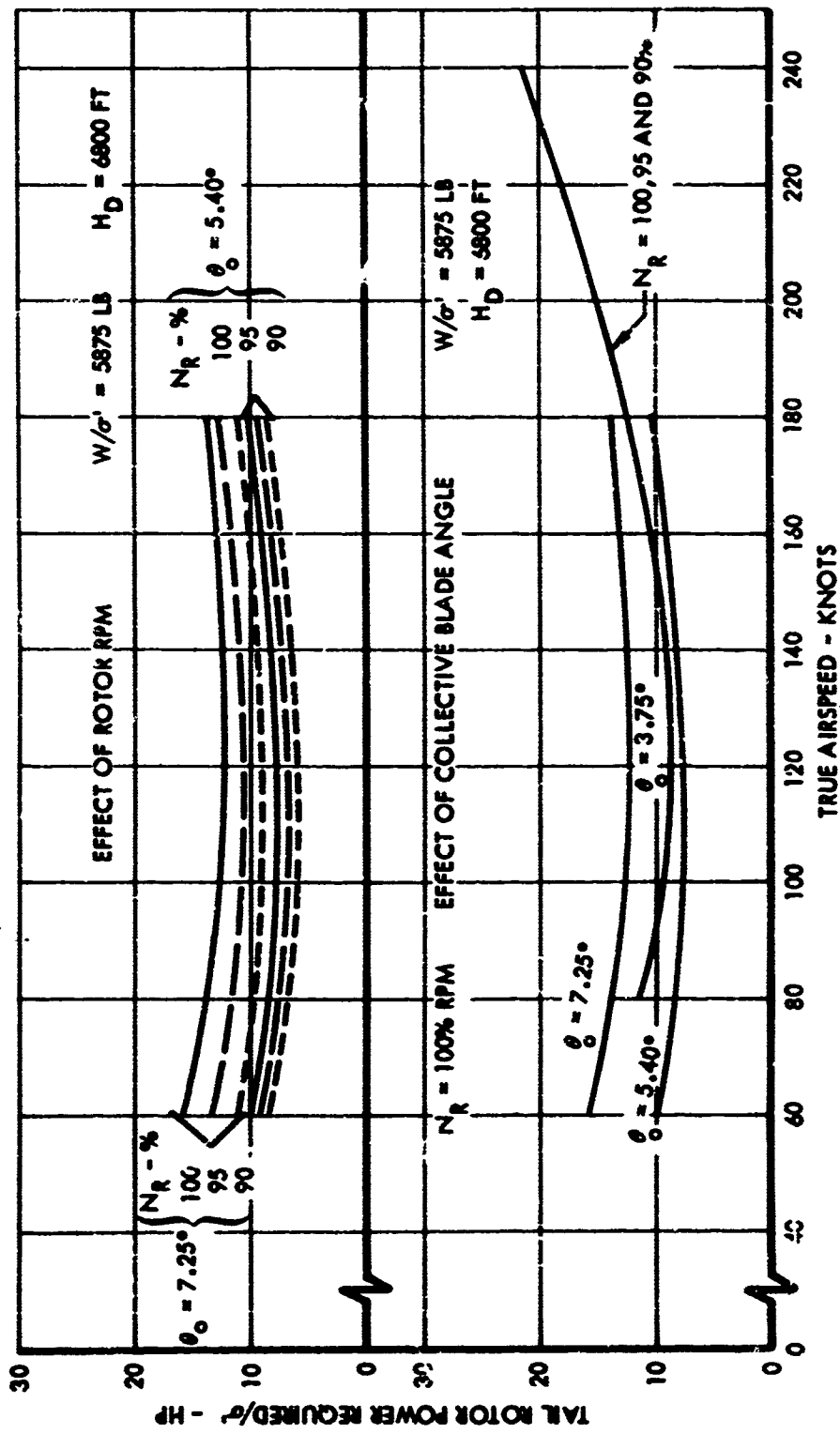


Figure 62. Tail Rotor Horsepower Required for Level Flight - Effect of Collective Blade Angle and Rotor RPM - Neutral CG.

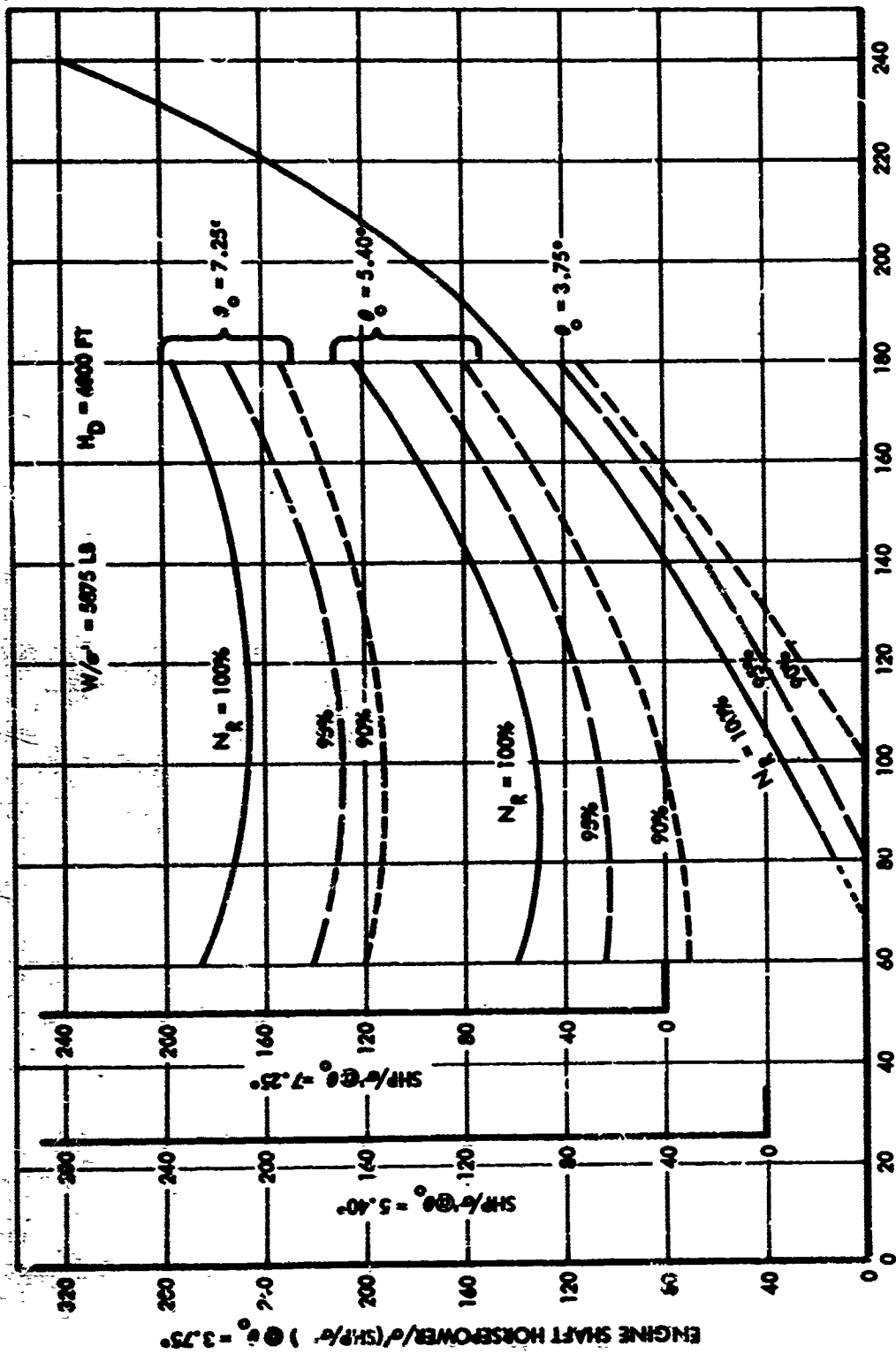


Figure 63. Engine Shaft Horsepower Required for Level Flight - Effect of Rotor RPM - Neutral CG.

rotor RPM is reduced. The antitorque requirement of the tail rotor is lower because the net torque of the auxiliary thrust engine and main rotor is decreasing as rotor RPM is reduced. Tail rotor power requirements over the airspeed envelope are rather small and are not significantly affected by operation at reduced rotor RPM settings. Hence, the variations of engine shaft horsepower shown in Figure 63 are a good indication of changing power conditions at the main rotor.

The variation of auxiliary thrust over the airspeed envelope is presented in Figure 64 as a function of rotor RPM and collective blade angle. These results exhibit the same trends as the engine shaft horsepower required data discussed in the preceding paragraphs. At a given airspeed and 100 percent rotor RPM, the auxiliary thrust required increases to compensate for the reduction in shaft horsepower as the blade angle is lowered. Auxiliary thrust required also increases as rotor RPM is reduced to provide sufficient power to offset the reduction in engine shaft horsepower. At the upper end of the airspeed envelope, the variation of thrust required with rotor RPM and collective blade angle also tends to approach a mean variation with airspeed.

Aside from comparing the shaft horsepower and auxiliary thrust required to maintain level flight on an individual basis, it is also of interest to examine this flight condition on a total power basis. Shaft horsepower and auxiliary thrust were combined in terms of equivalent shaft horsepower (ESHP), as defined below and further explained in Reference 1.

$$\begin{aligned} \frac{\text{ESHP}}{\sigma'} &= \frac{\text{SHP}}{\sigma'} + \frac{F_n}{\sigma'} \left(\frac{\text{KTAS}}{325} \right) \\ &= \frac{\text{SHP}}{\sigma'} + \frac{\text{THP}}{\sigma'} \end{aligned}$$

where, $\sigma' = \rho/\rho_0$

The variation of equivalent shaft horsepower with airspeed at 100 percent rotor RPM is shown in Figure 65 for collective blade angles of 3.75, 5.40, and 7.25 degrees. The equivalent power required varies slightly with collective blade angle. Although the 3.75-degree blade angle is optimum for high-speed flight and results in lower vibration and structural loads, it has the highest level flight equivalent power requirement. It appears that there is a small power tradeoff with collective setting, and the minimum equivalent power was obtained at the 5.40-degree blade angle. At 180 KTAS the equivalent power is 875 horsepower for the 5.40 degree blade angle and increases to 905 horsepower at the 3.75 degree setting, with a resultant difference of only 30 horsepower. Again it should be noted that minimum tail rotor power required was obtained with a collective blade angle of 5.40 degrees. Operation of a high-speed compound helicopter cannot be

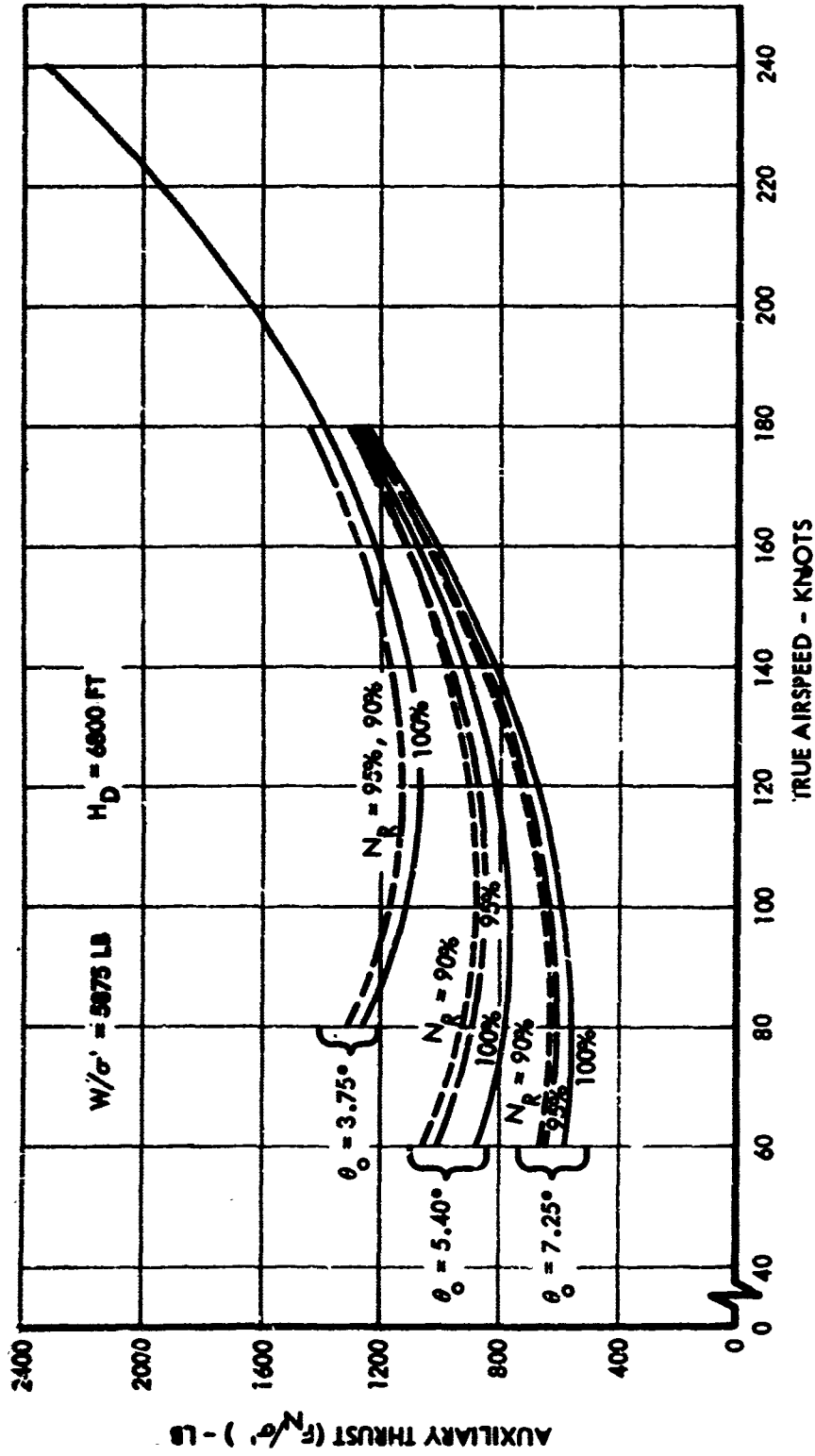


Figure 64. Auxiliary Thrust Required for Level Flight - Effect of Collective Blade Angle and Rotor RPM - Neutral CG.

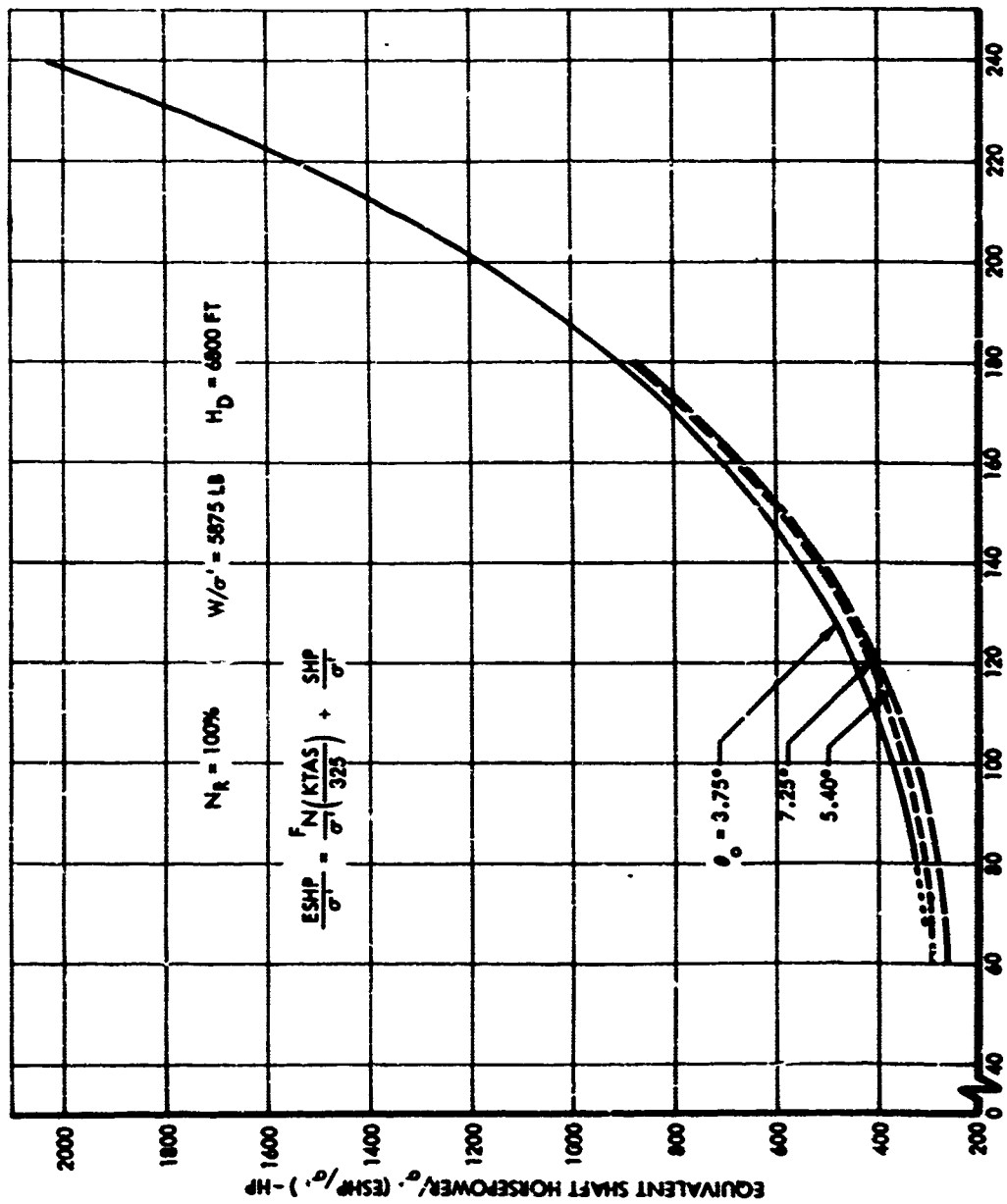


Figure 65. Equivalent Shaft Horsepower Required for Level Flight - Effect of Collective Blade Angle - Neutral CG.

based on power required alone. Effective use of the wing and rotor is obtained with a collective blade angle of 3.75 degrees and results in optimum overall aircraft performance from the combined effects of power required, handling qualities, vibration and structural loads.

Operation at reduced rotor RPM for a given collective blade angle also affects equivalent power. At the low collective blade angle of 3.75 degrees, there is an almost imperceptible change in equivalent power required with reduced rotor RPM. As the collective blade angle is increased to 7.25 degrees, these changes become more significant. However, the net result is that equivalent shaft horsepower required decreases with reduced rotor RPM. These data are shown in Figure 66.

POWER AND THRUST SHARING CHARACTERISTICS

The power sharing characteristics between the main and auxiliary engines are shown in Figure 67 as a function of collective blade angle at 100 percent rotor RPM. These data are expressed in terms of power fraction which represents the ratio of shaft horsepower to equivalent shaft horsepower required. Examination of these data indicates how the auxiliary thrust engine provides increasingly more of the total power required with increasing airspeed and decreasing collective blade angle. At a collective blade angle of 3.75 degrees and a true airspeed of 240 knots, shaft horsepower to the rotor represents only 16 percent of the total equivalent power required.

Power sharing characteristics at reduced rotor RPM levels are not significantly different from those shown in Figure 67 for 100 percent rotor RPM.

ROTOR/WING LIFT SHARING CHARACTERISTICS

The variation of rotor lift to gross weight ratio with true airspeed is presented in Figure 68 for collective blade angles of 3.75, 5.40, and 7.25 degrees at 100 percent rotor RPM. As expected, the rotor becomes increasingly unloaded with increasing airspeed at all collective blade angles as the wing becomes more effective and supports a larger share of the aircraft's weight. Lift is also transferred from the rotor to the wing as collective blade angle is reduced. Extrapolation of the data obtained at a collective blade angle of 3.75 degrees indicates that the rotor would be completely unloaded at a true airspeed of 240 knots for the specified test conditions.

An explanation of the lift sharing tradeoffs discussed in the preceding paragraph can be found by examining the change in fuselage angle of attack with airspeed. These results, valid only for the 1-g level flight condition, are presented in Figure 69. Shown are the body attitude changes necessary to maintain a constant total lift on the aircraft for the various collective blade angles and rotor RPM settings.

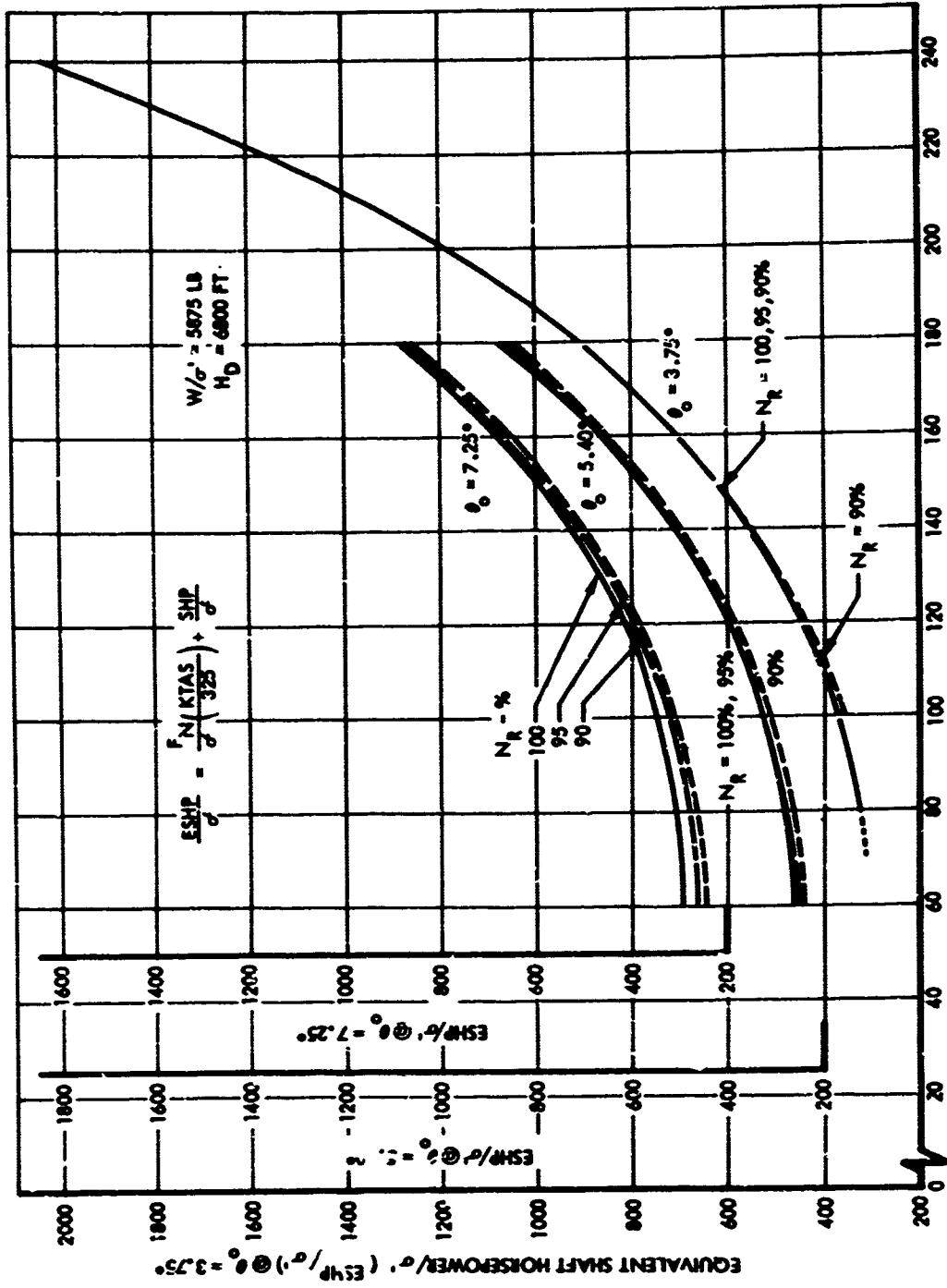


Figure 66. Equivalent Shaft Horsepower Required for Level Flight - Effect of Rotor RPM - Neutral CG.

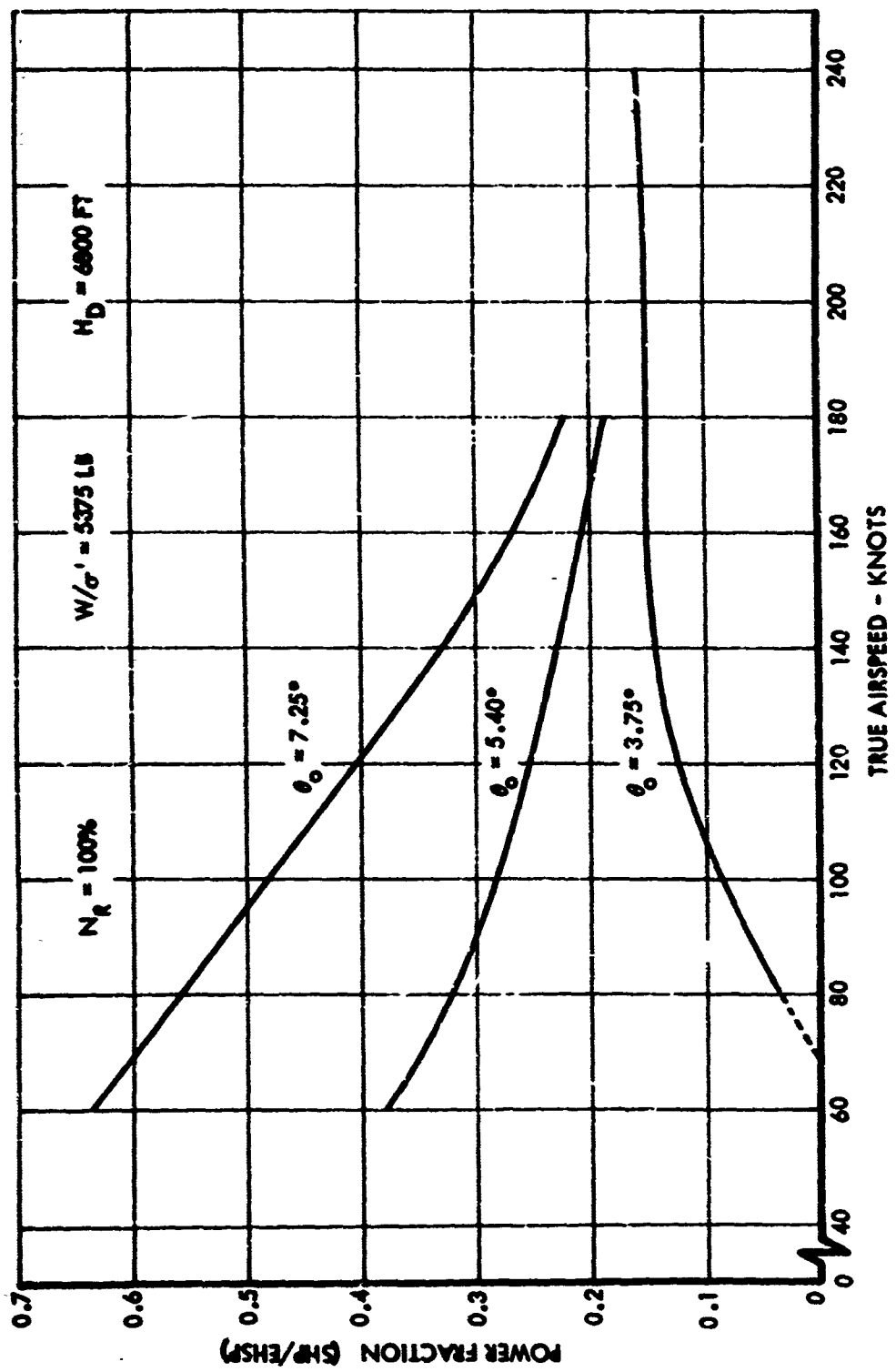


Figure 67. Power Sharing Characteristics in Level Flight - Effect of Collective Blade Angle - Neutral CG.

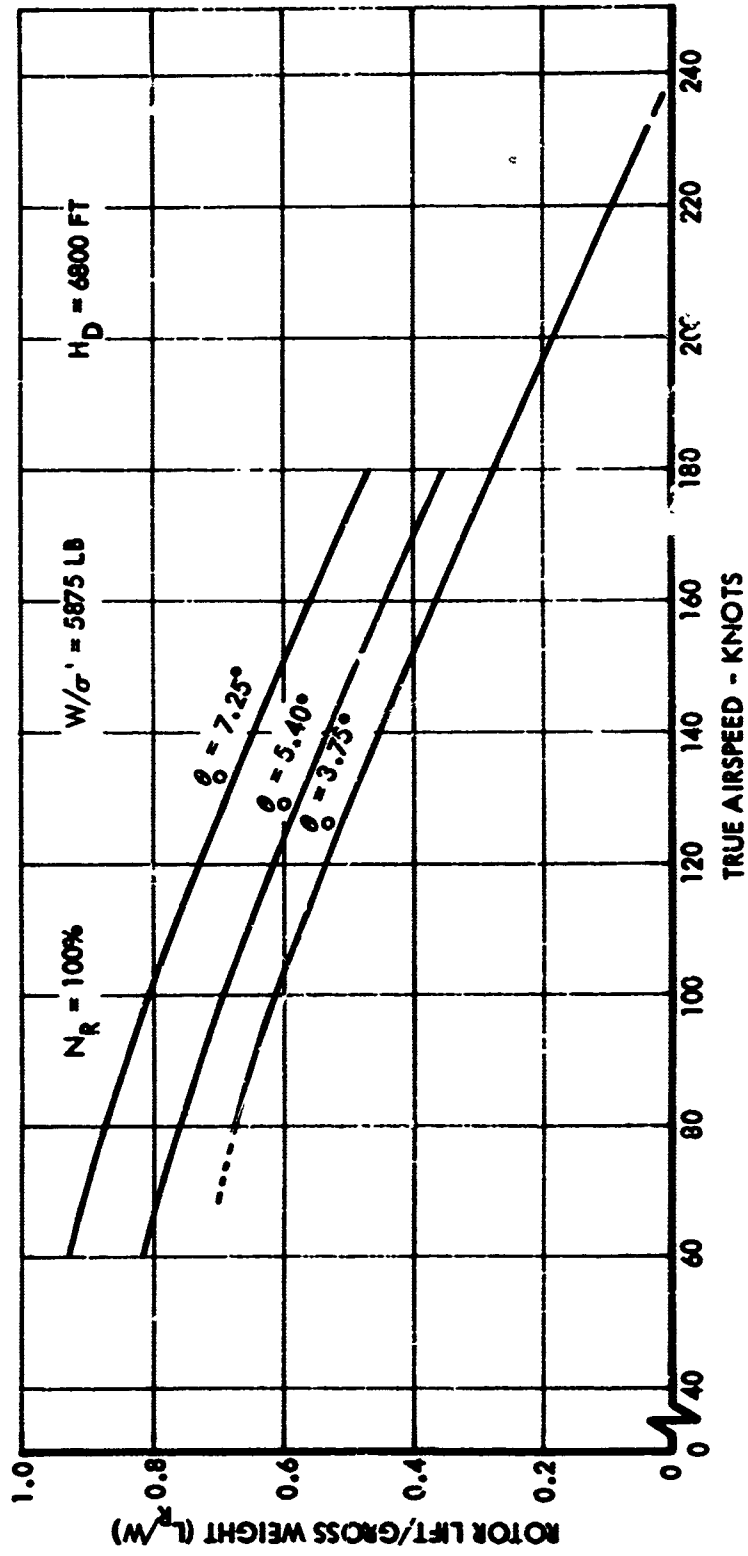


Figure 68. Rotor Lift Sharing Characteristics in Level Flight - Effect of Collective Blade Angle - Neutral CG.

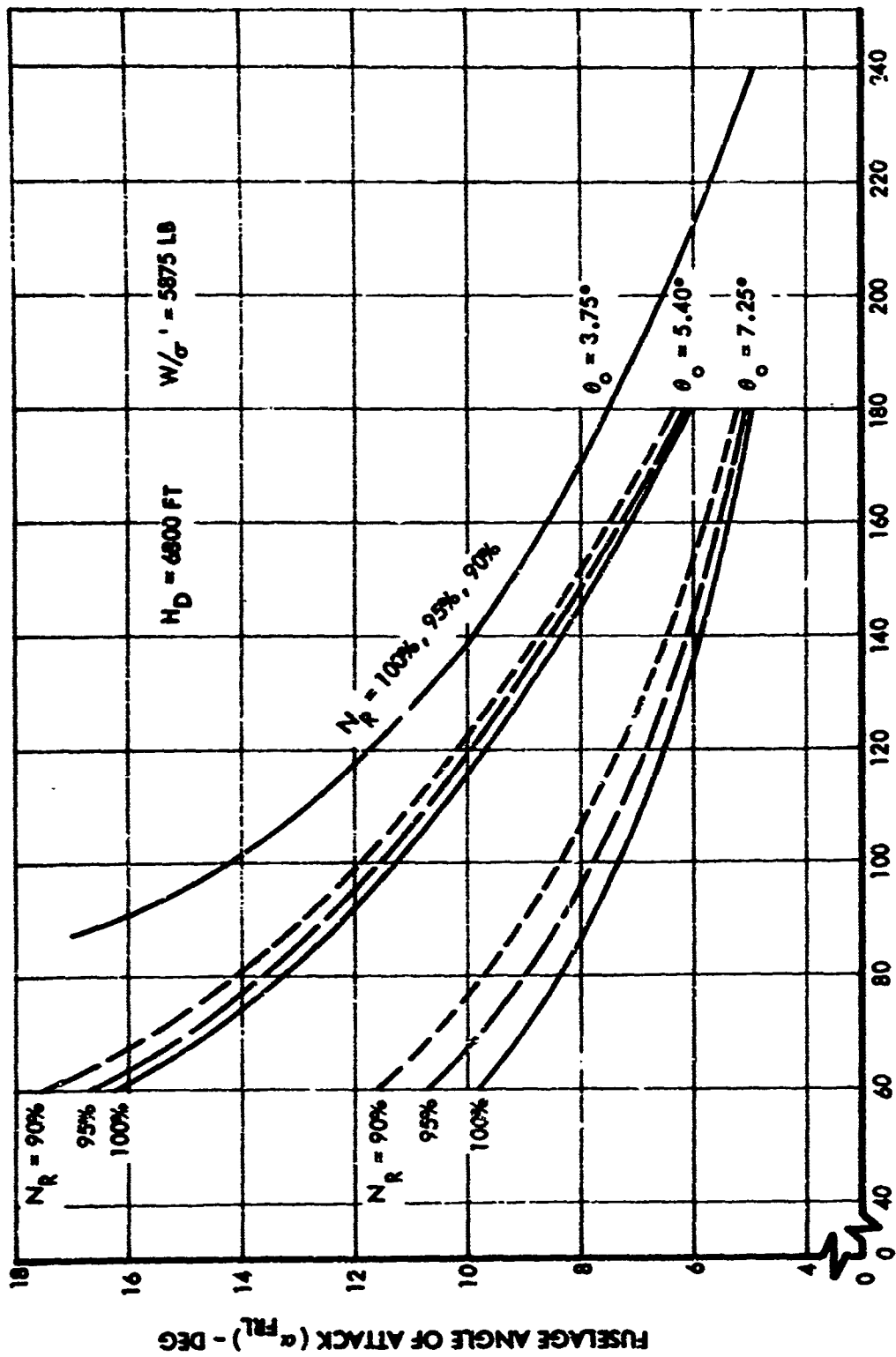


Figure 69. Angle of Attack Variation with True Airspeed - Effect of Collective Blade Angle and Rotor RPM - Neutral CG.

Examination of Figure 69 indicates that at any collective blade angle, as the rotor unloads with increasing airspeed, the fuselage angle of attack decreases at a decreasing rate. Since wing lift varies directly with dynamic pressure at a given angle of attack, smaller incremental changes in fuselage angle of attack are required at high speed to compensate for changes in rotor lift due to collective changes. Conversely, at low speeds, much larger fuselage angle of attack changes are required for the wing to produce its increment of the total lift with a change in collective blade angle.

The manner in which angle of attack varies with changes in rotor RPM at the various collective blade angle settings is consistent with the power required and rotor lift data shown in Figures 62, 63, 64, 66 and 70. As indicated by the presentation in Figure 69 the incremental changes caused by reducing rotor RPM are negligible at the 3.75 degree setting, but as collective blade angle is increased the effect of rotor RPM is more pronounced.

As shown in Figure 70, the lifting capability of the rotor decreases when operating at RPM settings below 100 percent. The decrease is not proportional to the square of the RPM reduction as a simple approximation might suggest. The reason for this is the corresponding increase in angle of attack which tends to cancel the lift loss somewhat. At high speeds, however, where angle of attack changes are quite small, the change in rotor lift is reasonably well defined by the percent RPM squared approximation.

ROTOR/WING LIFT SHARING CHARACTERISTICS IN TURNING FLIGHT

The lift sharing characteristics of the rotor/wing combination were also evaluated in maneuvering flight. The results shown in Figures 71 and 72 were obtained in turning flight during maneuvering stability testing, and they represent the changes in rotor and wing lift with increasing load factor as a function of true airspeed and collective blade angle.

Figure 71 indicates the fractional components of aircraft weight supported by the rotor and wing with increasing load factor and airspeed for a collective blade angle of 3.75 degrees. The total lift required to perform a maneuver is the product of load factor and aircraft weight and is, of course, the sum of wing and rotor lift. At a given load factor, the rotor becomes increasingly unloaded with increasing airspeed with the wing supporting a larger portion of the aircraft weight. In addition, the speed at which complete rotor unloading occurs increases with increasing load factor. For example, as shown in Figure 71, at 140 KTAS and a load factor of 1.0g the rotor carries 45 percent of the weight, with the wing supporting the other 55 percent. At a load factor of 1.50g the rotor lift increases to 80 percent of the weight while the wing lift has increased to 70 percent. For 1.0g flight at 220 KTAS, the wing supports 92 percent of the aircraft weight with only 8 percent of the weight being supported by the rotor. As load factor is increased to 1.50g, at 220 KTAS, the rotor

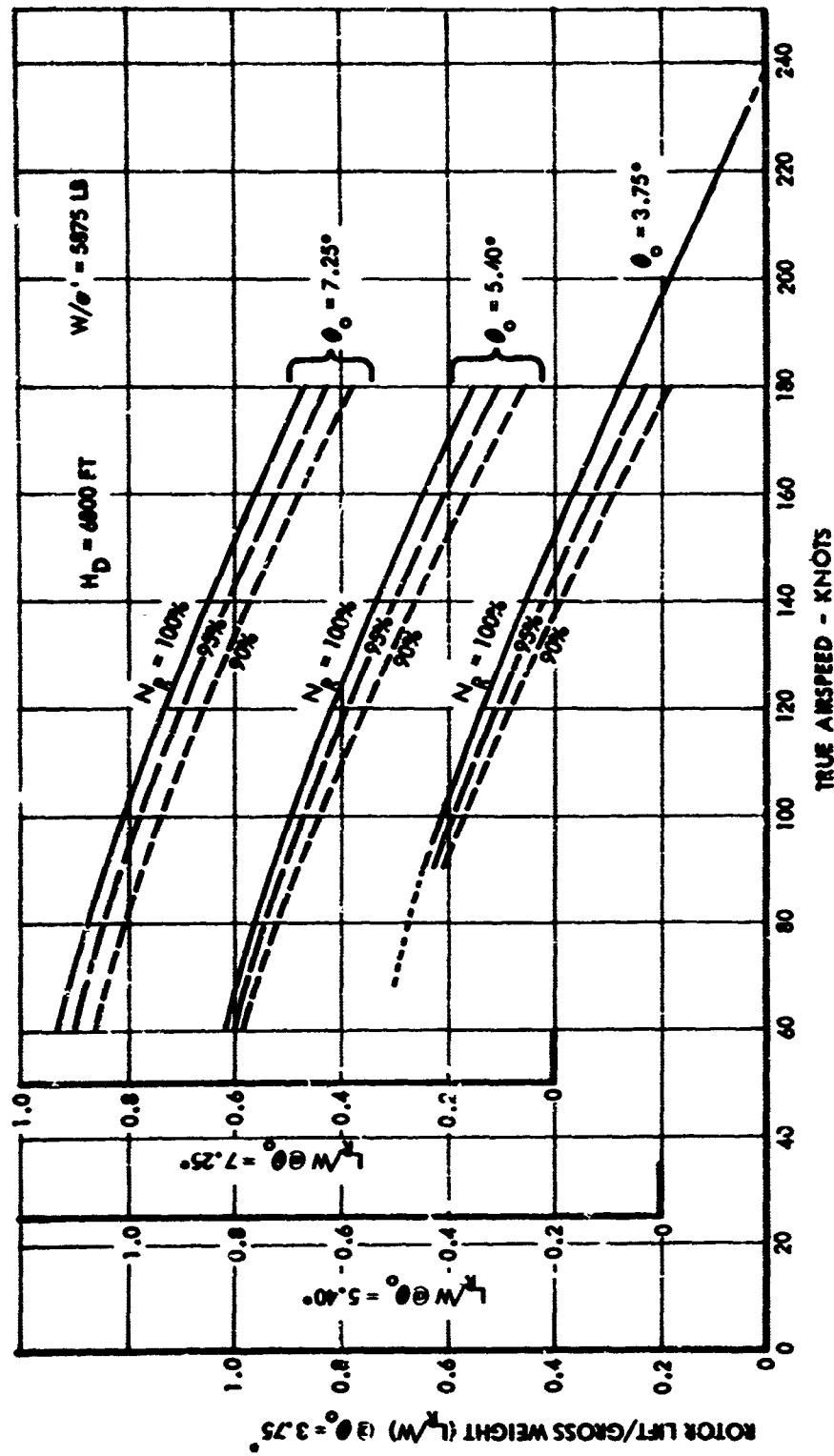


Figure 70. Rotor Lift Sharing Characteristics in Level Flight - Effect of Rotor RPM - Neutral CG.

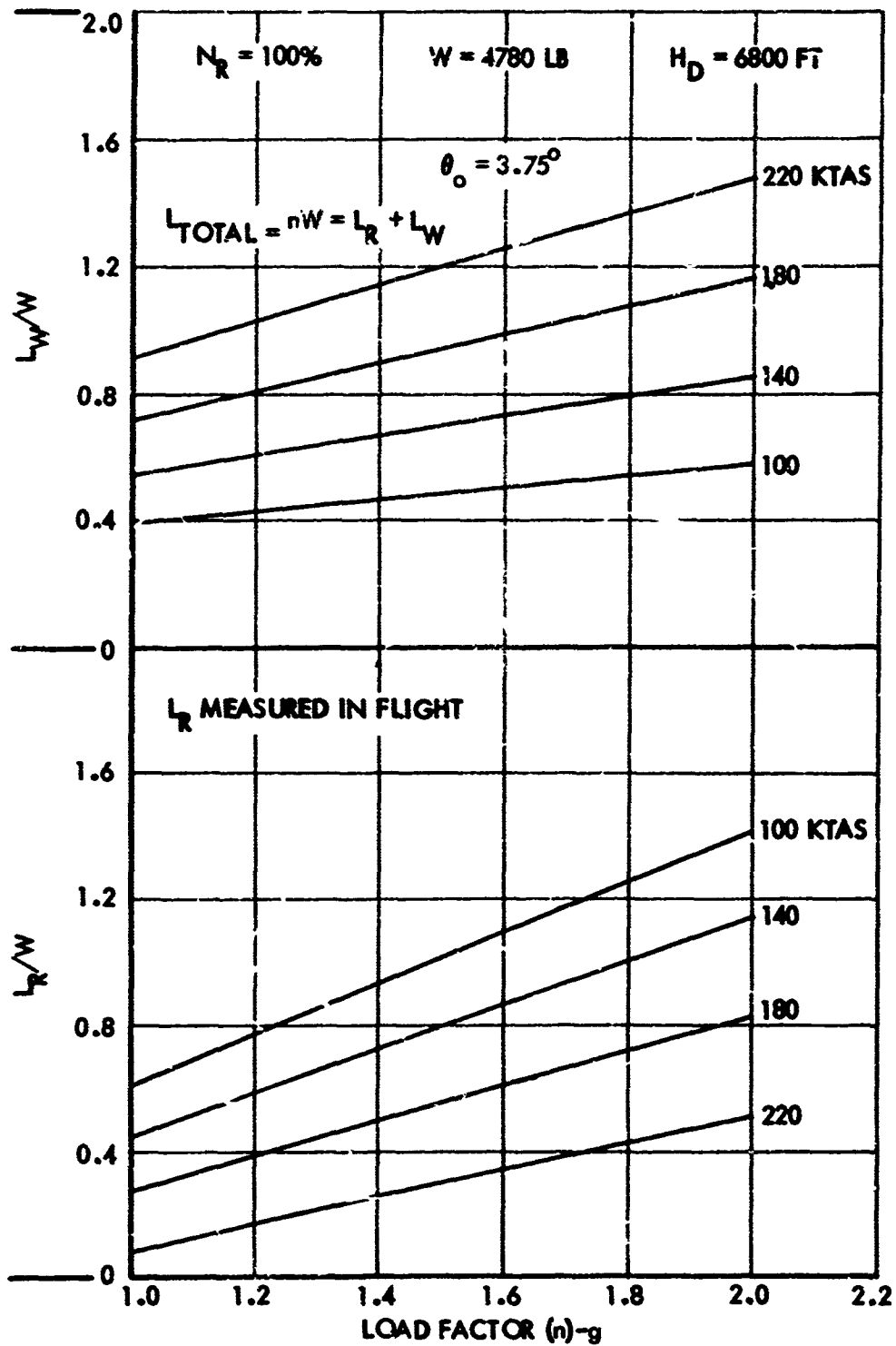


Figure 71. Rotor Lift Sharing Characteristics in Turning Flight - Effect of Airspeed - Neutral CG.

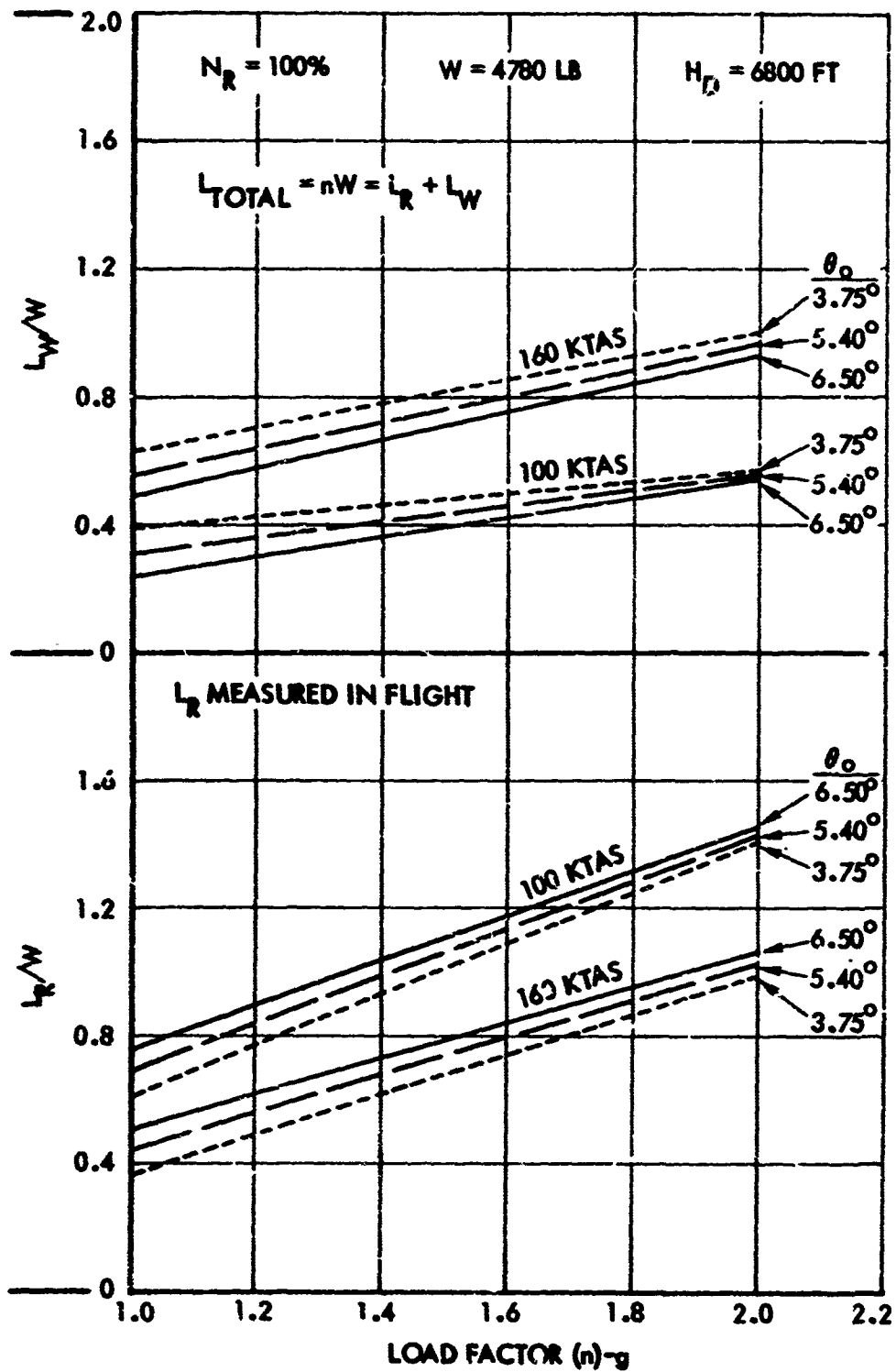


Figure 72. Rotor Lift Sharing Characteristics in Turning Flight - Effect of Collective Blade Angle - Neutral CG.

lift increases to 30 percent of the weight with the wing supporting 120 percent.

These examples illustrate that at higher airspeeds the wing is the principal source of lift at all load factors. It should be noted that the rotor incremental change of lift, referenced to the 1.0g rotor lift, is greater than is the wing incremental change, referenced to 1.0g wing lift. This, of course, reflects the greater lift slope (pounds/angle of attack) of the rotor.

Additional rotor/wing lift sharing characteristics in turning flight are shown in Figure 72 for various collective blade angles at high and low airspeeds.

Rotor RPM does not greatly affect the lift sharing characteristics shown in Figures 71 and 72. However, because of the decrease in level flight rotor lift as RPM is lowered, the wing will have to contribute a slightly larger share of the total aircraft lift in order to perform a turning maneuver at a given set of test conditions.

THEORETICAL COMPARISON

A study of the flight test data has been made to establish the correlation with the calculated performance charts of Reference 7.

Procedure

The correlation procedure consists of the following steps:

1. Use measured values of rotor lift, collective blade angle at the 3/4 radius station, tip speed ratio, advancing tip Mach number, and atmospheric density to identify the proper chart of Reference 7 and to calculate C_L'/σ .
2. Obtain C_D'/σ from the chart and convert it into rotor drag in pounds.
3. Determine the trim conditions of the aircraft by using trim equations derived from the forces shown in Figure 73. The trim equations are:

$$\Sigma \text{Vertical forces} = W - L_A \cos \phi_R - T_R \cos \alpha_R - F_N \sin (i_j + \alpha_\infty) = 0$$

$$\Sigma \text{Horizontal Forces} = F_N \cos (i_j + \alpha_\infty) - D_R - D_A \cos \phi_R - D_{TR} = 0$$

where

$$\alpha_R = \alpha_\infty - i_R$$

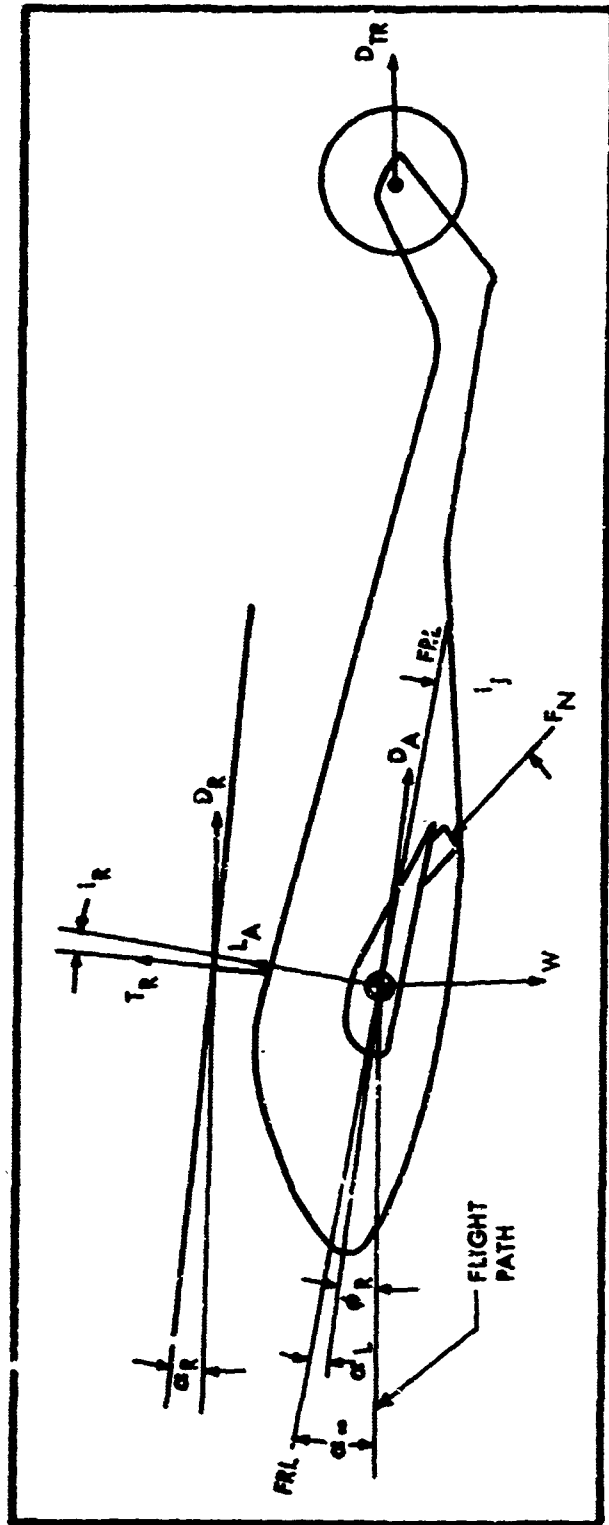


Figure 73. Forces Acting on the Aircraft

$$\phi_R = \frac{T_R}{2\rho\pi R^2 V^2}$$

$$D_{TR} = \frac{.010}{4} \rho \mu [\sigma \pi R^2 (\Omega R)^2]_{TR}$$

The lift and drag coefficients of the helicopter without rotor blades as a function of the local angle of attack, α_L , were measured during wind tunnel tests and are shown in Figure 74. An iteration procedure is used to determine the values of L_A , D_A , α_∞ , and F_N which satisfy the equilibrium equations.

4. Calculate turbine shaft horsepower using main rotor power based on C_Q/σ from the charts of Reference 7 and the following equation which accounts for transmission and accessory losses:

$$SHP = \frac{HP_{MR} + 1.01 HP_{TR} + 21}{.98}$$

where

$$HP_{TR} = \frac{.010}{8} [1 + \mu^2] \rho \left[\frac{\sigma \pi R^2 (\Omega R)^2}{550} \right]_{TR}$$

Results

The results of the correlation in terms of calculated and measured value of jet thrust (F_N), turbine shaft power (SHP), and angle of attack of the fuselage reference line (α_∞) are shown in Figures 75 through 77 for rotor speeds of 100, 95, and 91 percent of normal.

Figure 75 shows test results and calculated curves for 100 percent rotor speed. The highest forward speed used in this comparison at which steady trim conditions were recorded was 231 knots. At this speed, the advancing tip Mach number was 0.933. For engine shaft horsepower, two calculated curves are presented: one using the actual tip Mach numbers, and one using the lowest tip Mach numbers for which charts are available. The second curve is considered to represent incompressible data. It may be seen that the test data lie between the two calculated curves, which indicates that the section drag characteristics used in Reference 7 are somewhat conservative. Figures 75 and 77 show the correlation at 95 and 91 percent of normal rotor speed.

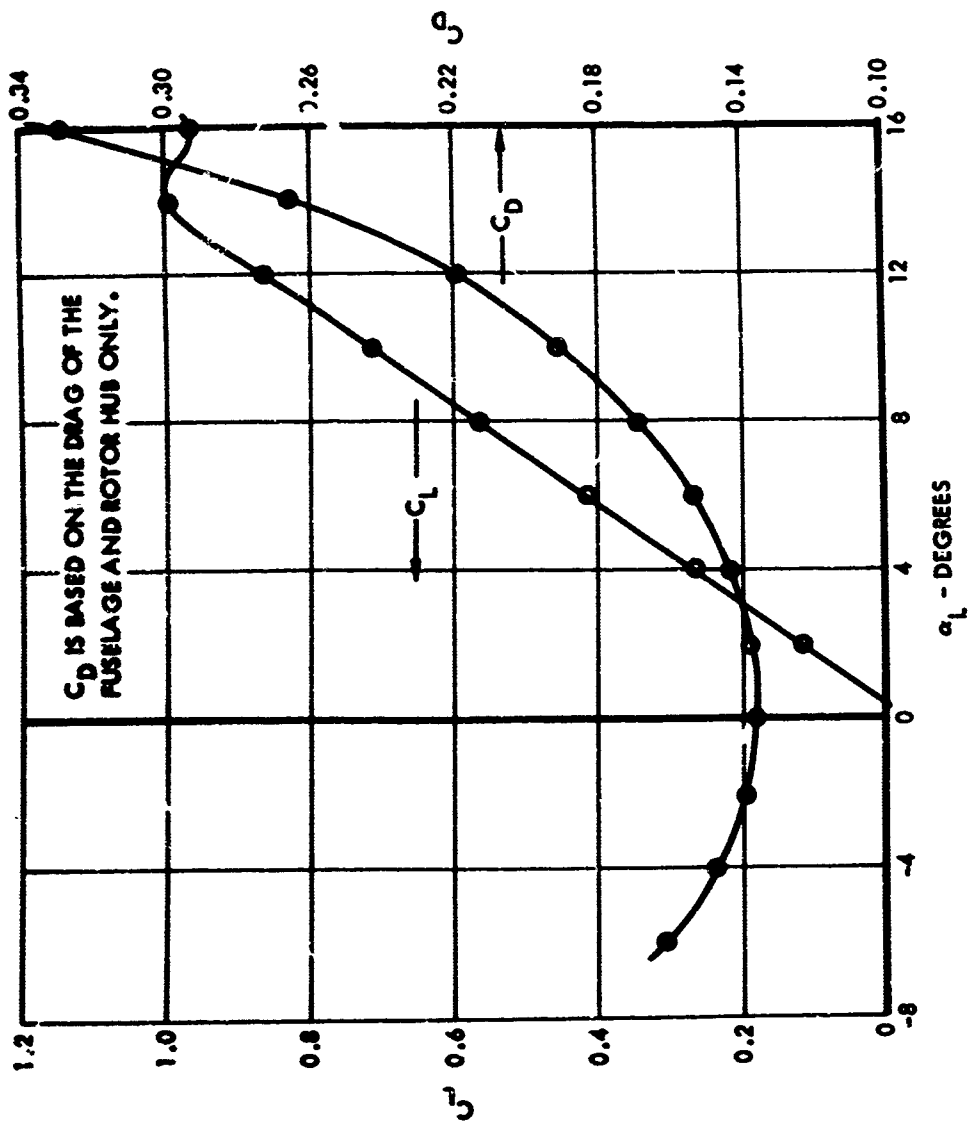


Figure 74. Helicopter Lift and Drag Characteristics

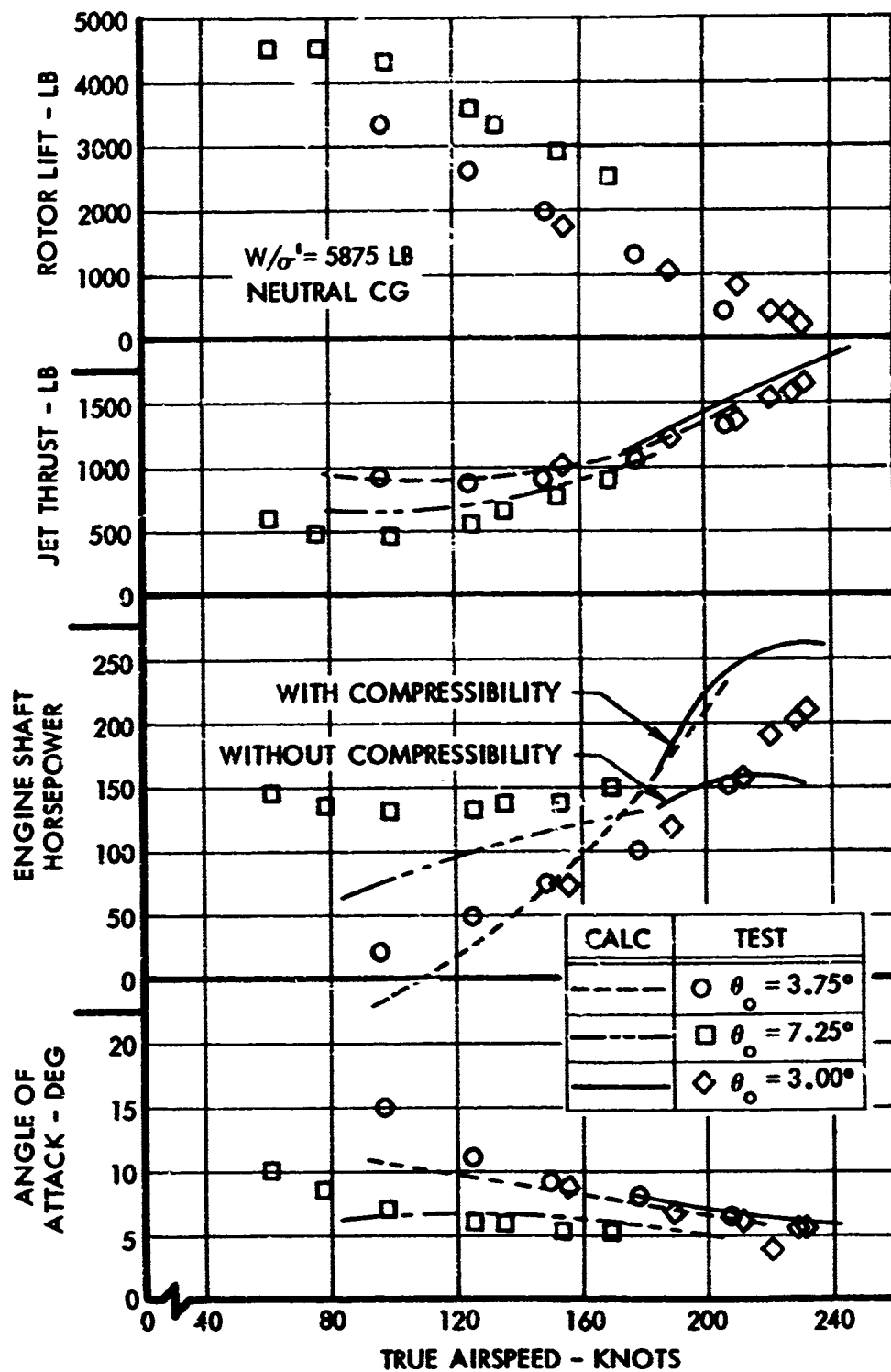


Figure 75. Correlation of Flight Test Data and Calculations at 100% Rotor RPM.

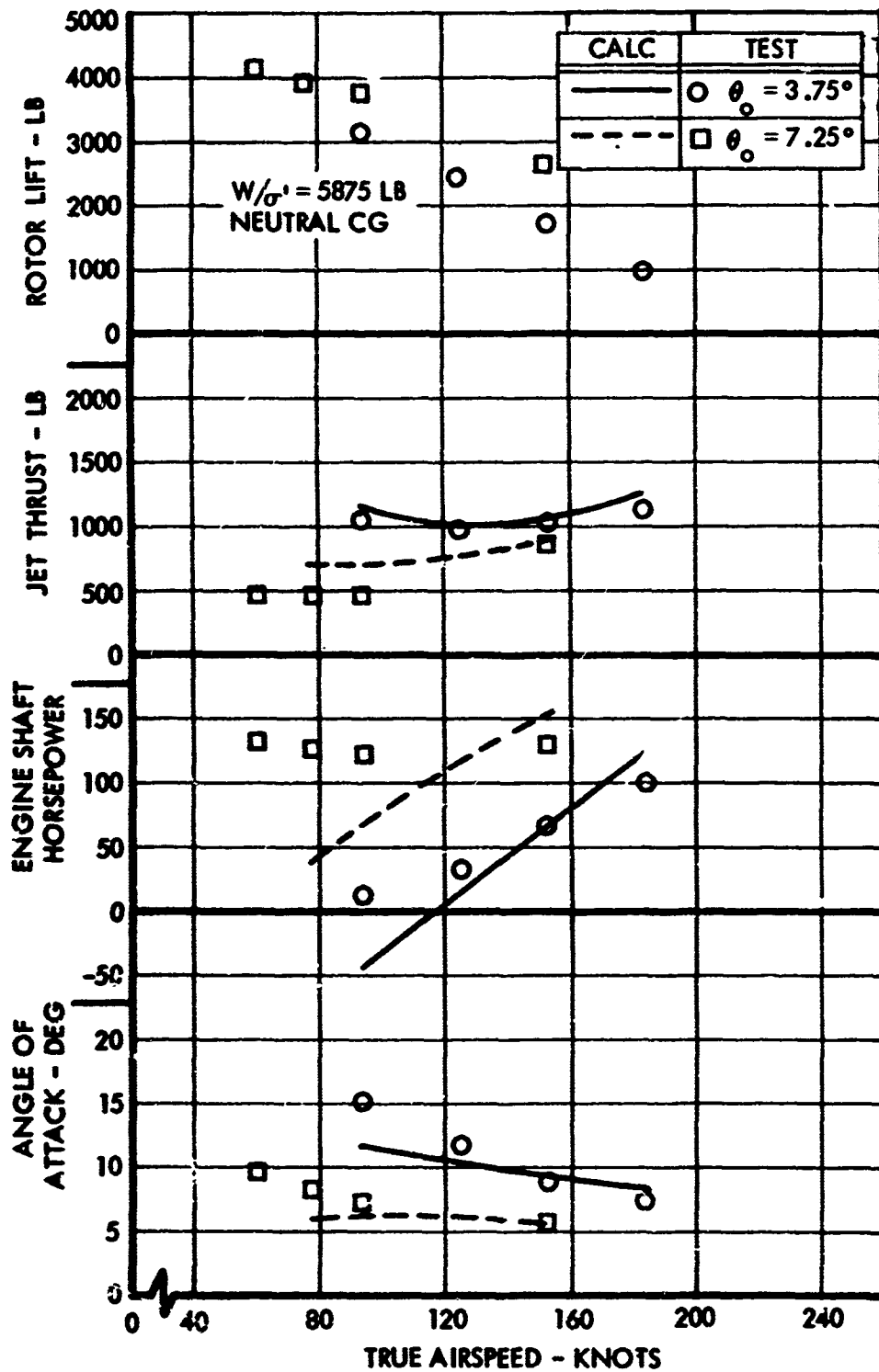


Figure 76. Correlation of Flight Test Data and Calculations at 95% Rotor RPM.

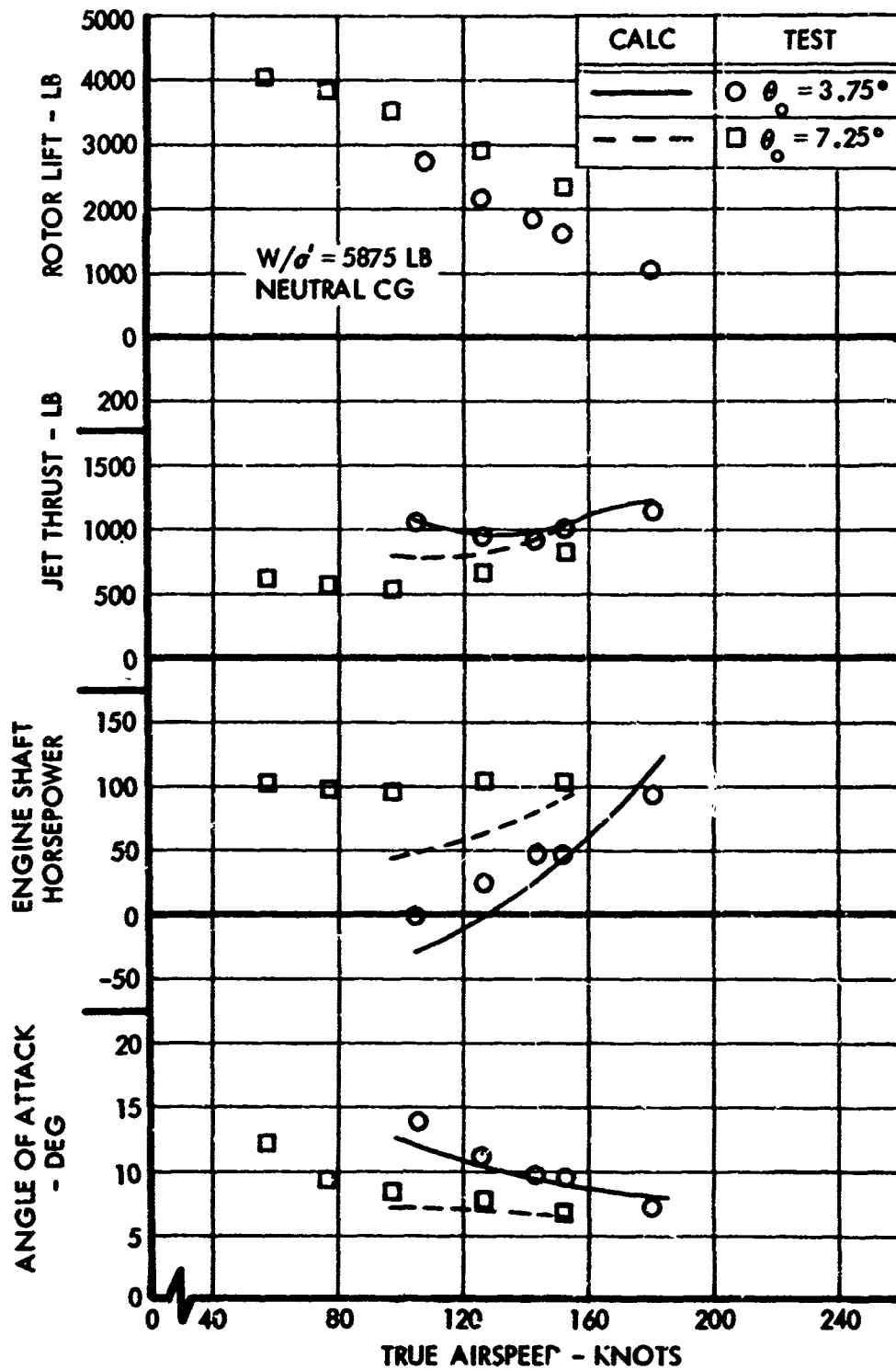


Figure 77. Correlation of Flight Test Data and Calculations at 91% Rotor RPM.

NASA PARTICIPATION

During the course of this program, NASA test personnel from the NASA Langley Research Center, Langley Station, Hampton, Virginia, evaluated the performance, handling qualities, and general flight characteristics of the XH-51A compound helicopter.

Check-out flights were performed by the NASA test pilot in the pure helicopter and compound flight modes. Static longitudinal stability, longitudinal and lateral control response, turning flight, hover maneuvers, autorotation entries, and accelerations and decelerations were evaluated at longitudinal/lateral system sensitivities of 66/200 percent, with a neutral center of gravity. Additional evaluations were conducted at forward center of gravity with longitudinal/lateral system sensitivities of 66/200 percent and 100/200 percent, respectively.

NASA participation amounted to 23 flights, for a total of 9.2 hours of flight time.

U.S. ARMY PARTICIPATION

At two intervals during the maneuverability program, Army test personnel from the U.S. Army Aviation Materiel Laboratories, Fort Eustis, Virginia, evaluated the performance, handling qualities, and general flight characteristics of the XH-51A compound helicopter to verify the contractor's test results.

Check-out flights were performed by the Army test pilot in the pure helicopter and compound flight modes. Level flight and steady turns were evaluated at longitudinal/lateral system sensitivities of 83/154 percent and 66/200 percent, respectively, at neutral centers of gravity. Various autorotation entries were performed to evaluate variations in entry technique. Static longitudinal stability tests were performed to compare the effects of changing system sensitivity, rotor RPM, and center of gravity. Nap-of-the-earth maneuvers were evaluated at the conclusion of the Army test program.

U.S. Army participation amounted to 15 flights, for a total of 5.5 hours of flight time.

CONCLUSIONS

- The objective true airspeed of 240 knots was exceeded.
- The maneuvering envelope was expanded beyond the specified objectives.
- Further expansion of the rotor RPM/airspeed envelope was limited by two factors. The first was an increase in vibration levels when operating at high to intermediate rotor RPM settings and is associated with operating at advancing tip Mach numbers in excess of 0.91. The second factor was a rotor plane oscillation which occurred at high speed with low to intermediate RPM settings.
- Maneuvering stability remained positive throughout the flight envelope and did not appear to be affected by changes in rotor RPM. Rotor overspeeds occur during maneuvering flight under certain combinations of airspeed, load factor, and collective blade angle.
- Autorotation entries were conducted in progressive increments over the airspeed envelope up to and including a true airspeed of 232 knots.
- Control response is unaffected by changes in rotor RPM and collective blade angle over the airspeed envelope. Short-period damping remains strong even at the lower RPM settings.
- Center of gravity location has a significant effect on handling characteristics. At neutral centers of gravity, longitudinal control response increases with increasing airspeed and is unacceptable at high speeds even with the longitudinal control system desensitized to 66 percent of nominal. However, at forward centers of gravity, longitudinal control response is nearly constant with increasing airspeed, which results in better high-speed handling characteristics.
- Simple geometry changes in the longitudinal cyclic control system were necessary to improve handling characteristics at high speed. A single lateral control system sensitivity of 200% of nominal is acceptable for use over the airspeed envelope.

- Lift and thrust sharing between the main rotor and auxiliary devices were evaluated over a broad portion of the flight envelope. At high speeds, the vibration and the structural loads favor a collective blade angle setting consistent with effective use of the wing and rotor.
- Some of the main rotor and other structural measurements exceeded endurance limit values at the extremes of the speed and load factor envelope, but the values were within safe limits for short-time operation of a research vehicle.
- For operation in rough air, the load factors encountered are about three-quarters of those for a typical airplane of about the same weight and in the same environment. Main rotor loads measured in rough air were more severe than those measured in level flight at comparable airspeeds. However, the effect of the load increase on fatigue life is not very severe.
- Increased gross weight and tail rotor torque limitations prevented a full evaluation of the hover maneuvering capability of the compound helicopter. However, the results of sideward, rearward, and low forward speed testing indicate that the handling characteristics are similar to those of conventional helicopters.
- Nap-of-the-earth flying is feasible in a compound helicopter. However, some maneuvers were limited by rotor overspeeds while pulling load factor at intermediate to high airspeeds.

RECOMMENDATIONS

The results of this program indicate some areas where additional study and flight research would prove beneficial in advancing the high-speed helicopter state of the art:

1. The high-speed stability and handling characteristics of the compound helicopter should be studied further. Center of gravity location has a significant effect on the high-speed boundaries of the maneuvering and rotor RPM/airspeed envelopes. Testing should be continued over a wider range of center of gravity locations to evaluate this effect on overall aircraft stability characteristics. This investigation would also examine improved methods for presentation of the stability parameters of compound helicopters.
2. Additional testing should also be conducted to evaluate further the conditions under which rotor plane oscillations are encountered at high airspeeds with low to intermediate RPM settings. Attention would be given to the effects on handling characteristics, structural loads, and vibration. After the problem is studied, techniques would be devised to delay or eliminate the rotor plane oscillation.
3. It is recommended that further studies be made to determine modifications to the XH-51A compound helicopter which would permit expansion of its operational envelope to speeds on the order of 300 knots and to increase its flexibility as a research tool.
4. Consideration should be given to providing for variations of blade taper ratio, blade twist, blade thickness ratio, blade camber, rotor rotational speed versus vehicle speed, and rotor coning angle. Also, increases in the installed power of both the auxiliary thrusting and primary rotor driving engines should be evaluated.

LITERATURE CITED

1. Wyrick, D. R., EXTENSION OF THE HIGH-SPEED ENVELOPE OF THE XH-51A COMPOUND HELICOPTER; USAAVLABS Technical Report 65-71, Lockheed Report 18917, U.S. Army Aviation Materiel Laboratories, Fort Eustis, Virginia, May 1965.
2. Foulke, W. K., EXPLORATION OF HIGH-SPEED FLIGHT WITH THE XH-51A RIGID ROTOR HELICOPTER; USAAVLABS Technical Report 65-25, Lockheed Report 18374, U.S. Army Aviation Materiel Laboratories, Fort Eustis, Virginia, June 1965.
3. UH-1B HELICOPTER FLIGHT LOADS INVESTIGATION PROGRAM; USAAVLABS Technical Report 66-46, U.S. Army Aviation Materiel Laboratories, Fort Eustis, Virginia, May 1966.
4. Schijve, J., THE ANALYSIS OF RANDOM LOAD-TIME HISTORIES WITH RELATION TO FATIGUE TESTS AND LIFE CALCULATIONS. Paper presented to the 2nd ICAF-AGARD Symposium, Paris, 16, 17, and 19 May 1961. Printed in: Fatigue of Aircraft Structures, Oxford-London, New York, Paris, Pergamon Press, 1963.
5. AIRPLANE STRENGTH AND RIGILITY-FLIGHT LOADS; Military Specification, MIL-A-8861 (ASG), 18 May 1960.
6. Webber, D. A., COMPARISON OF HELICOPTER AND AEROPLANE VERTICAL ACCELERATIONS IN TURBULENCE; Ministry of Aviation, Aeronautical Research Council, Current Papers, C.P. No. 878, London, Her Majesty's Stationery Office, 1966.
7. Tanner, W. H., CHARTS FOR ESTIMATING ROTARY WING PERFORMANCE IN HOVER AND AT HIGH FORWARD SPEEDS; NASA Contractor Report CR-114, November 1964.
8. Tanner, W. H., TABLES FOR ESTIMATING ROTARY WING PERFORMANCE IN HOVER AND AT HIGH FORWARD SPEEDS; NASA Contractor Report CR-115, November 1964.

UNCLASSIFIED

Security Classification

DOCUMENT CONTROL DATA - R & D

(Security classification of title, body of abstract and indexing annotation must be entered when the overall report is classified)

1. ORIGINATING ACTIVITY (Corporate author) Lockheed-California Company Burbank, California		2a. REPORT SECURITY CLASSIFICATION Unclassified	
		2b. GROUP	
3. REPORT TITLE RESEARCH IN MANEUVERABILITY OF THE XH-51A COMPOUND HELICOPTER			
4. DESCRIPTIVE NOTES (Type of report and inclusive dates) Final Report			
5. AUTHOR(S) (First name, middle initial, last name) F. P. Lentine, W. P. Groth, and T. H. Oglesby			
6. REPORT DATE June 1968		7a. TOTAL NO. OF PAGES 161	7b. NO. OF REFS 8
8a. CONTRACT OR GRANT NO. DA 44-177-AMC-36; (T)		8b. ORIGINATOR'S REPORT NUMBER(S) USAAVIABS Technical Report 68-23	
A. PROJECT NO. 1F121401A14301		9b. OTHER REPORT NO(S) (Any other numbers that may be assigned this report) Lockheed Report 20894 LF	
10. DISTRIBUTION STATEMENT This document has been approved for public release and sale; its distribution is unlimited.			
11. SUPPLEMENTARY NOTES		12. SPONSORING MILITARY ACTIVITY U.S. Army Aviation Materiel Laboratories Fort Eustis, Virginia	
13. ABSTRACT This report presents the results of a research program in maneuverability and rotor loads conducted by the Lockheed-California Company on the compound version of the rigid-rotor XH-51A helicopter. The principal objective of this program was to evaluate the maneuvering capability in terms of envelope expansion, longitudinal and lateral control power and damping, autorotation characteristics, level flight characteristics, and hover maneuvers. The testing included the evaluation of rotor RPM and control sensitivity changes over the target airspeed-load factor envelope for both neutral and forward centers of gravity. The maximum true airspeeds attained with a forward center of gravity were 262.7 knots at 95.5 percent rotor RPM in a shallow descent at a density altitude of 7750 feet, and 223.5 knots at 91 percent rotor speed at a density altitude of 7250 feet in level flight.			

DD FORM 1473

REPLACES DD FORM 1473, 1 JAN 64, WHICH IS OBSOLETE FOR ARMY USE.

UNCLASSIFIED

Security Classification

UNCLASSIFIED
Security Classification

14. KEY WORDS	LINK A		LINK B		LINK C	
	ROLE	WT	ROLE	WT	ROLE	WT
Agility Autorotation characteristics Compound helicopter Control response Hovering flight Maneuverability Performance Rigid rotor						

UNCLASSIFIED

Security Classification

6694-68

UNCLASSIFIED Security Classification